

The CLAS12 Superconducting Magnets

R. Fair^{a,1}, N. Baltzell^a, R. Banchimanchi^a, G. Biallas^b, V.D. Burkert^a, P. Campero-Rojas^a, L. Elementi^c, L. Elouadrhiri^a, B. Eng^a, P. K. Ghoshal^a, J. Hogan^a, D. Insley^a, V. Kashikhin^c, D. Kashy^a, S. Krave^c, O. Kumar^a, M. Laney^a, R. Legg^b, M. Lester^a, T. Lemon^a, A. Lung^a, C. Luongo^e, J. Matalevich^a, M.D. Mestayer^a, R. Miller^a, W. Moore^a, J. Newton^a, F. Nobrega^c, O. Pastor^e, S. Philip^a, R. Rajput-Ghoshal^a, V. Rao Gannig^a, C. Rode^b, N. Sandoval^a, S. Spiegel^a, D. Tilles^b, K. Tremblay^a, G. Velev^c, C. Wilson^a, M. Wiseman^a, G.R. Young^b

^a Thomas Jefferson National Accelerator Facility (TJNAF), Newport News, VA, 23606, USA

^b Thomas Jefferson National Accelerator Facility, Newport News, VA, 23606, USA (Retired)

^c Fermi National Accelerator Laboratory (FNAL), Batavia, IL, 60510 USA

^d SLAC National Accelerator Laboratory, Stanford, CA, 94025 USA (Previously with TJNAF)

^e International Thermonuclear Experimental Reactor Organization (ITER), St. Paul-lez-Durance 13067, France (Previously with TJNAF)

^f CEA Saclay, F91191 Gif-sur-Yvette, France

^g Michigan State University, East Lansing, MI, 48824 USA (Previously with TJNAF)

^h Old Dominion University, Norfolk, VA, 23529, USA

ARTICLE INFO

Keywords:

Superconducting, magnets, torus, solenoid, quench, mapping , toroid

ABSTRACT

As part of the Jefferson Lab 12 GeV upgrade, the Hall B CLAS12 system requires two superconducting iron-free magnets – a torus and a solenoid. The physics requirements to maximize space for the detectors guided engineers toward particular coil designs for each of the magnets which, in turn, led to the choice of using conduction cooling. The torus consists of 6 trapezoidal NbTi coils connected in series with an operating current of 3770 A. The solenoid is an actively shielded 5 T magnet consisting of 5 NbTi coils connected in series operating at 2416 A. Within the hall, the two magnets are located in close proximity to each other and are completely covered both inside and outside by particle detectors. Stringent size limitations were imposed for both magnets and introduced particular design and fabrication challenges. This paper describes the design, construction, installation, commissioning, and operation of the two magnets.

¹ The Manuscript received XXXXXX.

This work was supported by Jefferson Science Associates, LLC, under U.S. DOE Contract DE-AC05-06OR23177. The U.S. Government retains a non-exclusive, paid-up, irrevocable, world-wide license to publish or reproduce this manuscript for U.S. Government purposes.

Corresponding author: R Fair (e-mail: rfair@jlab.org)

Color versions of one or more of the figures in this paper are available online at XXXXXXXX

Digital Object Identifier (inserted by Publisher)

I. PHYSICS REQUIREMENTS AND TECHNICAL SPECIFICATIONS

The CEBAF Large Acceptance Spectrometer for 12 GeV (CLAS12) is a new detector system within Hall B at Jefferson Laboratory (JLab) designed to measure electron-induced reactions over a broad kinematic phase space. It consists of two large superconducting magnets, a 6-coil torus and a 5-coil solenoid. The solenoid magnet is located upstream of the torus magnet and provides a field to bend low-energy (300 MeV to 1.5 GeV) charged particles. The field also provides focusing and shielding for Möller electrons, which allows the detector system to run at high data rates. A homogeneous field at the magnet center is needed for polarized targets. The torus provides a bending field for high energy (0.5 GeV to 10 GeV) charged particles and mechanical support for 3 regions of drift chambers. A general overview of the physics requirements and experiment design is provided in Ref. [1].

Tables I and II summarize the physics requirements for the torus and solenoid superconducting magnets, respectively, while Table III provides a summary of the key design parameters for the two magnets. Figure 1 illustrates the locations of the two magnets relative to each other while Fig. 2 shows photographs of the two magnets.

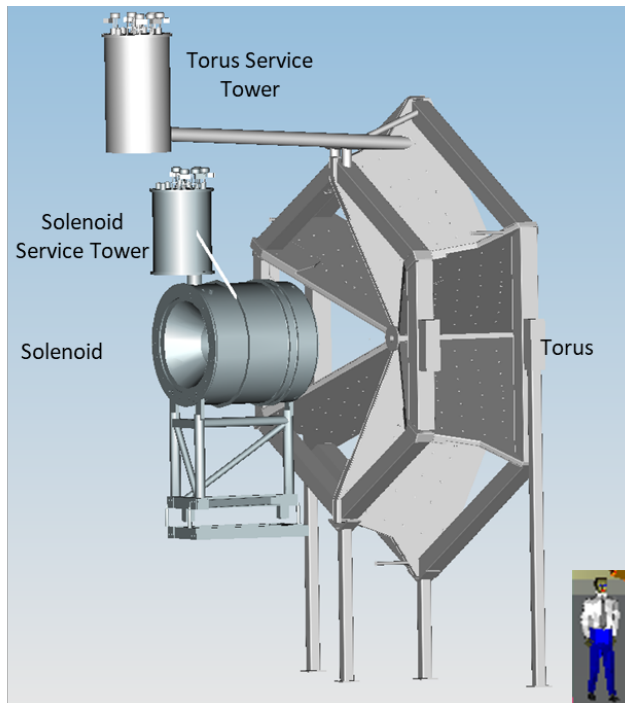


Figure 1: Simplified model illustrating the locations of the solenoid and the torus with respect to each other (no physics detectors are shown here).

TABLE I
 CLAS12 HALL B - TORUS PHYSICS REQUIREMENTS

Parameters	Requirement
Angular coverage (cone angle relative to the forward direction)	$\theta = 5^\circ - 40^\circ$ $\Delta\phi = 50\text{-}90\%$ of 2π
$\int B dl$ @ nominal current	2.83 T.m @ $\theta = 5^\circ$ 0.6-1.0 T.m @ $\theta = 40^\circ$
Access	Open access to field volume on either side of beamline

TABLE II
 CLAS12 HALL B – SOLENOID PHYSICS REQUIREMENTS

Parameters	Requirement
B_0	5 T
$L=1/B_0/B_{dl}$	$L = 1$ to 1.4 m
Field uniformity in target Area	$\Delta B/B_0 < 10^{-4}$ in cylinder 0.04 m length $\times 0.025$ m (100 ppm)
Field at HTCC PMTs	$B < 35$ G (for the four HTCC PMT locations) [2]
Field at CTOF PMTs	$B < 1200$ G (for the two CTOF PMT locations) [3]

HTCC – High Threshold Cherenkov Counter, CTOF – Central Time of Flight,
 PMT – Photomultiplier Tubes

TABLE III
 CLAS12 HALL B - SOLENOID AND TORUS MAGNET PARAMETERS

PARAMETER	DESIGN VALUE	
	SOLENOID	TORUS
Number of Coils	$2 + 2 + 1$ (2 inner + 2 intermediate + 1 outer shield)	6
Coil design	Helically layer-wound potted coils	Double pancake potted in aluminum case
Total number of turns	5096 $2 \times 840 + 2 \times 1012 + 1392$	1404 (117 $\times 2 \times 6$)
NbTi Rutherford cable	SSC 36 strands	SSC 36 strands
Nominal current (A)	2416	3770
Central field (T)	5	N/A
Conductor peak field (T)	6.56 1×10^{-4}	3.6
Required field homogeneity	Over a $\phi 25$ mm \times L40 mm cylindrical volume at magnetic center	N/A
Inductance (H)	5.89	2
Stored energy (MJ)	17	14
Warm bore (mm)	780	124
Outer diameter \times length	2.16 m \times 1.8 m	N/A
Inner bore length / opening angle	0.897 m/ 41°	N/A
Coil case thickness	-	Originally 100mm changed to 125mm
Total weight (kg)	18800	25500
Cooling mode	Conduction cooled	Conduction cooled
Supply temperature (K)	4.5	4.5
Temperature margin (K)	1.5	1.5
Stabilized conductor	W17 mm \times T2.5 mm copper channel	W20 mm \times T2.5 mm copper channel
Turn-to-turn insulation	0.004" glass tape $\frac{1}{2}$ lap	0.003" glass tape $\frac{1}{2}$ lap
Heat shield cooling	Helium boil-off	LN ₂ thermo-siphon

The torus magnet and the Torus Service Tower (TST) were designed and built at JLab; the Cryogenic Distribution Box (DBX), was designed at JLab and fabricated by Meyer Tool, while the coils were fabricated at the Fermi National Accelerator Laboratory (FNAL), USA [4, 5]. The solenoid magnet was designed and fabricated by Everson Tesla Inc., USA (ETI), while the Solenoid Service Tower (SST) and cryogenics were designed and fabricated by JLab. The magnets differ in their cooling schemes from that of more conventional bath-cooled superconducting magnets by using conduction-cooling methodology in order to comply with tight physical space

requirements. These requirements imposed certain size limitations on the design of the torus and solenoid magnet coils, which led to each magnet having their own unique issues for design, fabrication, installation, and control [6]. Leftover NbTi

Rutherford superconductor cable from the Superconducting Super Collider (SSC) project (which was terminated in 1993) was modified by soldering the cable into a C-shaped copper channel and then used to wind the coils for both the torus and solenoid.

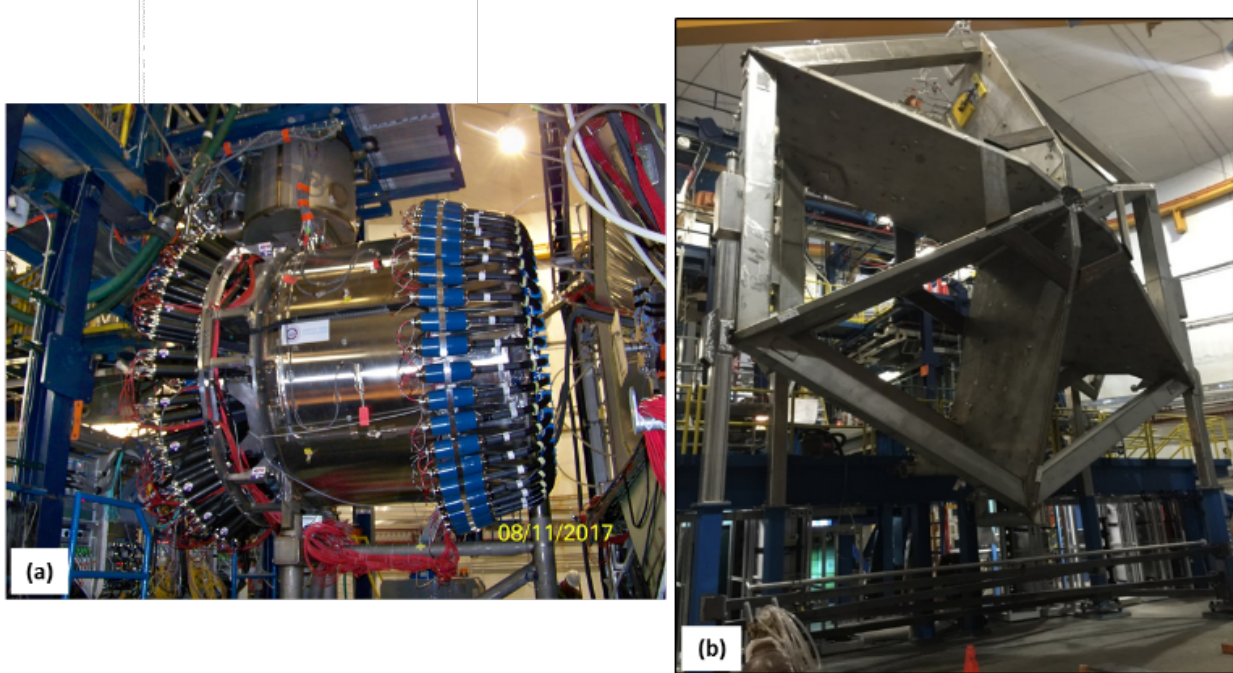


Figure 2: Magnets installed in Hall B – (a) Solenoid (with some detectors installed), (b) Torus (before drift chambers were installed between the coils).

II. PROJECT MANAGEMENT AND RISK MITIGATION APPROACH

The Hall B torus and solenoid magnets were part of the JLab 12 GeV Upgrade project, which included an upgrade to the accelerator and three of the four experimental Halls B, C, and D. The project involved the fabrication, installation, and commissioning of a total of 8 superconducting magnet systems [7]. Once the majority of the design work had been completed, a Magnet Task Force was set up at JLab in order to provide consistency in the management of the various activities, to promote the sharing of lessons learned between the different magnet systems and halls, and to provide a more focused effort. The task force leader had overall technical responsibility for all the magnets, including the Hall B torus and solenoid magnets, and oversaw the timely completion of all tasks. Key procurements (for example individual magnets and magnet power supplies) were overseen by the respective Subcontracting Officers (SOs) from the JLab Procurement Department with technical assistance being provided by Subcontracting Officer Technical Representatives (SOTRs). Multiple design and manufacturing reviews were held for each magnet and other key components, most of which were face to face. Progress tracking, problem-solving meetings, and teleconference calls were held with the various vendors on either a regular schedule or on an as-needed basis. JLab staff also provided oversight at the vendors' premises, especially during key manufacturing stages.

All critical tasks and systems of the magnets of the CLAS12 system, both torus and solenoid, were subjected to a detailed Risk Assessment and Mitigation (RAM) process. The process was used

to evaluate the overall magnet design and the robustness of its protection system and commissioning process. The magnet risk assessments were developed via a series of electromagnetic and electromechanical analyses, which included induced eddy currents, Lorentz forces, thermal loading, magnet-to-magnet interactions, and an assessment of magnet performance while in proximity to ferromagnetic structures. The assessments also included things like loss of control power, loss of main power, loss of cryogenic supply, and loss of vacuum. The risk mitigation approach was based on a Failure Modes and Effects Analysis (FMEA) carried out for each phase of the project: design, fabrication, installation, and commissioning [8]. FMEA is a tool used to eliminate or mitigate known potential failures, problems, and errors within systems. A failure mode is defined as the way a component could fail to meet its performance requirements or to function. More than 400 risk items were identified, categorized, and ranked; mitigation avenues were investigated for all risks, and implemented when warranted, either because the risk was deemed to be high, or implementation was easily achieved.

The potential failure modes were evaluated based on a Risk Priority Number (RPN), which is the product of three factors: the Severity ranking (S), the probability of Occurrence (O), and the probability of Detection (D). The RPN was used as a measure of overall risk and helped to identify and rank the risks of the potential failure modes. The end results of failures that lead to unsafe conditions or significant losses in functionality were rated high in severity. Larger RPNs indicated the need for corrective action or failure resolution. The FMEA process was used to assist in identifying potential failure modes early in the design phase.

Several of the key risks for the torus and solenoid (indicated by larger RPNs) are listed below and were addressed during the project:

- The system does not satisfy the physics requirements;
- Late delivery of key components and subsystems from vendors;
- Defects in the build and manufacture of thermal insulation (e.g. standoffs, multi-layer insulation);
- Insufficient helium mass flow in the cooling channel;
- Vacuum vessel cannot maintain required vacuum;
- Breakdown of the electrical insulation of the magnet system;
- Loss of control of the magnet power supply system;
- Loss of magnet protection due to a fault in the quench detection and protection system.

Some of the mitigation actions stemming from the FMEA included:

- Extensive use of mock-ups and practice builds for all quality-critical activities (e.g. conductor soldering into channel, conductor splices, distortion of vacuum jackets during welding, connection of hex beams to coils, mounting of instrumentation);
- Development of written procedures, before and in conjunction with the practice builds;
- Safety and risk-awareness meetings prior to each critical operation;
- Extensive use of in-process quality assurance (QA) checks;
- Detailed weekly and daily planning of installation activities in the hall;
- Vendor oversight by JLab staff.

Safety reviews, as well as Director's Reviews, Magnet Advisory Group Meetings, and U.S. Department of Energy Reviews, played a crucial role in developing the RAM process at JLab, as well as to guide the technical path, verify resources, and check project progress. Safety reviews in particular comprised two key sub-reviews - Pressure System Reviews (which checked against relevant design codes like ASME and also ensured all relevant documentation was in place), and Experimental Readiness Reviews (Cool down and Power-up reviews) before the magnet systems were signed over to the JLab Physics Division for operation.

III. DESIGN AND ANALYSIS

The coils for the two magnets utilized surplus Superconducting Super Collider (SSC) outer dipole conductor that consisted of 36 strands of 0.65-mm diameter multi-filament NbTi superconductor with a Cu:Sc ratio of 1.8:1, manufactured as a key-stoned Rutherford cable and soldered into a rectangular nominally dimensioned 2.5 mm × 20 mm OFHC copper channel for the torus and a 2.5mm × 17 mm channel for the solenoid (see Fig. 3 and Table IV for details). This Rutherford conductor had been in storage for many years, so sample lengths of conductor from each spool were tested to check for any degradation in performance. The superconductor for the magnets has a tested short sample performance of better than 11000 A at 4.2 K at 5 T and showed no discernable degradation when compared to its original specifications. The cable and copper channel underwent rigorous

inspection and cleaning processes prior to being soldered together. These were time-consuming and laborious processes.

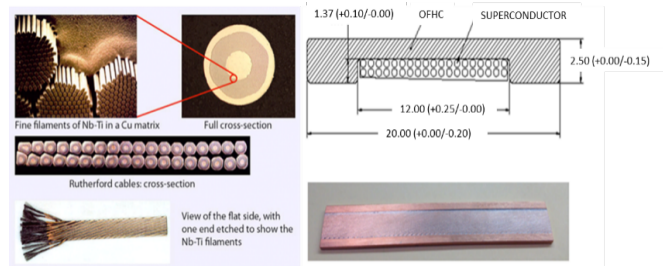


Figure 3: SSC Outer Dipole NbTi Rutherford Cable and cross-sectional view of the conductor with critical dimensions shown for the torus conductor.

TABLE IV
 TORUS CONDUCTOR SPECIFICATION

Parameter	Details
Rutherford type of cable (Superconductor)	NbTi
Conductor material (NbTi + Cu)	Cu-(NbTi) in rectangular Cu channel
Number of strands in the cable	36
Number of NbTi filaments in each strand	4600
Strand bare diameter (mm)	0.648
Copper to non-copper ratio	1.8
Twist pitch (mm)	15
Conductor size (bare) (mm x mm)	20 x 2.5
Conductor size (insulated) (mm x mm)	20.2 x 2.7
Minimum Short sample current at 4.22 K, 5 T (A)	>11000
RRR Cu (Cu-NbTi) – Strand	100
Minimum RRR Cu channel (design)	70

TORUS

Torus Magnet Design

The torus magnet has 6 double-pancake, trapezoidal-shaped coils wound with copper-stabilized NbTi Rutherford cable, which were vacuum impregnated with epoxy, wrapped with copper cooling sheets, assembled in aluminum cases, and then epoxy-impregnated a second time, to produce a coil cold mass (CCM) that operates at 4.5 K. Pre-formed multi-layer insulation (MLI) blankets were fitted to each CCM (see Fig. 4).

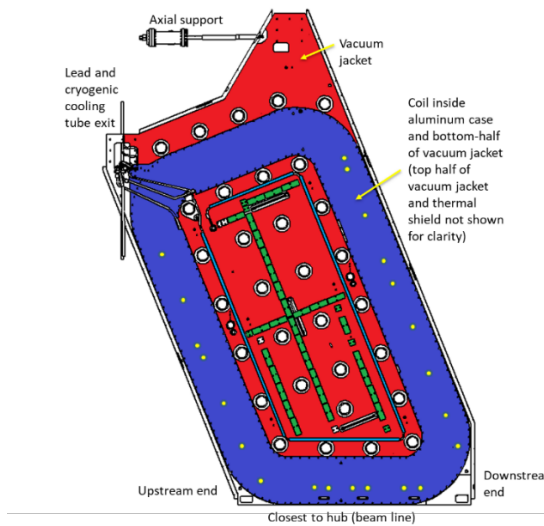


Figure 4: A torus magnet coil in its vacuum jacket.

Aluminum thermal shields, (cooled to 80 K by a liquid-nitrogen thermo-siphon), surround each CCM and themselves were covered with additional MLI blankets. The whole assembly is enclosed within a welded stainless-steel vacuum jacket. The 6 independent CCMs are mechanically held together at a cold hub positioned along the axis of the torus. The CCMs are connected to each other on their outer extremities via 12 hex beams, which are conduction cooled to 4.5 K. There are two hex beams per sector, upstream and downstream (see Fig. 5).

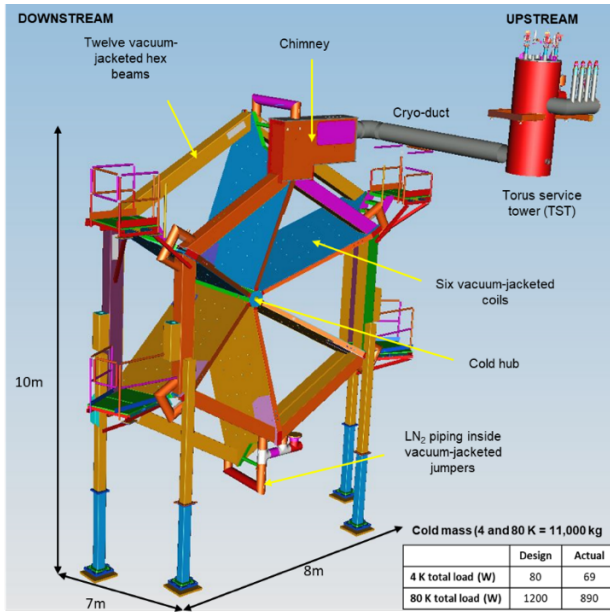


Figure 5: The torus magnet - key features, dimensions, and heat loads.

The six coils are electrically connected in series using soldered joints (splices). The system has three hydraulic circuits all supplied by the Torus Service Tower (TST) – supercritical helium to indirectly cool the coils, atmospheric helium running through the re-coolers and a liquid-nitrogen circuit for the thermal shields. A liquid-filled (4.5 K, 1.4 atm) helium re-cooler (tube-in-shell heat exchanger) is mounted to each upstream hex beam. The coil-to-coil splices are mounted to and cooled by these re-coolers. The re-coolers remove heat input at each coil before entering the next coil and thus maintain equal helium inlet temperatures to each coil. A small fraction of the boil-off from the re-coolers is used to cool the magnet's vapor-cooled current leads, the rest is sent back to the refrigerator. All six coils share a common vacuum space with two vacuum pumping systems being operated continuously - at the top and bottom of the torus magnet. A single distribution box (DBX) supplies both the torus and the solenoid magnets.

Torus Superconducting Coil Design

The torus magnet coils generate a toroidal magnetic field. The $\int B \cdot dl$ requirements outlined in Table I require a trapezoidal coil shape to be used. Figure 6a illustrates the magnetic field distribution on the coil surface. The peak field of 3.6 T is located at the coil inner bore surface and is almost half this value at the coil's outer radius. Figure 6b indicates the temperature distribution across the coil, with the “warmest” part of coil having the highest thermal radiation heat load near the lead exit due to the extended surface of the coil case at the hex rings.

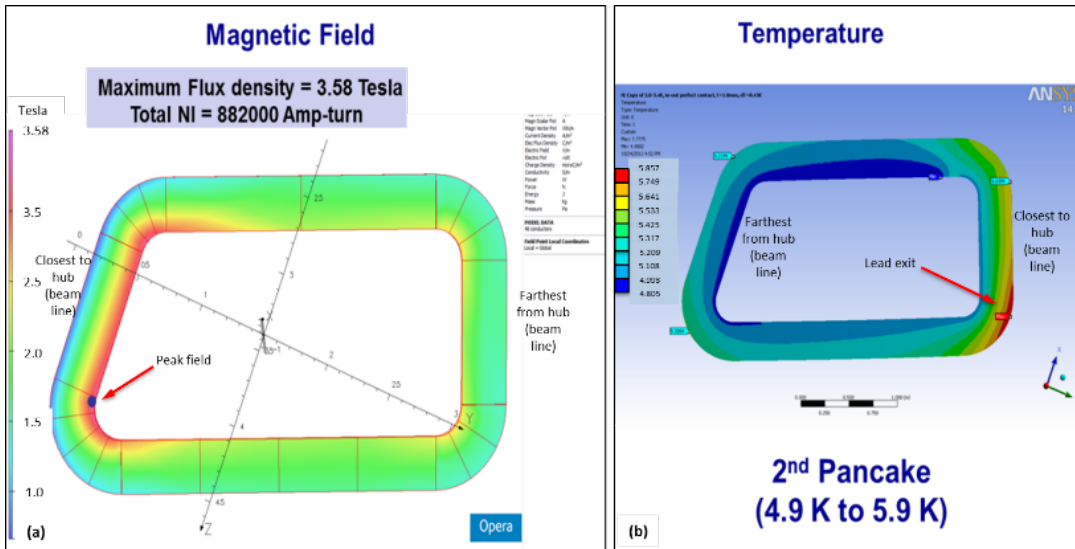


Figure 6: (a) Magnetic field distribution on the torus coil surface with the magnet at 3770 A. (b) Steady state temperature distribution on the torus coil surface (assuming 3x design heat load).

Figure 7 summarizes the performance of the superconducting Rutherford cable used for both the torus and solenoid magnets in

the form of a set of critical current curves at varying operating temperatures. The load lines for the torus and solenoid magnets are displayed as straight lines labeled I_{coil} .

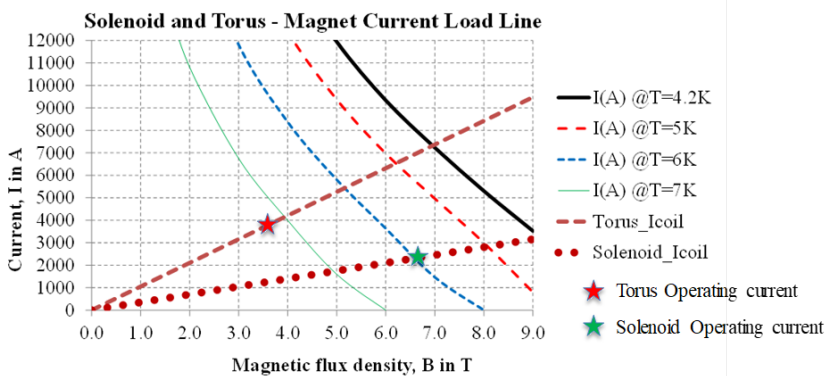


Figure 7: Superconducting Rutherford cable critical current vs. magnetic flux density - solenoid and torus magnet load lines (I_{coil}).
 (Note: the peak field calculation includes the detailed cable and strand geometry)

An assessment of the conductor stability for the torus is summarized in Table V.

TABLE V
 SUMMARY OF TORUS CONDUCTOR STABILITY ASSESSMENT

Operating Scenario (Hall B Torus)

Conductor temperature T_{op} (K)	5.3	K
Maximum field in the coil B_{max} (T)	3.58	T
Operating current I_{op} (A)	3770	A
I_c (at B_{max}) (A) at T_{op}	9836	
Summary		
Short sample performance (SSP)	<40%	38.33%
Stable for T_{cs} value (Margin)	Yes	>1.5 K
Stable for Beta (Adiabatic stability)	Yes	
Adiabatic flux jump stability	Yes	
Dynamic stability	Yes	
Adiabatic self-field stability	Yes	
Stable in term of twist pitch	Yes	
Stable for finite element size	Yes	

Several scenarios were evaluated during the design phase for different coil operating temperatures, different local magnetic field magnitudes, and also an examination of the effect of losing 2 out of the 36 strands from the conductor. As can be seen from Fig. 6 and Table VI, the torus coil design has a more than adequate temperature margin ΔT , which in all cases exceeds the usual design guidance of 1.5 K, suggesting that the magnet coils are somewhat tolerant, in particular, to temperature variations [9].

- Case #1: Operating temperature (T_{op}) 4.7 K (1st pancake), B_{max}
- Case #2: $T_{op}=4.9$ K (2nd pancake), B_{max}
- Case #3: $T_{op}=5.3$ K (2nd pancake), B_{max}
- Case #4: $T_{op}=5.3$ K (2nd pancake), B_{max} (assuming 2 lost strands)
- Case #5: $T_{op}=5.9$ K (2nd pancake), $B=1.5$ T (lead exit)

TABLE VI
TORUS MAGNET MARGIN AND SSP

Case	B _{max} (T)	I _c (at B _{max}) (A) at T _{top}	I _{op} (A)	% SSP (K)	T _{top} (K)	T _c (K)	T _g (K)	ΔT (K) = T _g (K) – T _{top} (K)
1	3.58	12076	3770	31.22	4.7	7.86	6.87	2.17
2	3.58	11332	3770	33.27	4.9	7.86	6.88	1.98
3	3.58	9836	3770	38.33	5.3	7.86	6.88	1.58
4	3.58	9285	3770	40.60	5.3	7.86	6.82	1.52
5	1.5	11467	3770	32.88	5.9	8.75	7.81	1.91

The coil turn insulation, pancake-to-pancake insulation, and the Turn-to-Ground insulation was designed as shown in Fig. 6 to meet the requirements in Table VII. A similar approach was used to define the solenoid coil insulation. The magnet coils are protected via an externally located dump resistor that is permanently connected across the magnet terminals. This resistor has a center tap that then feeds a ground-fault indicator. The presence of this center tap produces an expected maximum voltage across the magnet during a typical quench scenario of 250 V. However, in the extremely unlikely event that the center tap is lost, the voltage across the magnet terminals could increase to a peak of approximately 500 V. This hardware-related fault voltage, together with a safety factor, as well as a full protection analysis to calculate coil peak temperatures and voltages, was used to determine the overall design for the coil turn insulation, pancake-to-pancake insulation, and the Turn-to-Ground insulation (see Fig. 8 and Table VII) [9].

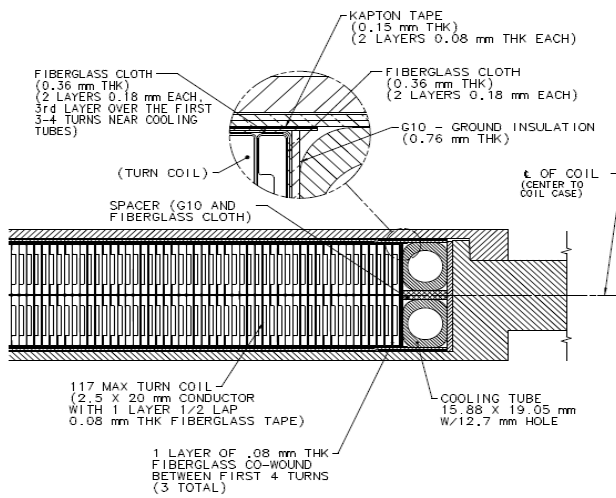


Figure 8: Partial construction detail for the torus coils, showing the conduction cooling mechanism and coil winding details. The coil cross section inside of the aluminum case is 353 x 45 mm.

TABLE VII
TORUS COIL ELECTRICAL INSULATION BREAKDOWN VOLTAGE

Material	E-Glass with Epoxy Thickness (mm)	G10 Thickness (mm)	Kapton Thickness (mm)
Insulation Region			
Turn-to-Turn Insulation (T-T)	0.3048	0	0
Turn-to-Turn Insulation (between pancakes)	0.3048	0.38	0
Turn-to-Ground (GND)	0.508	0	0.1524
Location	Turn-to-Turn	Pancake-Pancake	Turn-to-GND
Breakdown Voltage (kV) - calculated	7.01	15.75 kV	21.74 kV
Factor of safety	10 ¹	10 ¹	5 ¹

Breakdown voltage (kV) with safety factor used for design	0.7	1.58	4.35
Torus magnet 12 GeV (V) expected	< 10	< 120	< 250*

¹ Use safety factor of 5 where Kapton is used and 10 if no Kapton is used. [9]

* Rare hardware fault case resulting in approximately 500 V across the dump resistor

Electromagnetic and structural analyses of the coil pack and coil case assembly were carried out. The analyses focused on the cool down process, normal operation at full operating current (which also included gravity loads), as well as on conditions arising from coil misalignment, current imbalances, and quench events, to ensure that the aforementioned components were all within acceptable stress limits (see Table VIII) [8, 9-14].

TABLE VIII
TORUS STRESS SUMMARY

Component	Primary Limit (MPa)	Primary + Secondary Limit(MPa)	EM + Gravity [Primary] (MPa)		Cool down + EM [Primary + Secondary](MPa)	
			Peak	General	Peak	General
Case	184	552	350	70	380	300
Cover	184	552	130	45	430	350
Conductor	94	282	-	68	-	-181
Coil Pack Shear	15	45	5	13	40	20
Coil Pack Radial	94	282	-	-30	-	-120

Primary stresses were limited to the lesser of 2/3 times the yield strength or 1/3 times the ultimate tensile strength. Primary plus secondary stresses were limited to 3 times the primary stress allowable.

Torus Splice Design

The key drivers for the splice design were minimization of overall splice resistance, (which necessarily included contact resistance), and adequate quench protection. All conductors that are not within the main coil winding, (splices between the individual superconducting magnet coils, conductors between coils and current leads, and long runs of superconducting bus bar), have additional copper stabilizer to manage temperature rises during a quench event. The conductors that enter and exit the coil case also have stabilizer that runs to the outermost turn of each pancake. To design a “quench-tolerant” splice, the amount of copper has to be large enough to minimize peak temperatures during a quench event but also small enough to allow the development of a resistive voltage that can be detected and used to trip the fast dump interlocks to prevent the superconductor from burning out [15]. This “balancing act” is a critical part of the design of the quench protection system of any superconducting magnet. The Oxygen Free High Conductivity (OFHC) copper stabilizer bars extend over the entire splice length and are soldered to the assembly in the same operation that solders the splice.

To allow for a suitable design margin, the operating temperature of the splice has been assumed to be 5 K instead of 4.5 K. Using guidance from CERN, a joule heating limit (per splice) of 100 mW was selected, resulting in a maximum resistance of $7 \times 10^{-9} \Omega$ per splice [15]. This resistance corresponds to an operating current of 3770 A at 4.6 K with a background magnetic field in the region of 0.3 T, allowing for the magnetoresistance in copper. Splices are cooled via copper braids soldered to the helium re-cooler units located inside the upstream cold hex beams and they utilize a similar electrical insulation recipe to that used for the

coils. Space on the re-cooler units is limited and this constrained the allowable size of the splice design.

The key risk to the joint is the lack of even solder distribution and the inadvertent creation of voids within the solder and between the cables being joined. The cables are placed with the SSC cables facing each other and the keystone edges of the mating conductors lying on opposite sides of the joint to ensure a minimum gap between the cables. Several splice mock-ups were made and destructively tested to qualify the soldering fixture and fabrication procedure. A portion of the lip of the copper channel along the mating surfaces of the two conductors was removed to reduce the likelihood of void formation since the groove in the channel is deeper than the thickness of the Rutherford cable (see Fig. 9).

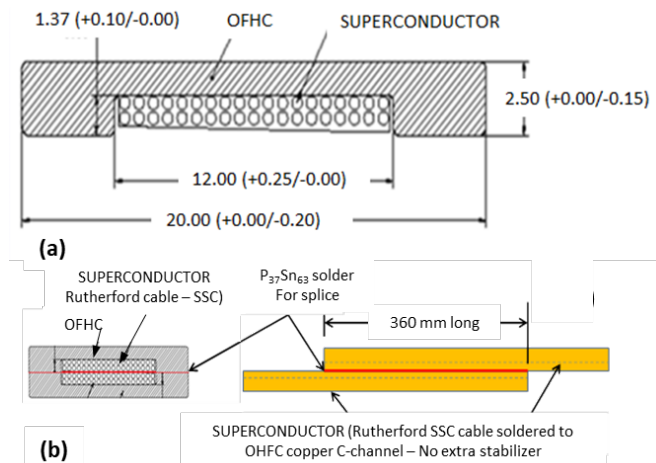


Figure 9: (a) Torus conductor - SSC outer cable soldered into a copper channel (dimensions in mm), (b) Typical layout of the test splice for joint resistance evaluation (without additional copper stabilizer).

$\text{Sn}_{60}\text{Pb}_{40}$ solder, having a liquidus of 188 °C to 190 °C, (and a melting point above 200 °C), was used to bond the Rutherford cable into the copper channel. Soft solder paste $\text{Sn}_{63}\text{Pb}_{37}$ (with a eutectic melting point of 183 °C) was used for the splice. Delamination of the Rutherford cable from the copper channel was avoided by careful control of the temperature during the soldering process using thermocouples for monitoring. The design of the soldering rig shown in Fig. 10 included open zones for direct viewing of the conductors during soldering, which allowed visual inspection of solder flow during the splicing operation.

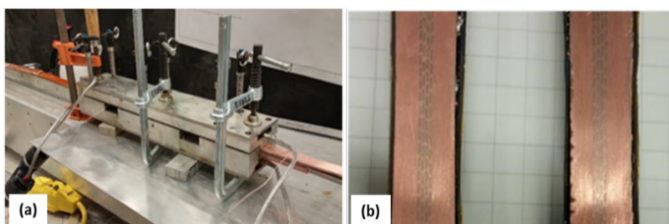


Figure 10: (a) Temperature-controlled aluminum block splicing rig. Cut-outs in the side of the rig allowed for visual inspection of solder flow, (b) Splice mock-up end-on view of the sectioned splice cut lengthwise showing void-free construction. NbTi strands and solder can be seen in the copper matrix. The outer-wrap is polyimide film and epoxy.

The splice insulation system is designed to accommodate a 2.5 kV standoff to ground (when cold) and incorporates polyimide film and a minimum tracking length of 1/2 inch. To improve thermal performance, physical gaps in the assembly were filled with two-part blue Styrofoam 2850 FT epoxy. The assembly was hi-pot tested (conductor-to-ground) only to 1 kV in air at atmospheric pressure to validate electrical isolation and integrity, as the full 2.5 kV standoff was designed to allow for any variation in the application of the insulation during the build of the magnet in the somewhat cramped conditions in the hall. This allows for a more than adequate safety margin.

Test splices with 360-mm-long soldered joints were prepared at JLab and critical current (I_c), n-value, and V-I data measurements were carried out at the University of Durham, UK up to 2000 A in one of two 15 T magnet systems (see Table IX). Due to a limitation of the measurement set up that could not accommodate the full length of the splice in the magnet, the resistance across the splice was also measured at a lower current and in an elevated magnetic field at LHe temperature. This additional measurement was carried out to allow characterization of similar splices for the Hall B solenoid magnet, that were likely to be located in higher fields of up to 4 T. Typical resistances measured for sample DR4686 are given in Table X.

TABLE IX
 CRITICAL CURRENT AND N-VALUE DATA FOR JLAB SPLICE SAMPLE# DR4562

Critical Current data			
E field criteria	10.5 T	10.0 T	9.5 T
100 $\mu\text{V}/\text{m}$	254 A	851 A	1708 A
10 $\mu\text{V}/\text{m}$	165 A	656 A	1415 A
n-Value			
10-100 $\mu\text{V}/\text{m}$	5	9	12

TABLE X
 RESISTANCE MEASURED FOR DR4686 AT VARYING MAGNETIC FIELD AT 4.2 K

Joint Length (mm)	Field at Field Centre (T)	Field at the top of the Joint (T)	Joint Resistance ($\times 10^9 \Omega$)
260	0	0	≤ 0.1
	0.5	0.13	0.70
	1	0.25	0.66
	2	0.50	0.68
	3	0.75	0.68
	4	1	0.7

The resistance of the splices measured at elevated magnetic fields was less than 1 nΩ in LHe (4.2 K), the maximum allowed design value was 7.0 nΩ. This splice design and associated insulation system, proven for the torus magnet, was shared with the vendor for the solenoid magnet who implemented a very similar system.

Torus Quench Protection Design

The torus magnet is protected via an externally located dump resistor that is permanently connected across the magnet terminals. This resistor has a center tap that then feeds a ground-fault indicator (see Fig. 12). Quench detection is via voltage taps located on either side of the splices between coils, thus allowing voltage detection across individual coils, splices, and long runs of bus bar.

At the operating current of 3770 A and with a total inductance of about 2 H, the torus magnet has a stored energy of 14.2 MJ. With

the $0.124\ \Omega$ dump resistor in circuit, any current decay under non-quench conditions will have a time constant of 16.7 s , with the magnet therefore running down to almost zero amps in about 5 time constants or 83.5 s . It should be noted that even during a “normal” fast discharge of current into the dump resistor (for example an interlock activating due a non-quench event) sufficient eddy current heating can be produced, which in turn would initiate a quench-back event that could then initiate a quench in one or all of the coils. During the quench event nonlinear superconductor normal zone growth and induced eddy currents in the aluminum cases and shields will decrease the effective discharge time due to the increase in effective resistance in the overall magnet circuit.

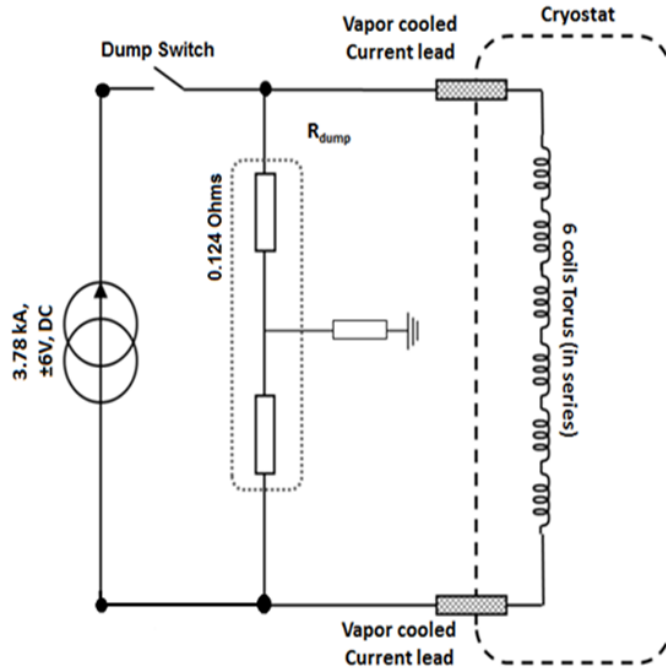


Figure 12: Torus magnet protection circuit.

Reference should also be made to Table IV for the conductor specification.

TABLE XI
 BRIEF SUMMARY OF CALCULATED CRITICAL PARAMETERS
 (TORUS)

Parameter (calculated)	COIL
Operating temperature, Θ_0 (K)	4.90
Current sharing temperature (K)	7.46
Temperature margin (K)	2.16
Short sample performance (%) at Θ_0	27.1
MQE (mJ)	49
Conductor length used for quench calculation (m)	2200 (per coil)
¹ Hot spot temp. (K) / Time to reach the corresponding hot spot temperature (s)	52 K / 60.68 s
Max. voltage, Line-to-Ground (kV)	> 2.5
Max. MIITs at 150 K ($10^6\text{A}^2\text{s}$)	149.6
Dump resistor, R_D (Ω)	0.124
² Maximum voltage across the R_D (V)	467

MIITs estimated with dump resistor ($10^6\text{A}^2\text{s}$)	77.2
Normal magnet time constant (τ), s	16.1
¹ All energy dumped in one coil (adiabatic condition)	
² Maximum voltage across the R_D for the worst case scenario = approximately 500 V as designed (with center tap present, dump resistor voltage = 250 V)	

Design and Selection of a Dump Resistor (R_D) for the Torus

An equivalent single-coil Wilson model [16] is used for quench analysis. The stored energy of the torus magnet is $\sim 14\text{ MJ}$ and is to be extracted via an external dump resistor to limit the maximum voltage to no higher than approximately 500 V in the event of a fast discharge or a quench.

1. The maximum design voltage limit of approximately 500 V was determined iteratively, via analysis of peak temperatures and voltages, as well as by including consideration of the hardware-related fault scenario with the center-tapped dump resistor, and necessitated the use of a $124\text{ m}\Omega$ external dump resistor.
2. The magnet time constant was calculated to be: $(L_{\text{Magnet}} = 2.0\text{ H})$, $\tau = L_{\text{Magnet}}/R_D = 2.0\text{ H}/0.124\ \Omega = 16.13\text{ s}$.
3. Table XI summarizes the critical parameters calculated for the magnet coil with a maximum hot spot temperature limited to no higher than 150 K. The adiabatic quench integral (also referred to as MIITs)
 - a. Maximum MIITs calculated, $MIIT_{S_{\text{max}}} = 149.6\text{ MA}^2\text{s}$
 - b. MIITs with R_D , $MIIT_{S_{\text{dump}}} = 77.2\text{ MA}^2\text{s}$
 - c. MIITs without R_D , $MIIT_{S_{\text{no-dump}}} = 236.8\text{ MA}^2\text{s}$

Note:

MIITs calculated with and without R_D are based on the energy extracted and on the time constant. The assumption and calculations are:

- a. The resistance of each coil (each CCM) above quench temperature is assumed to be, $r_{\text{coil}} = 10\text{ m}\Omega$;
- b. To keep the peak temperature to below 150 K, the decay time must be shorter than 10.53 s.

The time constant with dump resistor during discharge, $\tau_{R_D} = L_{\text{Magnet}}/(R_D + r_{\text{coil}} * 6) = 10.87\text{ s}$

MIITs with R_D , $(1/2)*(I_{\text{op}}^2/10^6)*[L_{\text{Magnet}}/(R_D + r_{\text{coil}} * 6)] = 77.2\text{ MA}^2\text{s}$

The time constant without dump resistor during discharge, $\tau_{\text{no}_R_D} = L_{\text{Magnet}}/r_{\text{coil}} * 6 = 33.33\text{ s}$

MIITs without R_D , $(1/2)*(I_{\text{op}}^2/10^6)*[L_{\text{Magnet}}/r_{\text{coil}} * 6] = 236.8\text{ MA}^2\text{s}$

The worst-case scenario was determined to be a single coil quenching and dissipating the entire magnet’s energy internally to that coil. The peak hot spot temperature for this scenario is estimated to be between 60 K and 75 K for that coil alone. Note that this calculation does not allow for the thermal capacity of the aluminum coil case, thereby allowing for an additional safety margin for the predicted coil temperature rise. In the case of a single double-pancake quench, all the other coils are driven normal by eddy currents generated within the superconducting strands and the copper cooling sheets, as the current decays

through the external protection dump resistor, once the dump switch opens to isolate the power supply from the magnet. This “quench-back” effect occurs within about 0.3 s [17] of the dump switch opening. All other coil failure modes see lower temperature excursions than that experienced for the single coil quench case.

The 0.124Ω dump resistor extracts $>50\%$ of the stored energy with a maximum terminal voltage <500 V (± 250 V with the dump resistor having a center tap configuration). The current decay, in the event of a quench or a fast dump, is enhanced by the growing normal zone that increases the coil resistance. The growth in coil resistance for this analysis assumes two values, 0.04 and $0.01 \Omega/\text{s}$; estimated to be the fastest and slowest resistance growth rates, respectively. This suggests that the energy extracted via the dump resistor will be between 43% and 63% of the total stored energy.

Quench Integral: The adiabatic quench integral or quench load, (also sometimes referred to as MIITs), is evaluated based on the Wilson Model [16] as indicated below for a worst-case scenario in the event of a quench, for the total decay time, 10.53 s in order to limit the maximum temperature to 150 K. The MIITs calculation uses only the material properties of the conductor to evaluate the time required to reach a certain temperature (we have selected 150 K for our case).

$$\int J(t)^2 dt = \int_{4.9K}^{T_m} \frac{\gamma \cdot C(T_{cond})}{\rho(T_{cond})} dT_{cond}$$

$J(t)$ = Current density (in copper only), T_m = maximum temperature, γ = Density of copper, C = specific heat capacity of copper, ρ = electrical resistivity of copper, T_{cond} = temperature of conductor, t = total time to reach T_m .

The required magnet protection is evaluated based on the assumption that the quench would start at one point and that point continuously increases in temperature under adiabatic conditions as the quench event progresses. MIITs is evaluated both with a dump resistor and without a dump resistor. The system heat loads were estimated using a Detailed Predictive Model (DPM) based on the Wilson model that assumes a fast dump releasing all the magnet stored energy. The DPM predicts that the torus is safe to operate for all energization states and fault scenarios up to the nominal operating current of 3770A. The analysis clearly indicated that an external dump resistor was necessary in order to limit the hot spot temperature to no more than 150 K, considering the required quench detection and electronics response times.

Characteristic parameters like Minimum Quench Energy (MQE) and Length of Minimum Propagation Zone (MPZ) have been calculated to guide the design of the splices, coil interconnects, and bus bars and to confirm overall magnet stability.

Design and Selection of Copper (Thermal) stabilizer – Splice and Coil Interconnects

The use of the FMEA process provided guidance on mitigating the lack of quench stability, for quenches initiating from the sections identified below.

1. Section of lead stabilizer – Lead exit starting from within the CCM up to the splice between coils

2. Splice stabilizer - for the actual joint between two coils
3. Splice within the Chimney
4. Splice inside the service tower – between start and end coil leads and the vapor-cooled current leads

The coil interconnects, lead exits, and any splices that do not have enough thermal capacity are likely to overheat and burn out during a quench event. Therefore, the design of these sections is critical for safe magnet operation. In order to achieve stable operating conditions, (as represented in the flow chart of Fig. 12), the following were considered during the design stage to make these critical elements as ‘quench tolerant’ as possible without compromising quench detection limits.

1. Thermal stability of each element - not to exceed the MIITs value.
2. MQE of each element $>$ MQE Magnet
3. Minimize the time to propagate the quench into the CCM (which has a larger thermal mass). The CCM thus acts as an “amplifier” and propagates the quench at a faster rate.
4. Quench detection voltage - a threshold minimum of 100 mV was selected.

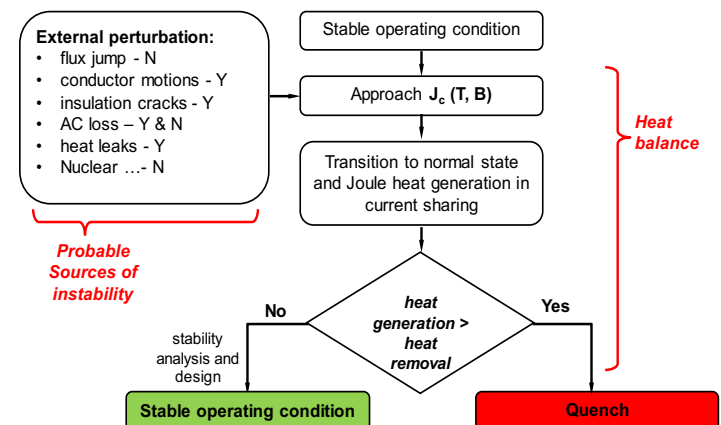


Figure 12: Flow chart representing the design evaluation for stable operation of a superconducting magnet.

The following scenarios were identified for magnet safety at the full operating current of 3770 A:

1. Coil, bus, lead, splice, and symmetric quench;
2. Detection time, based on MIITs (limited to a max. temperature of 150 K) with detection voltage threshold set to 100 mV.

Magnet Lead Between CCM to Inter-Coil Splice: Based on a MIITs evaluation and the plot shown in Fig. 13, the cross section of additional copper that needs to be added to the conductor is 70 mm^2 . With this additional copper added to a 1.0 m long conductor, the characteristic parameters are calculated to be:

- i. Quench velocity ($V_{Q_lead-coil}$) = 0.93 m/s
- ii. Time to reach coil ($t_{Q_lead-coil}$) = 1.08 s
- iii. Hot spot temperature rise during time for the normal zone to reach coil, $t_{Q_lead-coil}$ ($T_{Q_lead-coil}$) = 16 K
- iv. Voltage across lead ($V_{Q_lead-coil}$) = 6 mV (cannot be detected)

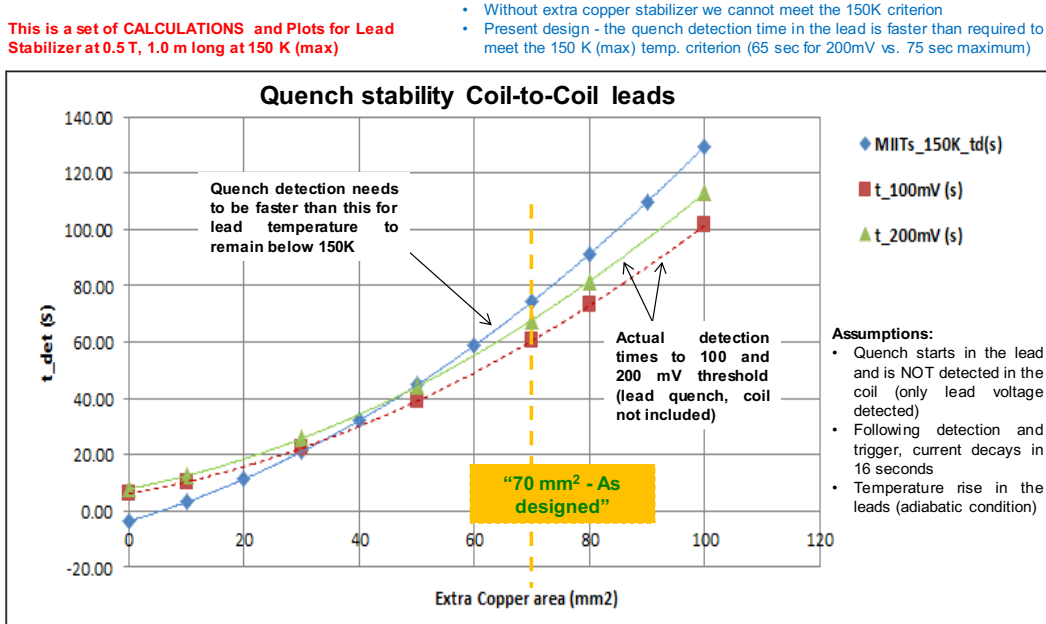


Figure 13: MIITs plot showing the variation of detection time with the additional copper applied to the conductor lead/bus bar (limited to a maximum hot spot temperature of 150 K).

Splice (mounted on top of the 4 K re-cooler): Based on a MIITs evaluation and the plot shown in Fig. 14, the cross section of additional copper that needs to be added to the conductor on either side of the splice is 50 mm², i.e. the total additional copper applied to a 350 mm long splice is 100 mm². The characteristic parameters are calculated to be:

- Quench velocity ($v_{Q_splice-lead}$) = 1.1 m/s;
- Time to reach splice end ($t_{Q_splice-lead}$) = 0.315 s;
- Hot spot temperature rise during the time for the normal zone to reach the splice end, $t_{Q_splice-lead}$ ($T_{Q_splice-lead}$) = 14 K;
- Voltage across lead ($V_{Q_splice-lead}$) = 4.5 mV (*cannot be detected*).

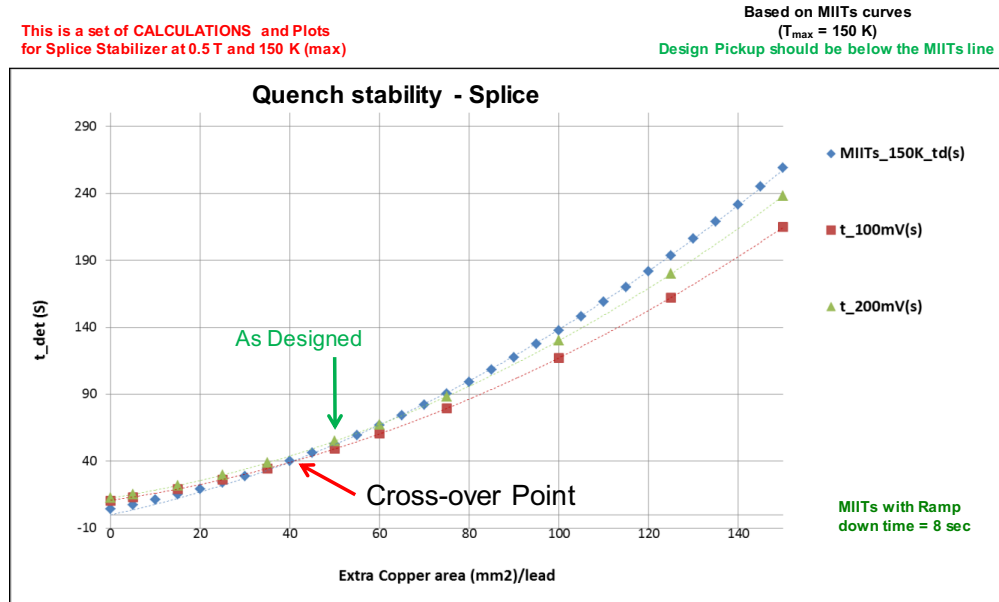


Figure 14: MIITs plot showing the variation of detection time with the additional copper in the splice (limited to a maximum hot spot temperature of 150 K).

Coil Quench (Field in the coil near the lead exit area, $B = 2.0$ T, $T_{OP} = 5.3$ K): Using the Wilson Model for quench analysis, and setting the quench detection threshold at two different levels – (a)

- 100 mV and (b) 200 mV, the times to quench the whole single coil (*length of conductor in each CCM is 2000 m*) are:
- Time to reach 100 mV (threshold) before detection (t_{coil_100mV}) = 825 ms;

- ii. Time to reach 200 mV (threshold) before detection (t_{coil_200mV}) = 1650 ms;
- iii. Hot spot temperature rise in the coil during the time to reach the 100 mV threshold, t_{coil_100mV} (T_{coil_100mV}) = 11.03 K;
- iv. Hot spot temperature in the coil during the time to reach the 200 mV threshold, t_{coil_200mV} (T_{coil_200mV}) = 14.60 K.

Therefore, considering the worst-case scenario with a quench initiating in the splice and not being detected, the quench will in fact propagate to the coil, which then actually “amplifies” the quench by rapidly propagating the normal zone within the coil

pack itself. Therefore, the time expected for detection of a quench for this worst-case scenario, with 100 mV and 200 mV detection thresholds are:

- i. Total detection time for 100 mV threshold (t_{det_100mV}) = $(1.08 + 0.315 + 0.825)$ s = 2.220 s;
- ii. Total detection time for 200 mV threshold (t_{det_200mV}) = $(1.08 + 0.315 + 1.65)$ s = 3.05 s.

The summary of the quench characteristic parameters for the locations identified are shown in Table XII.

TABLE XII
 BRIEF SUMMARY OF CALCULATED QUENCH CHARACTERISTIC PARAMETERS AT VARIOUS LOCATIONS

Description/Parameter Location	Magnet Coil	Splice on Re-cooler section (Joule heating)	Chimney splice, incl. Joule heating + secondary heating (Thermal) ²	Coil-to-coil Lead (no extra stabilizer)	Coil-to-coil Lead (with extra stabilizer as designed)	Torus-to-service tower bus bar (no extra stabilizer)	Torus-to-service tower bus bar (with extra stabilizer as designed)
Field (T)	3.58	0.2	0.2	0.5	0.5	0.20	0.2
Operating Current, I_{op} (A)	3770	3770	3770	3770	3770	3770	3770
Operating Temperature (K)	4.9	4.5/5.25	4.7/6.05	5.1	5.1	4.5	4.5
I _c (A)	13920	96630	77890	56890	56890	112900	112900
I _{op} /I _c	0.27	0.04	0.05	0.07	0.07	0.033	0.033
Additional copper (mm²)	-	100	140	0	70	0	40
Temp. margin (K)	2.16	3.86	3.07	3.78	3.78	4.61	4.612
MPZ (mm)	34.9	180	205	63	197	72	160
Adiabatic quench velocity (m/s)	2.82	1.03	0.95	2.66	0.93	2.33	1.126
MQE (mJ)	49	342	421	47	398	63	277
Length of Splice/Bus (mm)	-	350	350	1000	1000	8000	8000
Time to 100 mV (s)*/Temp (K)	<0.40/9	0.324 ¹	0.368 ¹	0.38 ¹	1.08 ¹	0.008/10	7.5/32
Time to 200 mV (s)*/ Temp (K)	<0.78/11	-	-	-	-	2.14/33	16.48/4
Quench protection current decay time (s)	10.4	247	367	12	90	12.6	49
Adiabatic hot spot temperature (K)	52	14	13	21	16	3.43 s / 39 K	7.1 s/32 K
MIITs (150K)	150	3516	5227	176	1284	179	697

*Temperature assumed ~10 K (Change in copper resistivity is negligible <25 K)

¹Time to reach one end of the splice

²Conduction and radiation thermal loads

Resistance of splice analyzed for 10 nΩ

1. Rutherford Cable coupling loss (parallel field), E _{pl_coup} (J)	220.6
2. Eddy current losses, E _{eddy} (J)	31.3
3. Hysteresis losses, E _{Hys} (J)	1246
4. Penetration Losses, E _P (J)	66.6
5. Self-Field Losses, E _{sf} (J)	82.8

Hi-Pot Test and Leakage Current Test

The instantaneous maximum voltage in the event of a quench across the dump resistor is about 467 V. An analytical model [16], [18] was used to calculate the maximum internal coil voltage of 110 V. The worst-case scenario with maximum voltage to ground could be, $V_{Max_L-G} = (467+110) = 577$ V. Therefore, additional ground (GND) plane insulation in vacuum, was employed at specific locations (e.g. coil, connectors, lead exit, and MPS). All voltage tests were carried out at 1 kV. Voltage tests between coil-to-GND, Line-to-GND, pin-pin (in the vacuum feedthroughs for

Parameters	Torus Magnet
Field (T)	3.58
Operating Current, I _{op} (A)	3770
Operating Temperature (K)	4.9
Charging time, τ_{ch} (s)	3600
RRR [-]	100
Inductance, L _{mag} (H)	2.0
Stored Energy (MJ)	14.2
Total AC Loss E_{TOTAL} (J)	1647

voltage taps), and pin-GND were carried out at every stage of the magnet assembly. Once the magnet was connected to the magnet power supply, the maximum hi-pot voltage was limited to 500 V. Leakage current values were also monitored during the hi-pot tests to confirm that tracking distances to ground were adequate.

Various quench scenarios derived from the FMEA process [8] were analyzed utilizing the Vector Fields (Cobham) quench codes that incorporate the ELEKTRA 3D (transient analysis) and TEMPO 3D (thermal analysis) software modules [19], as well as a JLab-developed Mathcad tool that also calculated inter-filament coupling losses. The analyses involved the examination of eddy currents generated during a quench event within the coils themselves, as well as in any nearby electrically conductive components such as the aluminum coil cases and aluminum thermal shields, and any subsequent forces produced by these eddy currents (see Fig. 15). These generated eddy currents, in particular the inter-filament coupling losses, can produce a phenomenon known as “quench-back” – i.e. the eddy currents produce a heating effect that then reflects back into the superconducting coils, thus speeding up the quenching of the coils – in effect providing a secondary form of quench protection.

Quenches normally start from the peak magnetic field region within a coil, (which is the inner bore coil surface for the torus), and then propagate through the coil to the outer radius, causing the current in the series-connected coils to decay very rapidly. This rapid current decay in turn induces large eddy currents and therefore large forces in the aluminum coil cases and thermal shields. Initial analysis suggested that the forces on the thermal shield would cause excessive deflection and permanent bending of the shield. Multiple iterations of segmentation were analyzed to reduce the eddy currents developed during a quench. Figure 9a shows the final segmentation employed for the shield and Fig. 9b shows the total force on the shield. The segmentation reduced the force by a factor of more than 5 [20].

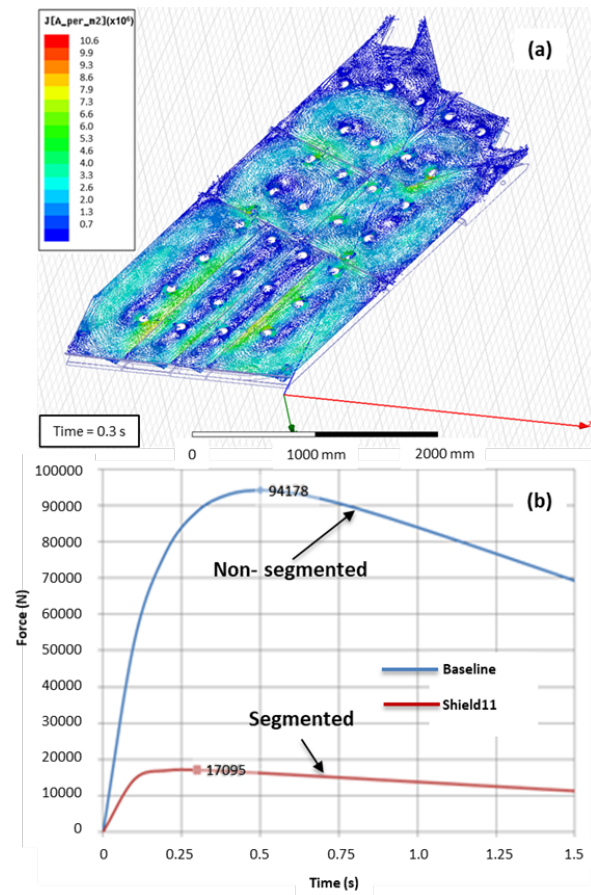


Figure 15: Torus segmented thermal shield performance during quench event – (a) current density vector plot, (b) Total force vs. time during a fast dump. The force reduction in segmented shield is about 1/5th that of a non-segmented shield design.

Based on the quench and normal operation scenario analysis, the observed results and mitigating actions are summarized in Table XIV [9, 20].

TABLE XIV
 TORUS - ANALYZED QUENCH AND NORMAL OPERATING SCENARIOS

	Quench Scenario	Results from Analysis	Mitigation
1	Normal magnet current decay from 3770 A with dump resistor connected across magnet terminals	The magnet system’s “normal” decay via the dump resistor (i.e. without a quench) will initiate a “quench back” after about 0.3 s, which will then cause all the coils to quench. The thermal shield can experience high forces due to the induced eddy currents during a quench.	This has been mitigated at the design stage by slotting or segmenting the shield in multiple locations and using a combination of two different grades of aluminum in its construction – one to preserve mechanical strength and the other to improve thermal conductivity. Bumpers between the shield and the coil case and vacuum jacket have also been incorporated in the design. The segmentation of the shields reduces the current density from 9.5×10^6 to 2.5×10^6 A/m ² ; with a corresponding reduction of out-of-plane forces from 94 kN to 17 kN.
2	One coil quench from 3770 A with full stored energy being dissipated amongst all 6 coils	Coil peak hot spot temperature = 53 K	None necessary as typical conservative design guidelines limit this peak hot spot temperature to no higher than 150 K

3	One coil quench from 3770 A with full stored energy being dissipated in only one coil	Coil peak hot spot temperature = 75 K	None necessary as typical conservative design guidelines limit this peak hot spot temperature to no higher than 150 K
4	A short in one coil that then causes the coil to quench (includes thermal stresses from cooling (395 K to 4 K), Lorentz forces due to a quench resulting from a single coil to ground short, and 110% gravity loading	A single coil short followed by a quench will disrupt the symmetry of the magnetic field, which can result in out-of-balance forces between the coils. The out of plane load generated by this load case is ~129 kN.	Damage to the cold mass that potentially could be caused by these non-symmetric forces has been mitigated by incorporating “coil case-vacuum vessel” bumpers. The vacuum vessel has also been designed to be capable of withstanding these forces.
5	Cool down stresses from 395 K to 4 K (includes stresses due to epoxy curing at 122°C)	The results from this analysis suggest that the coils are preloaded (compression) at room temperature. All stresses due to cool down are secondary stresses (self-limiting). Refer to Table IX.	
6	Normal operation (includes cool down stresses from 395 K to 4 K, Lorentz forces due to energization and 110% static gravity loading to allow for earthquake loads) - assumes perfect coil symmetry with no out of plane forces due to electromagnetic loads	The stresses from this load case are both primary (EM and gravity) and secondary (cool down). Refer to Table VIII.	
7	Current imbalance (includes thermal stresses from cooling (395 K to 4 K), Lorentz forces due to a current imbalance condition, and 110% gravity loading)- the current imbalance includes Lorentz forces from a 10% reduction of current (equivalent to losing ~12 turns in each pancake) in a single coil	This current imbalance generates a ~70 kN out of plane force on the coil. This analysis is also used to verify stresses due to out-of-plane EM forces resulting from imperfect coil locations. The maximum out-of-plane force due to imperfect coil locations is ~7 kN.	

0

SOLENOID

Solenoid Magnet Design

The solenoid is an actively shielded 5 T magnet designed and built by the Tesla Ltd. Group of companies. The magnet was designed by Tesla Engineering Ltd. (TEL), Storrington, U.K. and built by Everson Tesla Inc. (ETI) Pennsylvania, USA. The solenoid magnet has five coils in series (also wound with copper-stabilized NbTi Rutherford cable but with a slightly narrower copper channel, 17 mm instead of 20 mm as for the torus). The two main inner coils (Coils 1 and 2) are shrunk-fit inside a thick-walled stainless-steel bobbin, another two intermediate coils (Coils 3 and 4) are wound into separate pockets milled into the outer surface of the same bobbin and one long thin shield coil (see Fig. 16). The shield coil is wound onto its own bobbin but electrically connected in reverse to the other four coils as an “active shield” to limit the extent of the magnet’s stray field. This is important as there are many detectors mounted in close proximity to the solenoid that are sensitive to magnetic fields (see Fig. 17). Using two split-pair coils and one solenoidal coil allowed the required field strength and homogeneity to be obtained in a compact magnet volume that also satisfied the placement and location of the various physics detector packages [21].

All coils are supported via 8 radial and 8 axial supports and are conduction-cooled via copper cooling strips, which are potted with the coils and connected to a centrally located annular helium cooling channel. The magnet is cooled by a helium thermo-siphon connected to the magnet reservoir. Gas generated by the magnet is used to cool the thermal shield and also the magnet’s vapor-cooled current leads before being exhausted via the Solenoid Service Tower (SST).

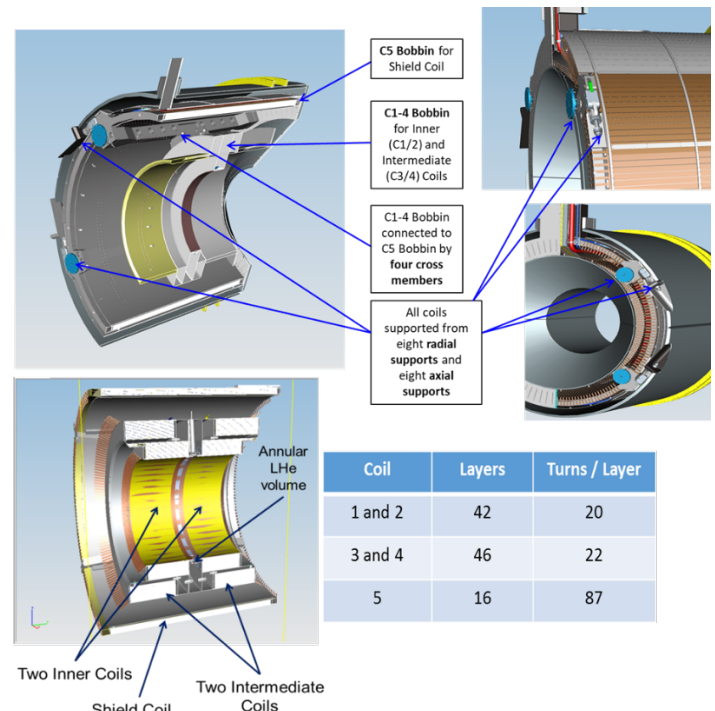


Figure 16: Cross-sectional views of the internal construction of the solenoid together with the coil winding details.

Coils “sticking and slipping” against their formers during current ramp-up, can cause spurious quenching, and necessitated the incorporation of slip planes consisting of Kapton and Mylar sheets placed between Coils 3, 4, and 5 and their respective bobbins to mitigate this problem. Forces and stresses encountered within the thermal radiation shield during quench events have been mitigated by slotting the shield. Temperature margins for each coil were quantified and resulted in improvements to the design and operation of the overall cryogenic cooling scheme.

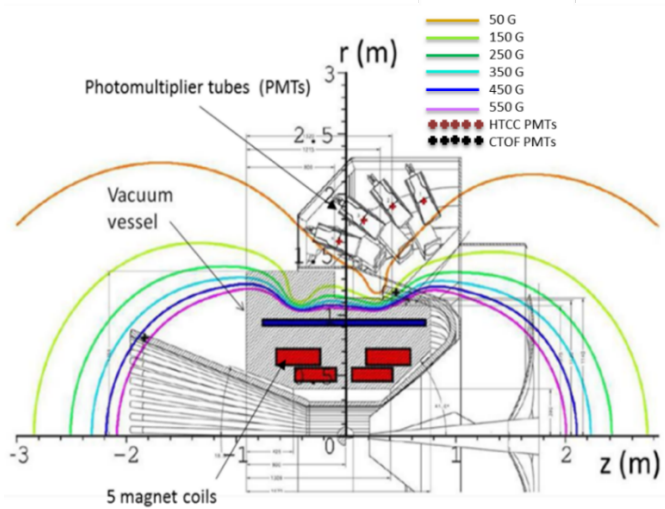


Figure 17: Cross-sectional view through the side of the solenoid showing the location of nearby PMTs and the stray field lines.

Coil manufacturing variations can degrade the magnetic field homogeneity from its required value of < 100 ppm (peak-to-peak) within a cylindrical volume of 25 mm diameter × 40 mm length located at the geometric center of the magnet. This homogeneous

magnetic field region will be required for polarized target experiments in the near future and a solution being developed is to incorporate small superconducting shims (Z1, Z2, X, and Y) on the 1 K shield that surrounds the target within the bore of the magnet. To quantify manufacturing variations for the solenoid coils and to check on the effectiveness of the winding and epoxy impregnation processes, a half-size practice coil was successfully wound, potted, and dissected.

Electromagnetic and cryogenic interactions exist between the torus and the solenoid magnet systems and had to be considered during the design stage.

Solenoid Superconducting Coil Design

The initial design of the coils indicated that the innermost Coils 1 and 2 had the smallest temperature margin (1.117 K), whereas design guidelines suggest at least 1.5 K for better stability (see Fig. 18 and Table XV). As a result, JLab made plans to enable operation of the magnet at sub-atmospheric pressures in order to obtain additional temperature margin and the complete magnet system was designed for this lower operating pressure. As it turned out, in practice the cooling of the coils was predicted properly and there were no unaccounted for heat loads, thus the sub-atmospheric mode of operation was not needed.

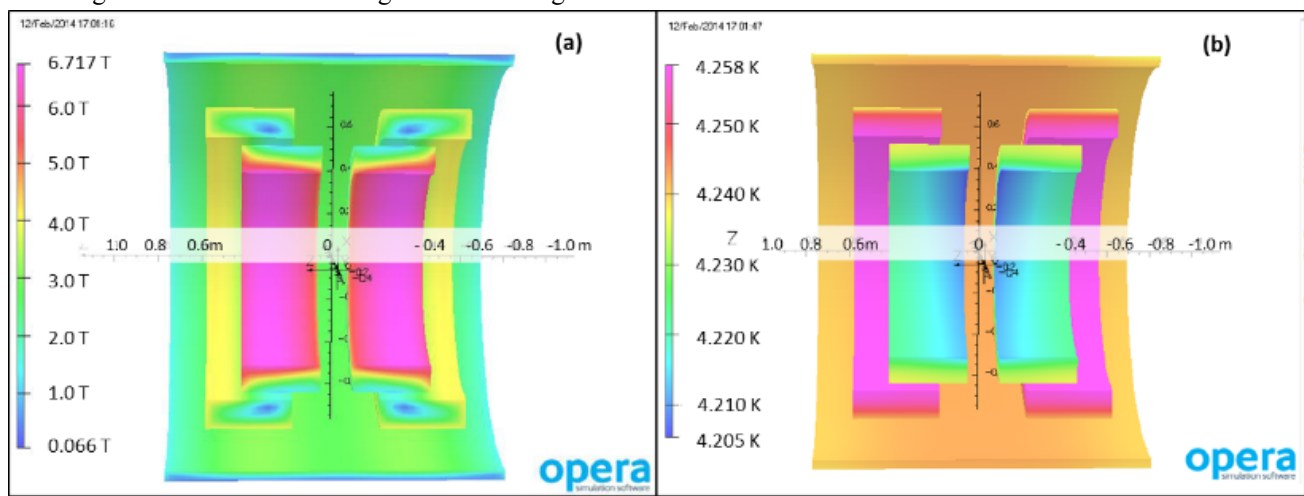


Figure 18: (a) Magnetic field distribution on the solenoid coil surfaces, (b) Temperature distribution in the coils at end of ramp up to full field. whole magnet and is used in conjunction with a dump switch. The dump resistor used for the solenoid is sized at 0.2Ω .

TABLE XV
SOLENOID – FIELD AND TEMPERATURE MARGINS FOR COILS

JLAB Thermal report							
Coil Number	T _{coil} (K)	B _{max} (T)	I _c (A)	SSP (%)	T _c (K)	T _{cs} (K)	ΔT (K)
1 and 2	4.68	6.56	6548	36.90	6.451	5.797	1.117
3 and 4	4.81	4.21	11022	21.92	7.578	6.971	2.161
5	5.62	3.05	10202	23.68	8.093	7.507	1.887

T_{coil}= Coil temperature, B_{max}= Maximum field in the coil, I_c= Critical current at B_{max} and T_{coil}, SSP= Short sample percentage, T_c= Critical temperature at B_{max}, T_{cs}= Current sharing temperature, ΔT= Temperature margin

Figure 19 illustrates the general protection scheme for the solenoid that was used as the basis for the quench and fault scenarios analyzed. As for the torus magnet, an external dump protection resistor (with a center tap) is connected across the

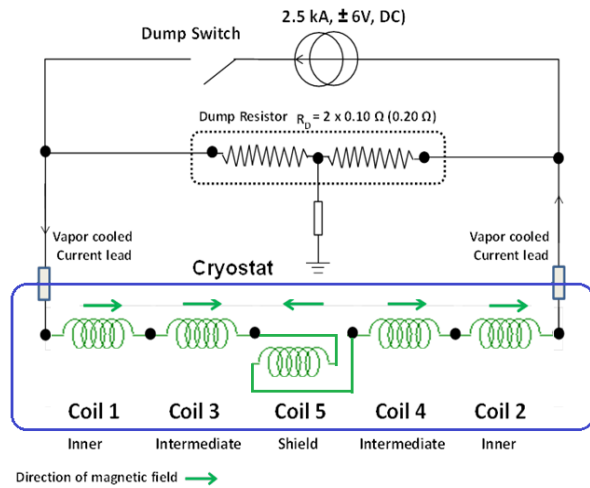


Figure 19: Solenoid magnet protection circuit.

Table XVI summarizes all of the analyzed quench and normal operating scenarios, together with observed results and any appropriate mitigation. Worst case peak coil temperatures did not exceed 108 K, while peak voltages across the coils did not exceed 156 V. High forces were predicted for the Al-1100 thermal shield during a fast discharge of the magnet and this was mitigated by slotting the shield. The studies also suggested that excessive training of the shield coil might be expected due to the potted conductor and resin being in tension; this was mitigated by the use of slip-planes between the coil and its bobbin.

TABLE XVI
SOLENOID - ANALYZED QUENCH AND NORMAL OPERATING SCENARIOS

	Quench Scenario	Results from Analysis	Mitigation
1	Quench initiating in C1, assuming presence of AC losses and electromagnetic coupling between coils	Peak temperature = 91 K, Peak voltage across coil = 102 V	No special mitigation was necessary as the coils are self-protecting and the coils are insulated for 1000 V to Ground.
2	Quench initiating in C3, assuming presence of AC losses and electromagnetic coupling between coils	Peak temperature = 87 K, Peak voltage across coil = 108 V	
3	Quench initiating in C5, assuming presence of AC losses and electromagnetic coupling between coils	Peak temperature = 79 K, Peak voltage across coil = 156 V	
4	Quench initiating in C1, assuming all the stored energy is dissipated in only one coil – i.e. no electromagnetic coupling with other coils	Peak temperature = 108 K, Peak voltage across coil = 96 V	
5	Quench initiating in C3, assuming all the stored energy is dissipated in only one coil – i.e. no electromagnetic coupling with other coils	Peak temperature = 99 K, Peak voltage across coil = 101 V	
6	Quench initiating in C5, assuming all the stored energy is dissipated in only one coil – i.e. no electromagnetic coupling with other coils	Peak temperature = 99 K, Peak voltage across coil = 156 V	
7	Quench initiation in C5 with all coil leads and splices between coils included	Peak temperature = 41 K	
8	Quench initiation in a coil splice	Peak temperature = 42 K	
9	Eddy current effects in the thermal shield due to a fast discharge of the magnet, the fastest rate being about 281 A/s	High forces experienced by the Al-1100 thermal shield.	The shield was designed with multiple slots, which significantly reduced eddy current formation and thus forces.
10	Training of the solenoid coils to full field	Preliminary analysis of the shield coil indicated that the potted conductor and epoxy were in tension and that this could potentially be a cause for multiple training steps to full field.	The shield coils (as well as Coils 3 and 4) were manufactured with slip planes between the coils and their formers (bobbins). Coil 5 (the shield coil) was also over-bound with multiple layers of glass cloth during the manufacturing process. As a result, there was minimal training of these coils to full field during

		commissioning. There were a total of 5 training quenches (C3: 937 A, C4:1014 A, C4:1035 A, C3:1059 A and C3:1066 A)
--	--	---

Additional analyses included assessment of forces on the coils due to the proximity of ferromagnetic components – for example the structural space-frame within the hall, the walkway that spans the left and right halves of the space-frame, and the Central Time-of-Flight (CTOF) detector [3] located close to the bore of the magnet with its multiple iron-shielded photomultiplier tubes. Eddy current analyses were also performed to verify and mitigate forces on electrically conductive components located within the bore of the solenoid – for example the copper heat exchanger for the Silicon Vertex Tracker (SVT) [22]. The results from the analyses were used to either confirm that there was minimal or no risk of damage to the magnet or the components in question, or to facilitate a re-design of the components to reduce the risk of damage. The CTOF shields exert a net force of about 5 kN. The magnet vendor (ETI) was provided with the detail of the CTOF shields and designed the z -restraints for a 4.9 kN force. The Central Neutron Detector (CND) shields exert a net force of about 400 N [23]. The other components are the steel hall space-frame structure (which provides staff with multi-level access within the hall to the magnets and electronics) and the stainless steel and aluminum mounting tube for the SVT and the Micromegas Vertex Tracker (MVT) [24]. The forces on the coils due to the hall structure depend on the magnet position; in the normal operational position the coil forces are about 500 N. Most of the material in the MVT and SVT inserts is non-magnetic. To counteract the 4.9 kN force from the CTOF detector shielding, an iron compensating ring was installed on the downstream end of the solenoid – bolted to the vacuum jacket's end closure plate. This compensating ring reduces the forces on the coils from the CTOF detector by about 3.6 kN. The total forces on the coils in the presence of all the components are summarized in Table XVII, indicating a resultant axial force on the coils (in the beamline direction) of about 2.4 kN with the compensating ring installed.

TABLE XVII

SOLENOID – FORCES ON COILS DUE TO PROXIMITY OF FERROMAGNETIC OBJECTS

Components close to the Solenoid Magnet	Fz (N)
Torus magnet	0
CTOF	4884
CTOF + compensating ring	1239
CND	414
HTCC	-35
Hall structure	499
SVT mounting tube (stainless steel)	196
SVT mounting tube (aluminum) during quench	22
SVT region 4 mounting tube (aluminum) during quench	76
Total without compensating ring	6056
Total with compensating ring	2411

Solenoid and Torus Interactions

A fast dump of the torus produces a voltage rise across the shield coil of the solenoid that can trigger the solenoid's quench protection system, thus causing the solenoid to undergo a fast dump itself. While the electromagnetic analysis predicts the sum of the overall forces on each torus coil to be zero, locally the load cells of the out-of-plane supports (OOPS) of the torus coils do experience a force. These OOPS, which are located in the center of the race track coil, show large changes in force when the torus is at field and the solenoid is energized. Electromagnetic analysis shows that the OOPS near the upstream leg of the torus coil will see a force change in the opposite direction of the one near the downstream leg. The OOPS are instrumented to read up to 8.9 kN of force, their failure load is 44.5 kN. Load changes of up to 4 kN were recorded. These changes in load are repeatable and nicely match those predicted by the analysis in magnitude and direction. All the OOPS are operating well below the maximum read-back value.

Table XVIII summarizes the level of electromagnetic interaction [25] between the solenoid and the torus under both normal and fault conditions; the analysis indicated that all force levels were well below coil buckling limits and therefore no specific design-related mitigation actions were necessary.

TABLE XVIII

SOLENOID + TORUS - ANALYZED INTERACTION SCENARIOS

Scenario	Results from Analysis	Mitigation
Torus-solenoid electromagnetic interactions. The following scenarios were analyzed: <ul style="list-style-type: none"> ▪ Solenoid alone under normal operating conditions; ▪ Solenoid and torus under normal operating conditions; ▪ Solenoid under fault conditions; ▪ Solenoid under fault conditions with various operating conditions of the torus. 	<ul style="list-style-type: none"> i. The long straight sections of the torus coils experience a force in the presence of the solenoid coils. The force on the straight coil sections closer to the solenoid is almost 3 times the forces on the far straight sections and varies from 1 kN to 6 kN. This force is balanced by other coils (so the net force is zero). These forces are in the x and y directions, there is no axial force on the torus coils. The forces and the x and y directions explain the slight buckling of the torus coils. The direction of the buckling depends on the relative directions of currents in both the magnets. This buckling phenomenon can be observed from the load cell data†. ii. Under certain fault conditions, the torus can exert very small torques on the solenoid magnet. iii. The worst but very improbable case (maximum torque) is for the torus with one of torus coils at 90% of full operating current (Fault #1) and no active shield in the solenoid, as a mitigation action solenoid was tested independent of torus magnet. iv. During subsequent post-commissioning runs, it was 	Overall these values are well within the design limits for coil buckling. The set limits on the load cell are well above this observed behavior.

discovered that there is some low-level coupling between the torus magnet coils and the shield coil (Coil 5) of the solenoid. The mutual inductance has been estimated as being approximately 0.2 H. So, if the torus quenches or undergoes a fast dump, it is likely that the voltage across Coil 5 of the solenoid will rise and exceed the threshold for quench protection, thereby causing the solenoid to undergo a fast dump also. This has happened at least once without any ill-effects for either magnet – apart from all the helium being lost from the reservoirs of both magnets.

[‡] Initial electromagnetic studies between the two magnets show almost no interaction. However, in this initial analysis each torus coil was modelled as one conductor and only the net force on that conductor was considered. A more detailed analysis was then performed modelling the torus coils as 8 sections: 2 long straight sections, 2 short straight sections, and 4 corner sections. The results from this subsequent analysis match closely to that observed during normal operation of these magnets.

Figure 20 illustrates the combined stray field maps of the torus and solenoid for various operating conditions.

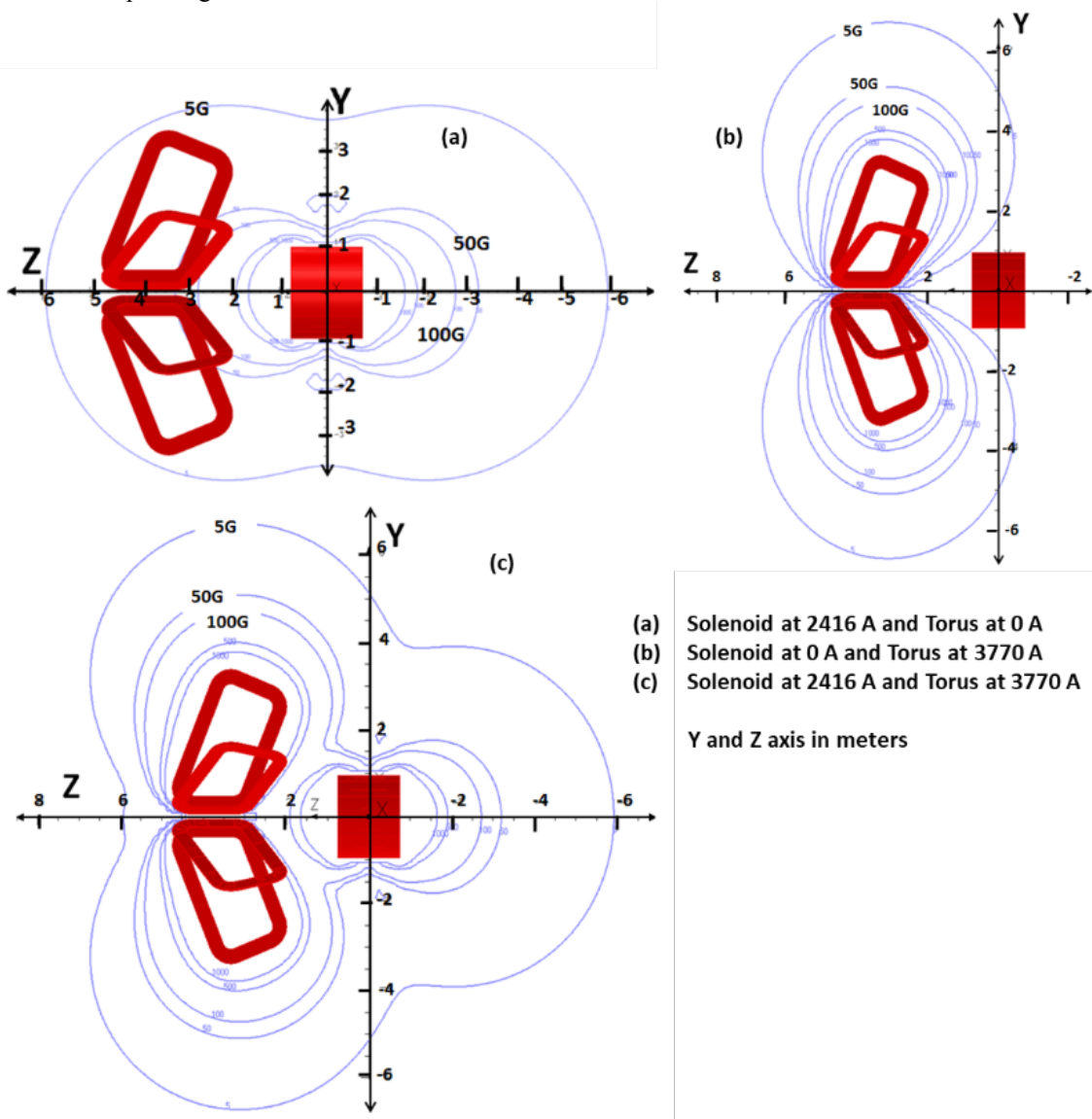


Figure 20: Solenoid and torus stray field maps for different operating conditions.

The common supply and return lines from the refrigerator supplies both magnets and a liquid-helium dewar that is used to fill cryogenic targets. These lines could produce coupling between the torus, solenoid, buffer dewar, and target, in particular

the warm return piping. Passive and active control elements have been put in place to minimize the potential for damaging the magnets due to these cryogenic coupling phenomena – for example, check valves on the vapor-cooled leads prevent reverse flow, automated vent valves allow flow to continue in the event of a pressure rise to prevent the leads from warming and remain

open until a magnet completes a controlled ramp down. There are also check valves in the torus and solenoid supply and return U-tubes to prevent back flow of hot gas from either magnet going into the other. These check valves also delay the instantaneous pressure rise that back flow would cause. Operational experience has shown that either magnet can be fast dumped and the system design allows the other not to be affected cryogenically.

IV. POWER SUPPLY, CONTROLS AND INSTRUMENTATION

Superconducting Magnet DC Power Supply

Each magnet is energized using identical superconducting magnet power supplies (MPS). This was a bespoke design from Danfysik based on their model 8500/T854 power supply [26]. The MPS DC output is low voltage, high current, designed for near zero resistance loads; however, the impedance seen at the magnet/power supply output terminals can go from purely inductive to an almost purely resistive state during a quench. Due to the requirements for high stability and low drift on a static magnetic field, a linear series-pass regulation topology was selected. The MPS output utilizes two-quadrant operation, allowing for smooth and continuous ramping of the current into the magnet [27]. The power supply is programmed to sweep magnet currents at predetermined rates at different current levels without user intervention. The MPS incorporates features designed to mitigate or prevent failure modes during magnet operation. These features include: controlled current ramping (up or down), a fast-opening dump switch and dump resistor (124 mΩ and 200 mΩ for the torus and the solenoid, respectively) to rapidly de-energize (fast dump) the magnet, a slow dump capability that utilizes the last-used ramp rate to run the magnet down, an integrated polarity reversal switch, and redundant DC current transducers for current-based interlocks. Additionally, a separate rack-mounted, PLC-based controller allows the programming of current ramp rates and the monitoring of interlocks and the overall health of the magnet. Salient MPS and energy dump specifications are given in Table XIX.

TABLE XIX
DC POWER SUPPLY AND FAST ENERGY DUMP SPECIFICATIONS

Description	Specification
Output current/voltage	± 4000 A / ± 6 VDC
Ramp rate	Variable: ±0.2 to ±3.0 A/s
Supply voltage	480 V/3-Φ/60 Hz.
Ambient temperature	15–35 °C
Cooling water (flow, temperature)	60 l/m, 15–35°C
Pressure	300 psig
Ground isolation	>1.0 MΩ
Quench protection	Fast DC output breaker
Absolute accuracy	-0/+100 ppm
Stability (30 min)	< ± 5 ppm
Stability (8 hours)	< ± 10 ppm
Magnet	IOP (A)
Torus	±3770
Solenoid	±2416
LTOT (H)	EST (MJ)
2.0	14.21
6.0	17.50
V _{DUMP} (V)	R _{DUMP} (Ω)
< 500	0.124
< 500	0.200
T _{MAX} (°C)	
	<350
	<350

The power supply is designed to react to a quench, which is detected by a set of hard-wired quench detector electronic units, and automatically switch power off to the magnet [28]. The hard-wired quench detection subsystem acts directly to open the dump

switch as part of the primary protection system. Voltages across the complete magnet including the magnet coils, vapor-cooled leads, bus-bars and all splices are continuously monitored by the quench protection system. The quench voltage detection thresholds were determined after carrying out a series of quench scenario simulations. An upper limit for the magnet power supply ramp rate was set based on the selected voltage thresholds and the magnet inductance.

The power supplies' default factory settings meant that there was a total time delay of about 750 ms between when the set quench threshold voltage was exceeded to the time when the dump switch was fully opened during a fault condition. Although this delay time would likely have been adequate for the torus and solenoid, operational experience with similar designs of power supply within the laboratory suggested that reducing this time delay would provide a larger safety margin in terms of minimizing peak hot spot temperatures within the coils. The overall time delay consists of three time components - (a) T_q is the time between when the quench starts within the superconductor and when the quench voltage threshold is exceeded, (b) T_{qi} is the time between when the quench voltage threshold is exceeded and the quench-interlock relay opens - this is a constant associated with the accompanying electronics, and (c) T_{dsw} is the time for the dump switch within the power supply to fully open. The control circuit for the dump switch was modified following consultations and instructions from the power supply vendor and the resulting total time delay has now been reduced to about 120 ms.

Magnet Current Leads and Ice-Management System

Water-cooled leads (WCLs) are used to connect each magnet power supply to the respective magnet's vapor-cooled leads (VCLs). Air-cooled multi-stranded (flexible) copper jumpers are used to transition between the hard connection points at the power supply end as well as at the magnet end (see Fig. 21). Tables XX, XXI, and XII summarize the main features of these current transfer components.

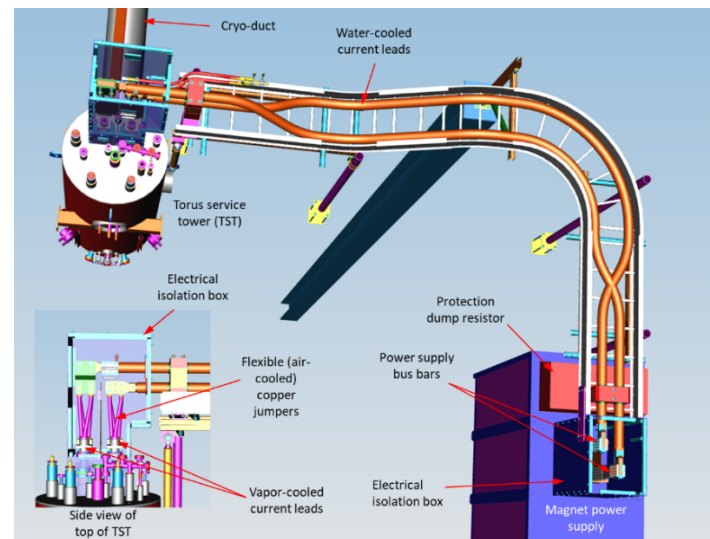


Figure 21: Torus – vapor-cooled leads, water-cooled leads, and flexible jumpers.
The set-up for the solenoid is similar.

TABLE XX
WATER-COOLED LEADS SPECIFICATIONS

Description	Torus	Solenoid
Operating current	4000 A	3000 A
Cable cross sectional area	2000 MCM	2000 MCM
Voltage drop per lead pair @ 4000 A (torus) @ 3000 A (solenoid)	1.1 V @ 50°C	1.3 V @ 50°C
D.C. resistance for both leads connected in series @ 50°C	274 $\mu\Omega$	475 $\mu\Omega$
Input water temperature	40°C	40°C
Output water temperature	50°C	50°C
Max. operating pressure rating	300 psig	300 psig
Test pressure	400 psig	350 psig
Insulation to ground voltage rating	2 kV	3 kV
Minimum allowable water flow @ 4000A (torus) @ 3000A (solenoid)	1.2 gpm	3.2 gpm

1 MCM (1 thousand circular mils) = 0.5067 mm²

TABLE XXI
 AIR-COOLED JUMPER SPECIFICATIONS

Description	Torus	Solenoid
Maximum design current	4000 A	3000 A
Jumper cross sectional area	3000 MCM	3150 MCM
Voltage drop for jumpers per lead @ 4000 A (torus) @ 3000 A (solenoid)	One jumper pair = 0.06 V @ 70°C	One jumper = 0.014 V @ 70°C
DC resistance for jumpers per lead @ 70°C	One jumper pair = 15 $\mu\Omega$	One jumper = 4.7 $\mu\Omega$

1 MCM (1 thousand circular mils) = 0.5067 mm²

TABLE XXII
 VAPOR-COOLED LEADS SPECIFICATIONS

Description	Torus	Solenoid
Rated operating current	5000 A	2500 A
Operating helium consumption @ 5000 A	20 liters/hr per pair	7 liters/hr per pair
Standby helium consumption	15 liters/hr per pair	6 liters/hr per pair
Minimum recommended lead gas flow per lead @ 5000 A / 4000 A (torus), @ 2500 A (solenoid)	118 SLPM / 112 SLPM	42 SLPM
Maximum allowable voltage drop per lead @ 5000 A (torus) and @ 2500 A (solenoid)	100 mV	100 mV
Allowable operating time with no gas flow	150 s	150 s

SLPM = Standard Liters per Minute

Band and cartridge heaters are installed at the top of the vapor-cooled leads where they exit the magnet service towers to keep ice-formation to a minimum (see Table XXIII).

TABLE XXIII
 LEAD HEATER SPECIFICATIONS

Description	Torus Specification (per lead)	Solenoid Specification (per lead)
Upper heater set – No. of heaters / power / voltage	1 / 400 W per heater / 120 VAC (Mica band heater 3" ID, 1.5" width)	2 / 150 W per heater / 115 VAC (cartridge heaters)
Central heater set – No. of heaters / power / voltage	2 / 300 W, 600W / 115 VAC (heater tapes) - proposed	1 / 600W / 115 VAC (Mica band heater)
Lower heater set – No. of heaters / power / voltage	1 / 600W / 115 VAC (heater tapes) - proposed	2 / 300 W, 600W / 115 VAC (Mica band heaters)

In case of heater failure, an ambient vaporizer is installed between the VCL and the warm return piping. The piping between the VCL and the vaporizer is vacuum jacketed. These features keep water from dripping onto the detectors.

Controls and Instrumentation

Depending on where instrumentation was mounted on the magnet, all selected sensors had to be compatible with cryogenic temperatures and magnetic fields with regard to reliability and reproducibility of read-outs with all detectors in their final locations.

The cycling of large currents in the superconducting magnets during ramp-up and ramp-down operations results in heat loads caused by eddy current effects. This phenomenon, together with the level of ambient noise within the experimental hall, guided some of the instrument choices. The risk analysis also identified the various forces that arise during operation of the torus and solenoid magnets, viz. eddy current forces, Lorentz forces, thermal loading, and also the electromagnetic and cryogenic interaction between the torus and solenoid magnets. Therefore, for safe magnet operation, it is necessary to monitor and control all of the following parameters - temperatures, pressures, pressure drops, liquid levels, mass flows, vacuum levels, voltages, strains, and loads (see Table XXIV) [6, 29, 30]. Extensive instrumentation was used to verify the design under various operating conditions during commissioning and to allow flexible, reliable, and safe control of all subsystems by non-expert personnel post-commissioning.

Instrumentation is monitored using the following key electronic subsystems:

- a. JLab-designed multi-sensor excitation low voltage chassis (MSELV or LV chassis) + National Instruments Compact Real-Time Input Output controller or cRIO (slow DAQ refers to slow data acquisition) - Magnet temperatures and strains [31];
- b. National Instruments cRIO (fast DAQ refers to fast data acquisition) – Magnet-related voltages;
- c. Cryo-Con readout units – Cryogenic system temperatures (Cryo-Con refers to Cryogenics Control Systems Inc.);
- d. Programmable Logic Controller (PLC) – Cryogenic system pressures, vacuum levels.

Monitoring and control of the entire system (including valves and flow indicators) were performed by Allan Bradley PLCs. The design of the sensor read-back MSELV chassis was based on the requirements of the torus and solenoid instrumentation in terms of quantity and types. Commercially available readout boxes for sensors are usually limited to a certain number of channels and the multi-functional capability of these devices usually means that these devices are expensive. The motivation to accommodate all of the sensor types (temperature, pressures, strains, loads, and magnetic field – termed “slow data”) that would be used on both magnets, together with a reduced set of functions, to only meet the required control system needs of the magnets and no more, led to a JLab-designed and developed FPGA-based MSELV chassis that sets the excitation current or voltage for a sensor and also provides read back [6, 32]. The data read-back would then be routed to a NI-cRIO (the slow DAQ system) that would pass data

to the PLC for control of the various subsystems and interlocks. The majority of instruments are powered and read out via the LV chassis:

1. The MSELV sends the unscaled raw readouts to the NI-cRIO via individual RS232 ports. Each port is selectively assigned based on instrument type, temperature, strain, etc. The NI-cRIO takes the raw data for each instrument and converts it to engineering units from specified calibration tables. This “slow” data is sampled at 1 Hz.
2. The cRIO device puts scaled sensor readouts into arrays, based on instrument type, and sends these arrays to the PLC via Ethernet.

3. The PLC interrogates these data sets and then uses prescribed routines (cool down, power up, etc.) to force action on valves, heaters, power supplies, etc. The PLC also transfers this data to an EPICs IOC (input-output controller) to allow for archiving and site-wide system control (e.g. the cryo compressor in the End Station Refrigerator can use one of our cryogen liquid levels to help determine cryogenic heat load).
4. In parallel another cRIO (fast DAQ) uses its 24-bit ADCs (Analog to Digital Converters) to monitor the voltage taps. This cRIO directly sends 10 kHz data to the EPICs IOC for offline analysis. In parallel, it also sends the voltage tap data to the PLC at a rate of 5 Hz for the redundant (secondary) protection system.

TABLE XXIV

TORUS AND SOLENOID MAGNET SYSTEM SENSORS AND VOLTAGE TAPS

(A) Torus Magnet System

Measurement	Voltage		Temperature (4 K)		Temperature (77K)		Strain		Load Cell	Hall Sensor		
Sensor/wiring type	8 mil Kapton insulated-multi-strand copper wire (pair)		Cernox™(1070) – 4 wire		Calibrated PT100 – 4 wire (Omega F2020-100-B)		Cryogenic series 350 Ω (CFLA-6-350) 4-wired/3-wired for measurement		Load Cell - FUTEK FSH02239 (2000 lbs), 4 wire, 300 K			
Sensor location / No. of sensors	Magnet	23	Magnet	54	Thermal shield	60	Coil Cold Mass (CCM)	24	OOPS	26		
	Zero-flux current transducer	2	Cooling tube	12	Current - leads	2+2	Axial sup	6	FMEA result	3 (Hub)		
	FMEA Result	1 (Power supply-One bus bar)	Splices	6+2	Axial sup	3	Vert sup	8				
	Line-GND/dump resistor	1	VCL in Cryostat	2+2	Vert sup	4	FMEA result	24 (Hex)				
Connection wiring	Copper		Constantan multi-core harness		Constantan multi-core harness		Constantan multi-core harness		Copper			
Wire gauge	24 AWG		36 AWG		36 AWG		36 AWG		28/32 AWG			
Signal amplitude	Magnet	300 V pk	3 mV (300 K) to 50 mV (4.2K)	0.1 V (77K) to 0.5 V (300 K), actual excitation Current = 2.5 mA	0-5 V for resistance measurement the variation is 0-0.5 Ω or 10 μV – 1 mV (CFLA-6-350)	~ 2.0 mV/V	~ 1.00 mV/kg (at 298 K)					
	Dump R	250/500 V pk										
	ZFCT	50 mV										
	PSU	6V										
Sampling rate	> 2 kHz		100 Hz		100 Hz		100 Hz		100 Hz			
Excitation current or voltage	n/a		0.20-20 μA		1-5 mA		0-10 V (2.5 V in operation as chosen)		0-10V (2.5 V in operation as chosen)			
No. of channels	24		71		61		38		26			
Multiplexed	NO		YES		YES		YES		YES			
Control	Primary - hard wired to quench detection/Secondary - PLC		PLC		PLC		PLC		PLC			
Fast DAQ	FPGA		FPGA		FPGA		FPGA		FPGA			

1

(B) Solenoid Magnet System

Measurement	Voltage		Temperature (4 K)		Temperature (77K)		Load Cell		Hall Sensor											
Sensor/wiring type	8 mil Kapton insulated-multi-strand copper wire (pair)		Cernox™ – 4 wire (4.2 – 325K)		Calibrated PT100 – 4 wire		Load Cell, 4 wire, 300 K (Force)		Cryogenics hall generator (axial), HGCA-3020, 4 wire											
Sensor location / No. of sensors	Magnet		21	Magnet	26	Thermal shield	18	8 (LCM307)	0-10 kN (axial)											
	Zero-flux current transducer, Power supply bus							8 (KMR300kN)	0-165 kN (radial)											
Connection wiring	Constantan/manganin/copper		Constantan harness		Constantan harness		Copper		Copper											
Signal amplitude	Magnet		718 V pk	3 mV (300 K) to 50 mV (4.2K)	0.1 V (77K) to 0.5 V (300 K), actual excitation Current = 2.5 mA	~ 2.0 mV/V	~ 1.00 mV/kg (at 298 K)													
	Dump R																			
	ZFCT																			
	PSU																			

21

Sampling rate	> 2 kHz	100 Hz	100 Hz	100 Hz	100 Hz
Excitation current or voltage	n/a	0.20-20 μ A	1-5 mA	0-10V (2.5 V in operation as chosen)	100 mA
Control	Primary - hard wired to quench detection/Secondary - PLC	PLC	PLC	PLC	PLC
Fast DAQ	FPGA	FPGA	FPGA	FPGA	FPGA

Analog data collection from other devices not listed above are: Pressure transducers, EV electric valves, PV pneumatic valves, RV pressure relief valves, VCL lead heaters, VCL lead flow indicators, vacuum pump control (gauges and gate valve), bus-bar water flow switches, magnet power supply water flow, and temperature monitors.

Magnet Quench Protection and Control Electronics

The magnet Quench Protection System (QPS) was developed for both magnets based on the analysis of several quench scenarios and is comprised by primary and secondary subsystems [28]. Parallel path voltage taps from multiple locations throughout the magnet (magnet coils, splices, bus-bars, leads, etc.) feed both of these subsystems. The voltage taps feeding the primary protection subsystem are hardwired directly from the magnet to the Danfysik Quench Detector units – i.e. with no electronics or any software manipulation in between.

The secondary quench protection subsystem is also fed from the same voltage tap locations but this time the information is acquired by a fast data acquisition system (Fast DAQ), using a National Instruments cRIO device, and then routed to a PLC that performs summations and subtractions of various voltages to provide back-up for the hard-wired primary subsystem. A quench-induced voltage that exceeds pre-set voltage thresholds will trigger the primary system closely followed by the secondary system.

Each of the hardwired Quench Detection (QD) modules consists of four input channels; each input channel is a differential channel consisting of an upper and lower channel. These upper and lower channels accept voltage signals that are then subtracted from each

other. The resultant voltage is compared with a pre-set voltage threshold (set by the operator). If the resultant voltage is higher than this threshold and remains above this threshold for a pre-set time period, then the QD will trip and fast dump the magnet—i.e. the dump switch will open to isolate the magnet from its power supply and the magnet will run down through the external dump resistor. Between 43-63% of the stored energy within the magnet is extracted and dissipated in the external dump resistor. The remainder of the energy is dissipated within the magnet coils and cryogenic system itself. Figure 22 illustrates a set of typical voltage taps for the solenoid magnet, feeding both the primary QPS (i.e. to the quench detector units, QD-U) and also to the secondary QPS (DAQ).

The secondary QD system routes voltage tap data from the magnet via Knick isolation amplifiers (iso-amps) [33, 34] to a second dedicated NI-cRIO having eight four-channel N9239 24-bit analog input modules. The voltage tap data are then manipulated by the PLC to produce summed and subtracted voltages that are then routed to the various interlocks.

Two sets of thresholds are employed here - one set to initiate a controlled ramp down and a second set that is deployed as a backup for the hardwired QD and also acts directly on the fast dump contactor.

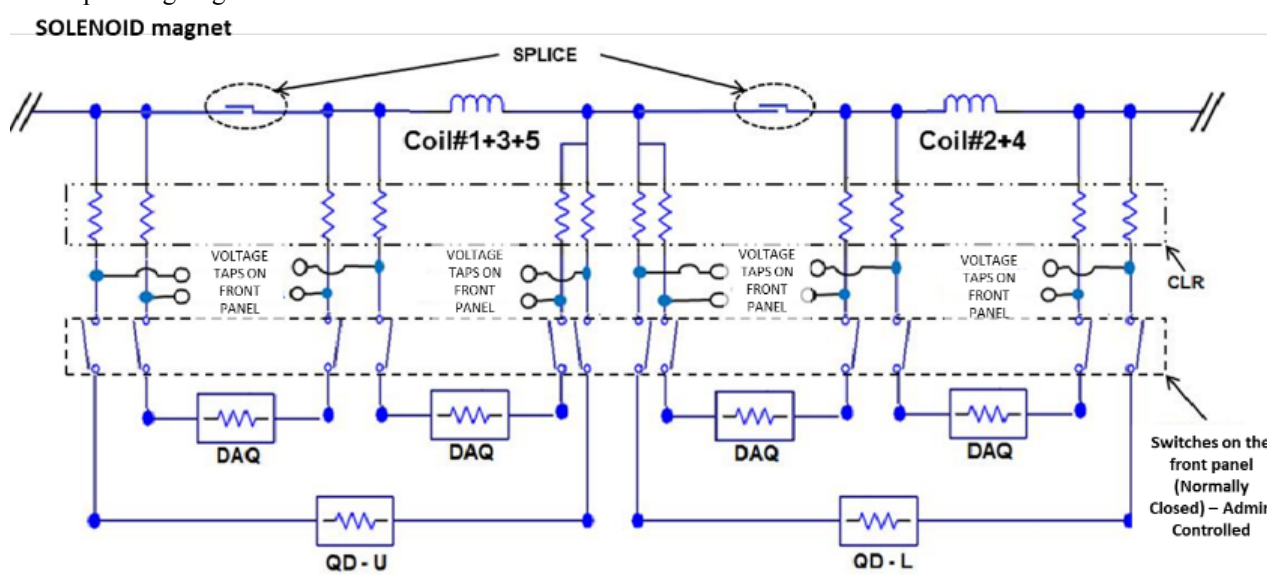


Figure 22: Schematic arrangement of a typical section of the solenoid magnet for impedance-matching simulations – Current Limiting Resistor (CLR), Op-Amp, QD board.

The design of the quench protection and voltage tap subsystems was driven by the anticipated levels of voltages developed during a magnet quench. The quench protection provides valuable data during a quench event via data capture of the voltage and temperature waveforms. The magnets are continuously monitored during ramp up, steady state operation, and also ramp down—i.e. the QPS is always active—so inductive voltages across coils during ramp up and down operations are also captured and have been used during the commissioning process to ensure the correct

balancing of voltages between the various coils and thus QD channels.

The same cRIO also feeds VT waveform data to EPICS at 10 kHz for online review via parallel Ethernet communications. The primary and secondary voltage thresholds for the torus and solenoid are summarized in Table XXV, which also provides the full list of interlocks that are managed by the control system.

TABLE XXV
TORUS AND SOLENOID MAGNET HARDWARE AND SOFTWARE INTERLOCK THRESHOLDS

Torus Magnet System			
	Acceptable Operating Range	Actual Trip Limit	Expected Threshold
Hardwire Interlocks (FAST DUMP)			
Liquid Helium Level (SC probe)	21-110 %	<20 %	<20 %
Liquid Helium Level (Diff Press)	21-110 %	<20 %	
Vapor Cooled Lead Temp	4.5-15 K	>15 K	>10 K
Danfysik QD's	>200 mV, 100 mV(VCL), >2250 mV		Varies across sections identified
PLC Interlock - I (Fast Dump)			
Current Limit (Hard coded)	Not to exceed \pm 3880 A	3850 A	\pm 3880 A
Software Quench, 2nd Threshold	Coil voltages are compared >350 mV, VCL >125 mV		Coil voltages are compared >350 mV, VCL >125 mV
PLC Interlock - II (Controlled Ramp Down)			
CCM Load Cell	Top 600 lbs, bottom 1300 lbs	Top 600 lbs, bottom 1300 lbs	Top 600 lbs, bottom 1300 lbs
Vertical Support	-9500 lb		-9500 lb
Coil Compartment 1st Threshold	Coil voltages are compared >250 mV		Coil voltages are compared >250 mV
Vacuum	$>5 \times 10^{-5}$ atm		$>5 \times 10^{-5}$ atm
Pressure Helium Tank	PT8120 < 2.3 atm		PT8120 < 2.3 atm
Supercritical Helium Pressure	2.4-3.0 atm	<2.3 atm	
Pressure Nitrogen Tank	<2.0 atm		<2.0 atm
LL Helium Tank	<90 %		<90 %
LL Nitrogen Tank	<90 %		<90 %
VCL Flow	\pm 15 SLPM of SP		\pm 15 SLPM of SP
VCL Temp	>10 K		>10 K
VCL Voltage	80 mV		80 mV

Solenoid Magnet System			
	Acceptable Operating Range	Actual Trip Limit	Expected Threshold
Hardwire Interlocks (FAST DUMP)			
Liquid Helium Level (SC probe)	21-110 %	<20 %	<20 %
Liquid Helium Level (Diff Press)	21-110 %	<20 %	
Vapor Cooled Lead Temp	4.5-20 K	>20 K	<15 K
Danfysik QD's	>200 mV, 100 mV(VCL), >1500 mV		Varies across sections identified
PLC Interlock - I (Fast Dump)			
Current Limit (Hard coded)	Not to exceed \pm 2500 A	2500 A	\pm 2500 A
Software Quench, 2nd Threshold	Coil voltages are compared >350 mV, VCL >125 mV		Coil voltages are compared >350 mV, VCL >125 mV
PLC Interlock - II (Controlled Ramp Down)			
Axial Support	0-8000 lbs		
Radial Support	0-18000 lbs		
Coil Compartment 1st Threshold	Coil voltages are compared >250 mV		Coil voltages are compared >250 mV
Vacuum	$>5 \times 10^{-5}$ atm		$>5 \times 10^{-5}$ atm
Pressure Helium Tank	PT8120 < 2.3 atm		PT8120 < 2.3 atm
Supercritical Helium Pressure	2.4-3.0 atm	<2.3 atm	
LL Helium Tank	<90 %		<90 %
VCL Flow	\pm 15 SLPM of SP		\pm 15 SLPM of SP
VCL Temp	4.5 - 15 K		>17 K
VCL Voltage	80 mV		80 mV

at 4.6 K that flows in cooling tubes located on the inner diameter of the coil. Two layers of copper sheet are soldered to the cooling tubes on each side of the double pancake and completely encase the coil, providing the main path for conduction-cooling. To allow for visual inspection of the coil potting quality the coils were first potted without the copper sheets. Ground plane insulation was then added followed by the installation of the copper sheets. The coil was then positioned and potted for a second time within its aluminum case (see Fig. 23).

V. FABRICATION AND ASSEMBLY

TORUS

The individual coils are housed in an aluminum case that is approximately $2 \times 4 \times 0.05$ m³ [35]. The conductor is insulated with fiberglass tape and each of the coils is wound as a double pancake. Each coil is conductively cooled by supercritical helium

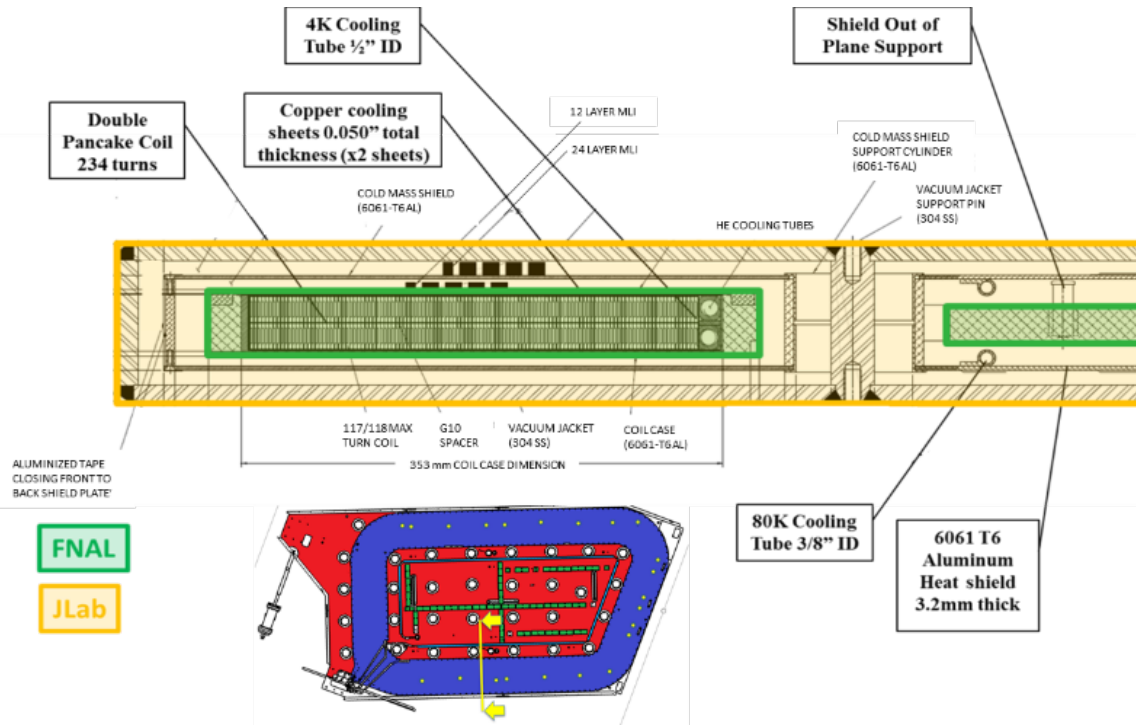


Figure 23: Coil and cryostat design (FNAL – components fabricated by Fermi Lab, JLab – components fabricated by JLab). The lower inset figure shows the coil in its aluminum case and vacuum jacket with the two viewing arrows indicating the cross-sectional view being displayed in the upper part of the figure

The aluminum coil case is surrounded by a 3-mm-thick aluminum thermal shield cooled to 80 K by thermo-siphon-driven liquid nitrogen circulating through tubes welded to the shield. The shield is supported off of the coil case by thin-walled support arms and low thermal conductivity bumpers. The shield is constructed of Al-6061, which provides mechanical strength to the shield, with high thermal conductivity Al-1100 strips epoxied to the shield to reduce peak temperatures at maximum temperature regions on the shield. As large eddy currents can be induced in the thermal shield during fast discharges of the magnet coils, the shield has been segmented to reduce these effects.

The six coils make up a hexagonal assembly where the hex beams carry the elements to make the hydraulic and electrical connections between coils; they also contain re-coolers that are tube-in-shell heat exchangers (see Fig. 24a). The re-coolers recool the helium that exits each coil before it enters the next and also provide cooling for the inter-coil splices (see Fig. 24b). The design is a coiled tube in a shell and works equally well both during cool down and at steady state at 4 K. During cool down variable temperature gas is transferred into the shell side. At steady state the shell side is filled with liquid helium by a thermo-siphon from the reservoir in the Torus Service Tower (TST). All coils, hex beams, and the service tower share a single vacuum space that is pumped on by two 8 in turbo-molecular pumps.

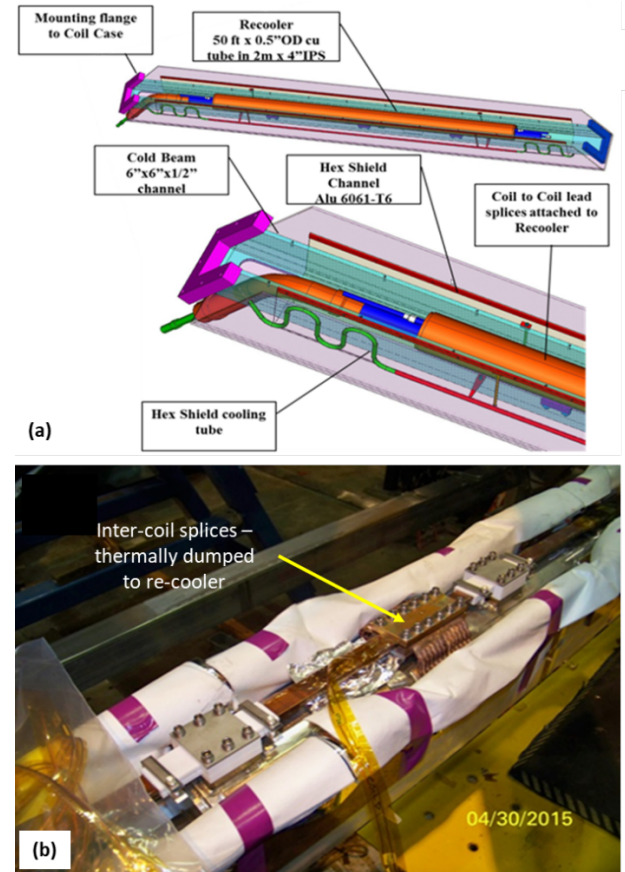


Figure 24: (a) Typical hex beam detail, (b) Coil splice (soldered joint) attached to re-coolers.

Three axial supports, (aligned in the beam direction), together with 4 vertical supports, 2 lateral out-of-plane supports (OOPS), and 24 coil OOPS support the entire torus cold mass (see Fig. 25). Any sag in the coils due to gravity, installation misalignments, or forces that arise from the energization of the solenoid are managed by the coil OOPS. The OOPS design consists of a fiberglass tube epoxied to spherical bearings. The bellows at the vacuum case maintain vacuum, allow adjustment in the out-of-plane direction, and allow force-leveling between upstream and downstream OOPS. The bellows also allow movement of the coil during cool down. The assembly includes a room temperature load cell connected to the data acquisition system so that the out-of-plane force seen by each coil is always known. The axial and vertical supports are stainless steel links with strain gauges mounted near the warm end. Each end has a spherical bearing rod-end and they connect the cold mass to the vacuum jacket. The vertical supports take the entire gravity load for the 25 Ton cold mass, while the axial supports react to any loads in the beam direction to adjust the magnet in the pitch and yaw directions and to handle the seismic loads.

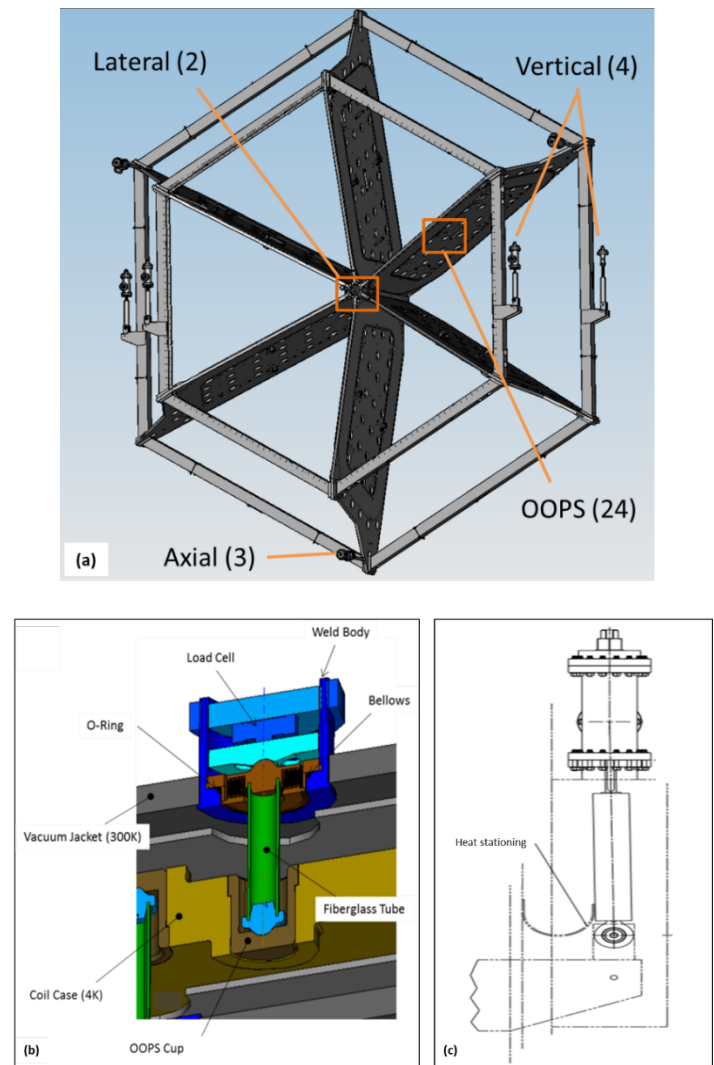


Figure 25: (a) Cold mass support system, (b) Out-of-Plane support, (c) Vertical support.

A top-level summary of the key manufacturing steps of the torus magnet construction is given in Table XXVI followed by detailed descriptions of the various steps.

TABLE XXVI
 A SUMMARY OF THE KEY MANUFACTURING STEPS - TORUS

Manufacturing Step	Location
1 Superconducting Rutherford cable soldered into C-shaped copper channel	Advanced Engineering Systems (AES) LLC, PA, USA
2 Clean and inspect conductor (supplied by JLab)	
3 Wind cooling tube and apply ground insulation	
4 Insulate conductor	
5 Wind first pancake layer, set coil dimensions	
6 Turn-to-turn short tests	
7 Install ground insulation on coil OD	
8 Install layer-to-layer insulation	
9 Wind second layer, set dimensions, repeat tests	
10 Install ground insulation, and molding hardware	
11 Push into potting mold and flip assembly	Fermi National Accelerator Laboratory (FNAL)
12 Install ground insulation on first pancake	
13 Form leads	
14 Close and seal the mold	
15 Vacuum impregnate the coil, cure the epoxy	
16 Remove from the mold – full coil electrical test	
17 Survey conductor location on both sides	
18 Solder copper cooling sheets on each side of coil	
19 Position coil in aluminum case	
20 Vacuum epoxy impregnate and cure	
21 Final electrical test	
22 Ship to JLab	
23 Apply multi-layer insulation (MLI) to coil case	
24 Fit thermal shield and insulate with MLI	
25 Fit vacuum jacket and transport to hall	
26 Install torus	
27 Fabricate distribution box	JLab
28 Fabricate torus service tower (TST)	
29 Install distribution box	
30 Install TST	
31 Commission torus	

Conductor Manufacture

Jefferson Lab contracted with Advanced Engineering Systems (AES) to solder the Rutherford cable into a copper channel for the two magnets. Soldering required bonding the superconducting cable to the channel and also bonding together the two layers of the key-stoned cable. Bonding between the strands adjacent to the channel was nearly perfect, but the bonding between the layers was more difficult. The main reason for the difficulty of the inter-layer bonding was the age and cleanliness of the cable. Many trials of soldering were done and much of the iteration had to do with perfecting cleaning methods. The torus magnet had a Minimum Quench Energy (MQE) of 47 mJ. The following limits were therefore set as requirements based on a factor of safety of 10 or 4.7 mJ. An acceptable void area was determined to be about 82 mm², which implied a 9 mm diameter or approximately 4 x 20 mm² void. Similarly, the solenoid MQE is 20 mJ and an acceptable void area is 30 mm², which translates to a 6.2 mm diameter or 5.5 mm x 5.5 mm² void. A continuous automatic void monitoring system was attempted with limited success and thus improved process control was the only solution. Control of overall dimensions was also extremely important, so wiping the exterior surfaces free of solder was a key step in the fabrication process.

Another key element of the process was to make each production length of conductor as a single run thus minimizing any deterioration of quality associated with the line starting and stopping. This required multiple shifts to keep the line running around the clock. To check the quality of the soldering process, cables were peeled from the channel and then strands removed from one layer to expose the center solder joint. Once the process was optimized, each soldered length of conductor had several meters removed, about 50 m in from its beginning and end, and inspected to ensure that good quality soldering was being achieved. The flux used was SUPERIOR #75 warmed to 38°C together with 60/40 tin/lead solder. After soldering, the surface solder layer was removed from the copper using buffering wheels on 4 sides to improve epoxy bonding with the glass fiber insulating cloth that would be applied later. The completed conductor was then shipped to the Fermi National Accelerator Facility (FNAL) to start the coil winding process.

Although this is certainly a viable way forward for fabricating a stabilized conductor, this approach was the only one afforded to the JLab team as the Rutherford conductor was already available (i.e. surplus from the SSC project). For future projects, conductor design should consider a more conventional fabrication approach – e.g. extruded conductor and stabilizer in one for instance.

Coil Winding and Impregnation

The Magnet Department at FNAL was contracted to wind, insulate, vacuum pressure impregnate the torus coils, and install them in their individual aluminum coil cases before shipping them to JLab. Because of the large size of the coils, FNAL had to develop new tooling and processes to support coil production operations [5, 35]. At FNAL the conductor was de-spoiled and cleaned once again before being wound onto a specially prepared spool. These spools were also electrically insulated so that the conductor could be hi-pot tested during insulation application. The conductor was then insulated with an automated machine that applied $\frac{1}{2}$ lap 0.08-mm fiberglass tape insulation around the conductor immediately prior to the start of winding. Coils were wound by first winding the 2 turns of cooling tube around the winding mandrel, followed by winding of the coil. The coil was wound as a double pancake by winding 117 turns of the first layer with the cable for the second layer supported on an insulated spool above the coil winding table (see Fig. 26). A 0.38-mm-thick sheet of G10 was placed upon the first pancake so it would be in-between the coil pancakes, then winding the second layer for a total length per coil of \sim 2000 m (see Fig. 27). The ground insulation between the conductor and copper cooling tubes or copper sheets varies in thickness but has a minimum of 4 layers of 0.18-mm glass cloth. After each coil layer was wound, G10 shims were installed between the cooling tube and the first turn at the hub and the first 0.7 m of the upstream and downstream straight sections; shims were not applied along the radii at the corners near the hub. The primary purpose was to ensure coil-to-coil uniformity in the high-field area (close to the hub region) and to push the extra material caused by “dog-boning” to the outer portions of the coil where it would have little effect on the field or physics of the CLAS12 detector system. The “dog-boning” of a winding of conductor occurs when multiple layers of insulated wire are wound around mandrels that have straight and circular sections such as a rectangle with rounded corners. As additional

layers are added, the inner layers are compacted against the winding mandrel at the corners. This compaction tends to decrease the tension in the conductor of the inner turns. If enough compaction occurs then the conductor in the straight sections can go into compression, thus causing it to bow and create space between the turns. In order to avoid producing spaces between turns, pressure along the straight sections can in some cases re-establish the desired conductor location and spacing, the extra material then moves to the corners and this can create a shape that for long narrow coils resembles a dog-bone. As a result, this creates an uneven spacing of conductors with decreased packing density in some portions of the winding. Another cause of dog-boning is that during winding some portions of the conductor can be bent enough to yield into a permanent bend, and unless it is over-bent it will still have portions of it that are not yielded and the conductor will try to spring back into a straighter geometry. This effect produces different levels of radial stress around the winding and thus varies the compaction of the coil, which can affect the packing density.

After potting, the coils were removed from the potting mold and the FNAL survey team used photogrammetry to provide JLab with actual locations of the conductors around the perimeter of each coil (discussed later).

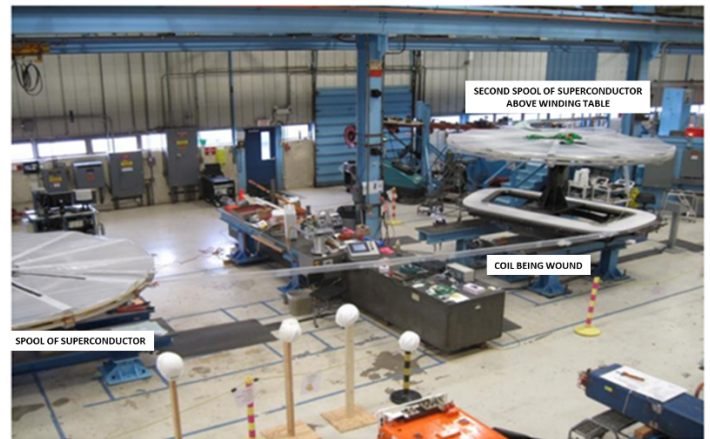


Figure 26: Partial view of the coil fabrication shop at FNAL showing a coil being wound. The aluminum spool with cleaned conductor is positioned on the winding table at left. The second spool is seen above the winding table.

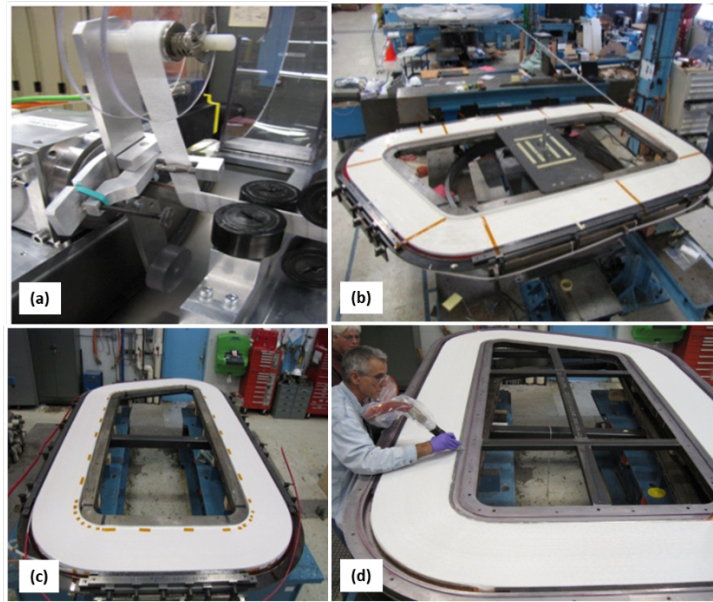


Figure 27: (a) Conductor being insulated, (b) The start of the 2nd pancake winding, (c) After 2nd pancake winding, (d) Coil in the potting mold.

During winding, the coil was also subjected to a turn-to-turn short test measurement capable of detecting both “hard” and “soft” (of about $1\ \Omega$) shorts between adjacent turns. Additional copper stabilizer was added to the leads before an initial Vacuum Pressure Impregnation (VPI) in a sealed mold with Composite Technology Development, Inc. CTD-101K epoxy. The impregnation procedure was designed, and qualified, for proper degassing, and to prevent outgassing of the epoxy during impregnation. The temperature of the coil and of the mold was driven and maintained via resistive heating of the coil itself. Temperature uniformity was monitored and controlled via sensors mounted along the mold. The coil was then allowed to soak for 24 hr at 58°C before the cure cycle began. The cure cycle took place over 3 days with gel, cure, and post-cure stages. A layer of polypropylene mesh was incorporated between the mold and a peel-ply adjacent to the coil to allow a uniform epoxy flow over the surface of the coil, as well as to provide a route for trapped and evolved gases to escape to one of the 3 main vacuum pump-out ports (see Fig. 28).



Figure 28: (a) Potting mold closed up ready for potting, (b) Hot box with potting mold installed, magnet leads, and fill/vent tubes penetrating. The box is sloped for bottom fill, (c) Top cover removed from potting mold after coil potting, (d) Coil removed from mold and flipped, cleaned up, and ready for cooling sheet attachment, (e) Coil aligned in coil case, (f) Coil case cover installed over the coil.

Upon removal from the mold, a thorough visual inspection was carried out of both sides of the potted coil to check potting quality. After initial potting, two sheets of 0.635-mm annealed OFE copper were soldered to the cooling tubes on each side of the coil and then folded over the outside of the coil. Two layers of 0.006-in Kapton were installed on the inner layer of copper for ground insulation and an additional layer of glass was installed between the Kapton and coil to aid in epoxy flow between the two during the second coil potting. The coil was then placed into its Al6061-T6 aluminum coil case and a second impregnation step was carried out using the same basic procedures as developed for the first potting (see Fig. 28f). The difference in thermal expansion between aluminum and copper ensured an adequate preload on the coils after cool down. After the second potting, the coil case modules had their cooling tubes formed, received their final round of quality control tests, and were then shipped to JLab for installation into their individual vacuum jackets and ultimate assembly in Hall B.

As part of the Quality Assurance plan, a practice coil was fabricated by FNAL and delivered to JLab. Following the 80 K test on the practice coil and a subsequent dissection, the coil was discovered to have several “dry” areas where the epoxy had not penetrated fully (see Fig. 29). A team was formed to investigate and address this problem and included experts from the USA and overseas organizations. Over a four-month period, this team reviewed the impregnation process and carried out multiple trial runs on coil samples. An improved impregnation process was developed and implemented. This resulted in the successful

production of six coils and two spares. The improvements to the impregnation process were also shared with the vendor for the solenoid magnet.

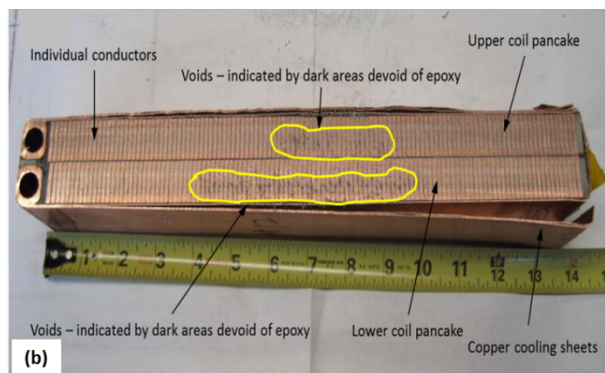
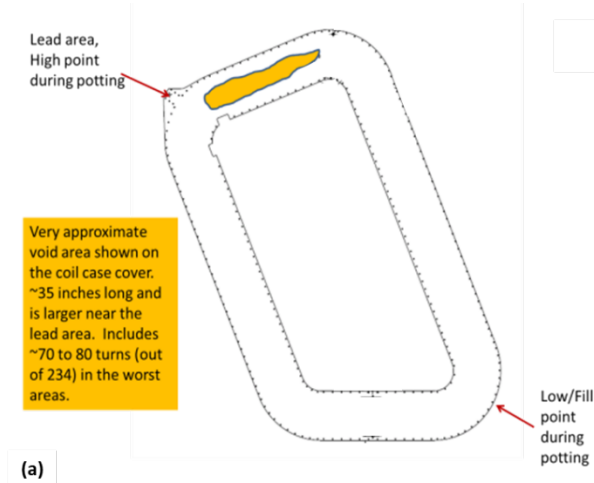


Figure 29: (a) Voids identified on the practice coil, (b) Sectioned coil indicating problem areas.

Key changes in the fabrication for the torus coils included:

1. Changing of the sequence assembly by attaching the copper cooling sheets after first potting thus allowing complete visual inspection;
2. Adding material (polypropylene mesh and peel ply) in the coil potting mold to take up the space left by the copper and ground plane and to allow resin distribution and removal of the spacer;
3. Fine tuning of resin degassing and infusion process.

80 K Cold Test and Cryostating

A “Cryostat Factory”, set up at JLab, facilitated the assembly of each coil as it arrived from FNAL. Upon arrival, each coil was inspected, instrumented with temperature sensors and strain gauges, and underwent a cool down test to 80 K (see Fig. 30) to assess the robustness of the coil’s electrical insulation and its structural integrity, as well as to test the efficacy of the employed conduction cooling method [36]. Table XXVII summarizes the results obtained from the 80 K test, data extrapolation to 4 K, and comparison with the results obtained from the finite element analysis. The results indicated that the conduction-cooling system was indeed functioning as designed with more than adequate safety margin.



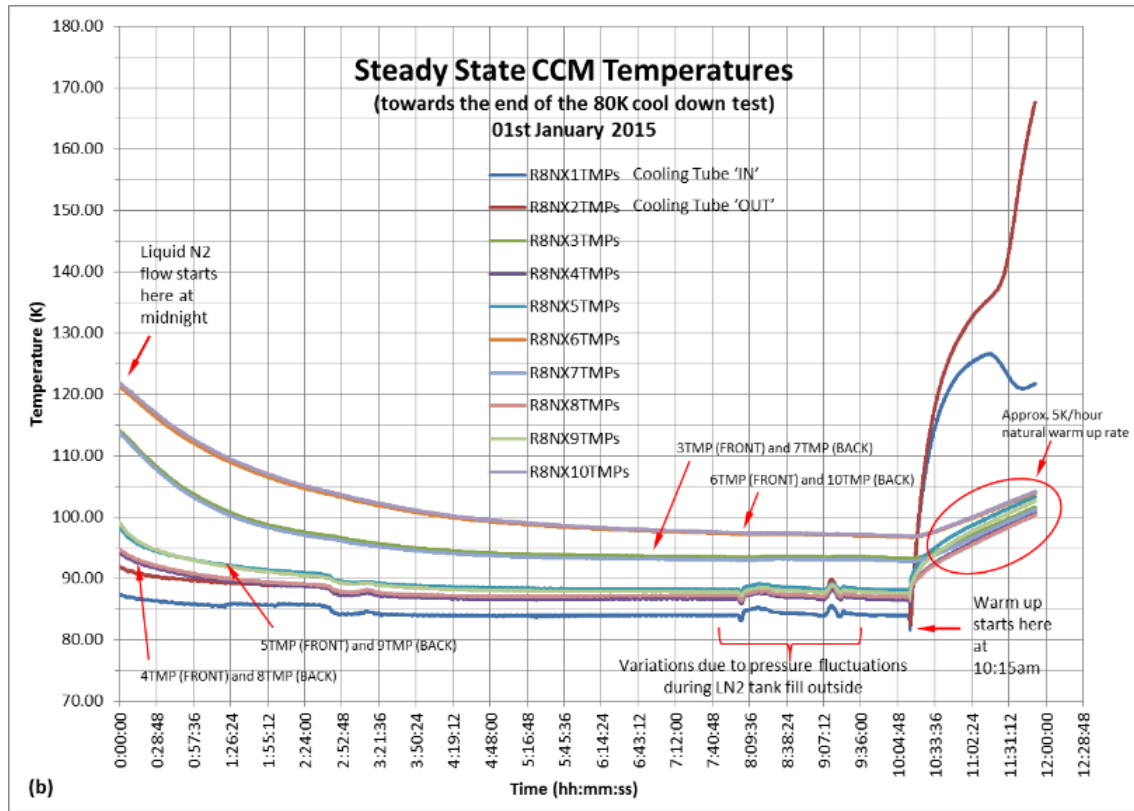


Figure 30: (a) Coil placed in large “foam” box being prepared for the 80 K test, (b) Cool down curve during 80 K test.

TABLE XXVII
 80 K DATA CORRELATION TO CALCULATED RESULTS

LOCATION	80 K Test	80 K Test	4 K Scaled	4 K Scaled	4 K
	Result Front	Result Back	Result Front	Result Back	ANSYS FEA
Temperature difference at hub (bore) K	4.00	3.10	0.12	0.09	0.251
Temperature difference at downstream hex K	7.20	4.80	0.22	0.15	0.834

Consistent with the program risk mitigation approach of practicing every quality or schedule-critical procedure, the Cryostat Factory practiced cryostating a full-scale empty coil case, which was later disassembled and returned to FNAL for use on a production CCM. This early practice allowed refinement of the assembly procedures and construction time estimates.

After warm-up from the 80 K cold test, the CCM was then wrapped in multi-layer insulation (MLI), fitted with its MLI-covered nitrogen-cooled thermal shield (see Fig. 31), and vacuum jacketed before being moved to the experimental hall for final system assembly (see Fig. 32).

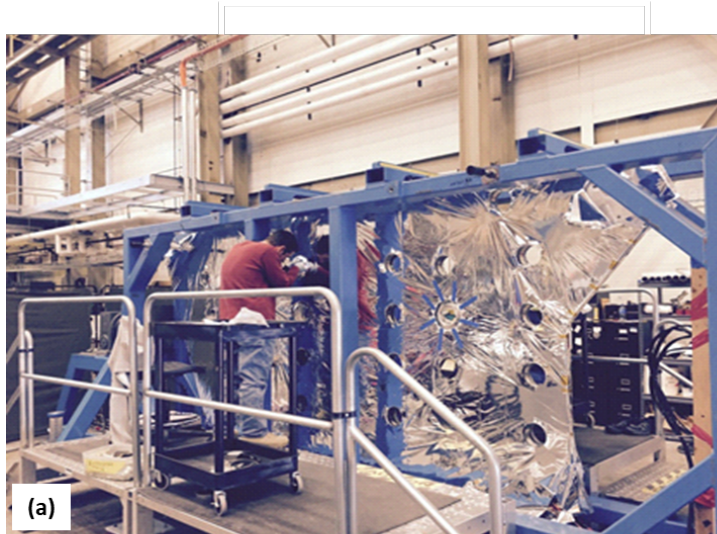


Figure 31: (a) Applying Multi-Layer Insulation (MLI) to coil case, (b) coil with thermal shield installed and in rotatable jig (to allow fitting of instrumentation on the other side).



Figure 32: (a) Soldering additional copper stabilizer to the leads as they exit from the vacuum jacket, (b) Stabilized leads bent to required shape and insulated – ready for transport to the hall, (c) Welding shut the vacuum jacket.

SOLENOID

The superconducting Rutherford cable for the solenoid was soldered into its copper channel by Advanced Engineering Systems LLC, using the same process as for the torus conductor described earlier, and transported to Everson-Tesla Inc. in Nazareth, PA, where it was de-spooled, inspected, cleaned, and re-spooled prior to the start of winding. The solenoid magnet was fabricated at Everson-Tesla and the whole process was overseen by JLab engineers.

A top-level pictorial view of the manufacturing and build sequences with a summary (see Table XXVIII) of the overall magnet construction at the solenoid vendor (ETI) follows (see Figs. 33-38):

TABLE XXVIII
 A SUMMARY OF THE KEY MANUFACTURING STEPS - SOLENOID

Manufacturing Step	Location
1 Superconducting Rutherford cable soldered into C-shaped copper channel	Advanced Engineering Systems LLC, PA, USA
2 Conductor inspected and cleaned	
3 Conductor insulated with glass-cloth and wound onto bobbin (coil former)	
4 Leak check and pressure test of C1-4 bobbin cooling channels and pipe work	
5 Wind Coil 1 (inner coil) and epoxy pot	
6 Wind Coil 2 (inner coil) and epoxy pot	
7 Wind Coils 3 and 4 (intermediate coils) on common C1-4 bobbin and epoxy pot	
8 Wind Coil 5 (shield coil) and epoxy pot	
9 Cool down Coils 1 and 2 (using LN ₂ boil-off) and shrink-fit into C1-4 bobbin	
10 Assemble Coil 5 over C1-4 bobbin using 4 cross-member beams	
11 Rivet and solder thermal “copper fingers” between all coils	
12 Assemble thermal shield and C1-4 bobbin into vacuum jacket	Everson-Tesla Inc (ETI), PA, USA
13 Fit suspension links	
14 Leak check and pressure test of internal circuits	
15 Weld shut vacuum jacket	
16 Leak check	
17 Ship to JLab	
18 Fabrication of solenoid service tower (SST)	
19 Installation of SST and solenoid	
20 Commissioning of solenoid	JLab



Figure 33: (a) Central cooling channel with helium “buttons” installed – the copper cooling sheet fingers were later soldered to these buttons, (b) Inset picture showing a helium button before welding into channel (the “fins” on the button face the inside of the channel), (c) One of the two inner coils being wound, (d) One of the two inner coils after epoxy potting was completed (the slotted copper cooling sheet can be seen on the inner surface of the coil, potted in with the coil).

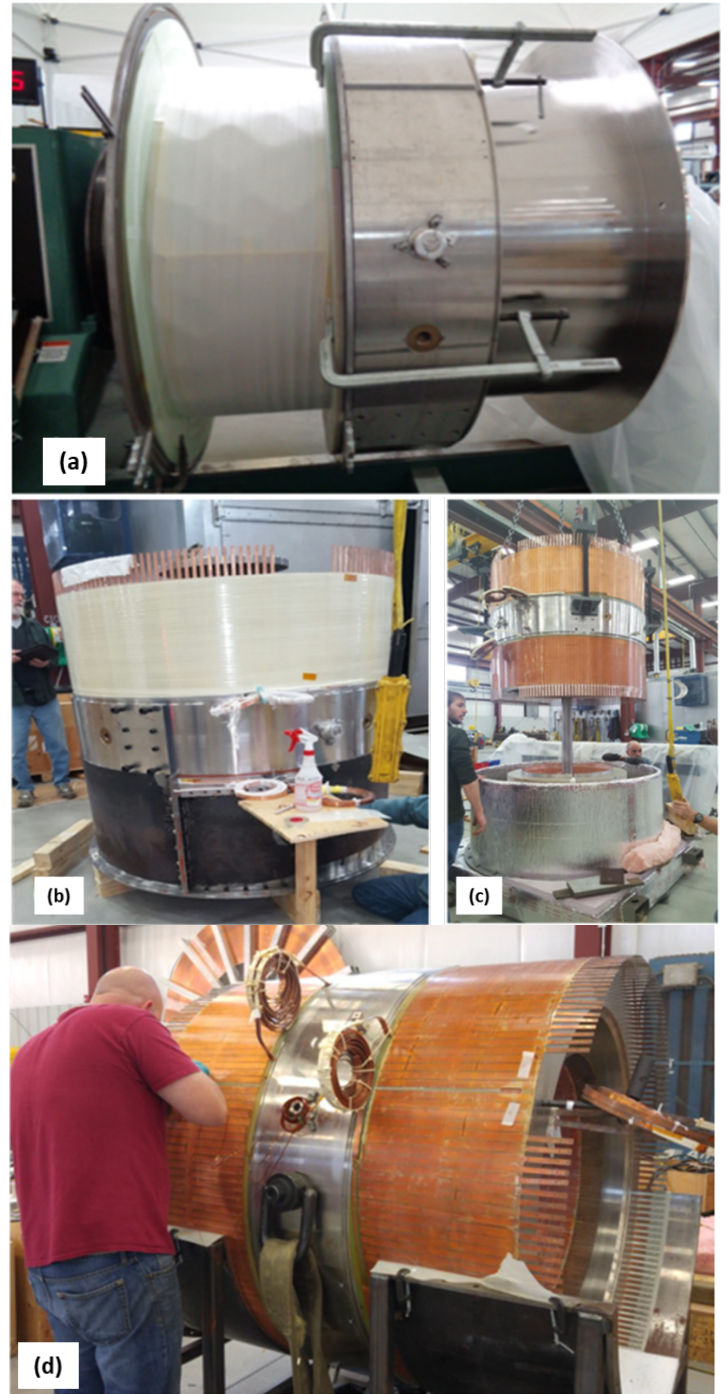


Figure 34: (a) Coil 3 being wound into its pocket on the Coil 3-4 bobbin, (b) Coil 4 (lower coil in the picture) having its potting mold being fitted around it in preparation for epoxy potting, (c) Coil 3-4 bobbin being lowered over one of the two inner coils for the shrink fit operation (the copper cooling sheet with fingers can be seen potted in with Coils 3 and 4 on their outer surfaces), (d) Coils 1 and 2 assembled within the Coil 3-4 bobbin and Coils 3 and 4 being instrumented with CERNOX temperature sensors.

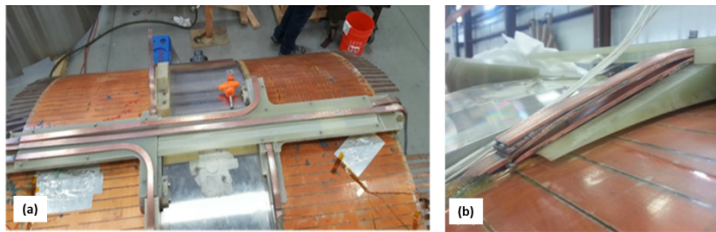


Figure 35: (a) Coil leads being routed on the outside of Coils 3 and 4, (b) Additional copper stabilizer being soldered to leads.



Figure 36: (a) Stycast being painted onto the outer diameter of Coil 5 after epoxy potting before being overwrapped with additional glass fiber cloth tape, (b) Inserting Coils 1-4 into the Coil 5 bobbin, (c) All five coils assembled together.

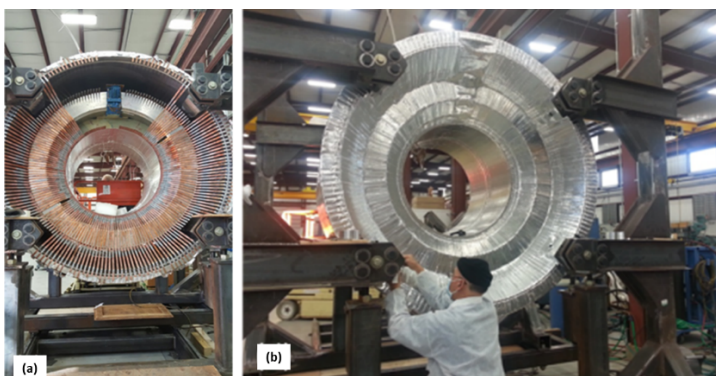


Figure 37: (a) Copper cooling 'fingers' being riveted and soldered across all coils – these fingers provide the conduction cooling path from the central helium annular channel to each individual coil, (b) Fingers being taped over with aluminum tape.



Figure 38: (a) Cold mass inserted into vacuum jacket, (b) Thermal radiation shield end cap being installed, (c) Solenoid in shipping cradle and transport fixture being loaded onto air-ride low-loader truck bed at vendor's site.

VI. INSTALLATION IN EXPERIMENTAL HALL

Torus

Installation in Hall B used the “rotating-spit” method (see Fig. 39a). Individual coils assembled in their individual vacuum cases, (with a portion of the vacuum case open to enable attachment to the central hub, see Fig. 39b), were transported into the experimental hall. The first coil was attached to the central hub, after which two adjacent hex beams were attached. This sub-assembly was then rotated before the next coil was attached and so on until all the six coils were assembled (see Fig. 40). During the installation process, this whole sub-assembly was freely rotatable around the central axis which allowed critical operations (like splicing or welding) to be performed at a convenient and safe location and orientation.

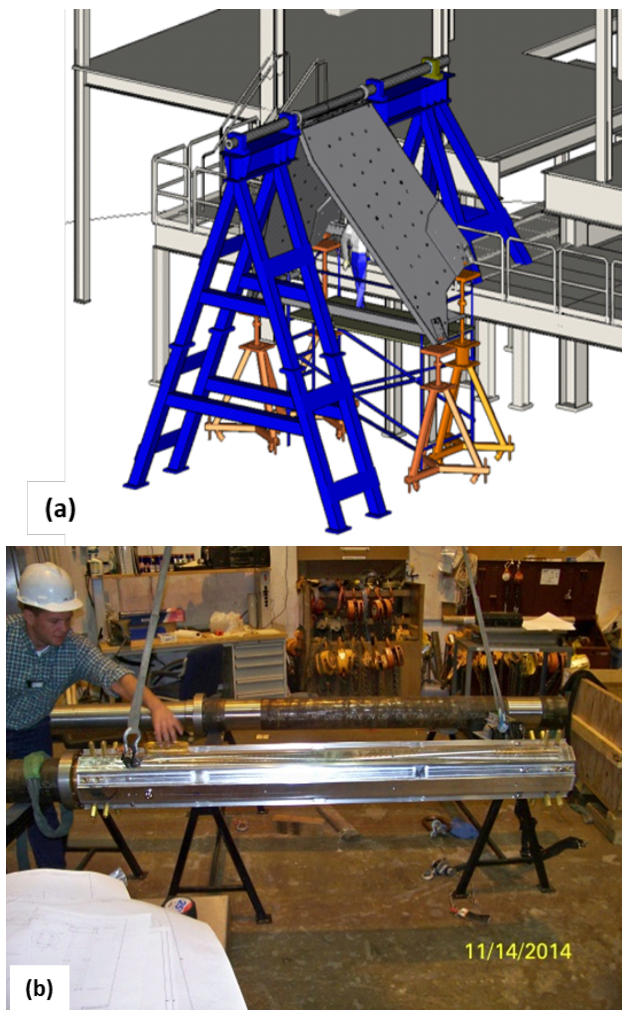


Figure 39: (a) Installation philosophy used the “rotating-spit” method, (b) Inspecting the hub before lifting into place on the “spit”.

Quality Assurance (QA) checks played a vital role at key stages of the very involved installation process within the hall (see Figs. 41-47). The QA checks included three major categories: a) electrical checks, b) leak and pressure checks, and c) survey checks. For each coil-to-coil splice, a room-temperature resistance measurement was made across the splice and also between the coil start and end leads. The coil inductance was also measured using an inductance (LCR) meter, with extrapolation to the corresponding DC value. Once the splice was fully insulated, a hi-pot to ground test was carried out to verify the integrity of the insulation and to confirm adequate tracking distances to ground. Likewise, full instrumentation checks were carried out as each of the hex beams was fitted, and also each time the coils were rotated.

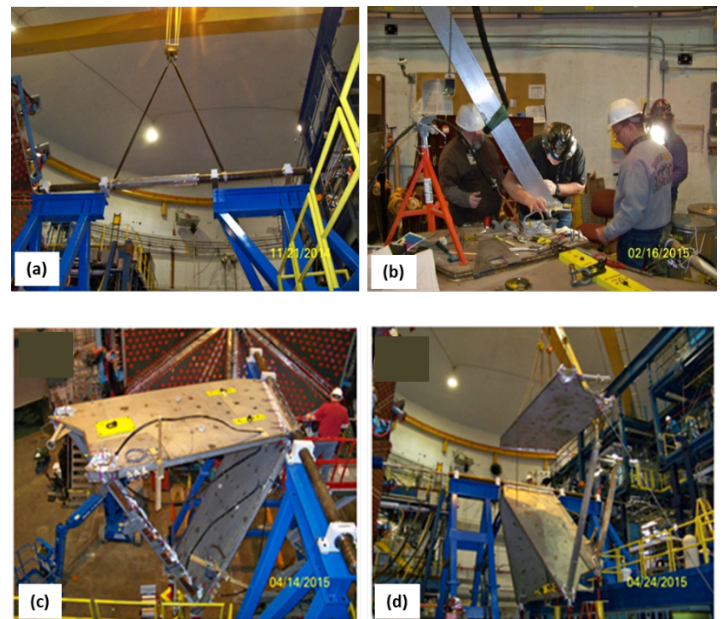


Figure 40: (a) Installing the hub, (b) Trial fit of a hex beam to a coil (c) Hex beams fitted between the coils (d) Third coil on the crane with torus rotated and hex beams installed to accept it.



Figure 41: (a) Splice soldering using purpose-built temperature-controlled heating rig, (b) Applying MLI to the splice joints, (c) Load testing an axial support.

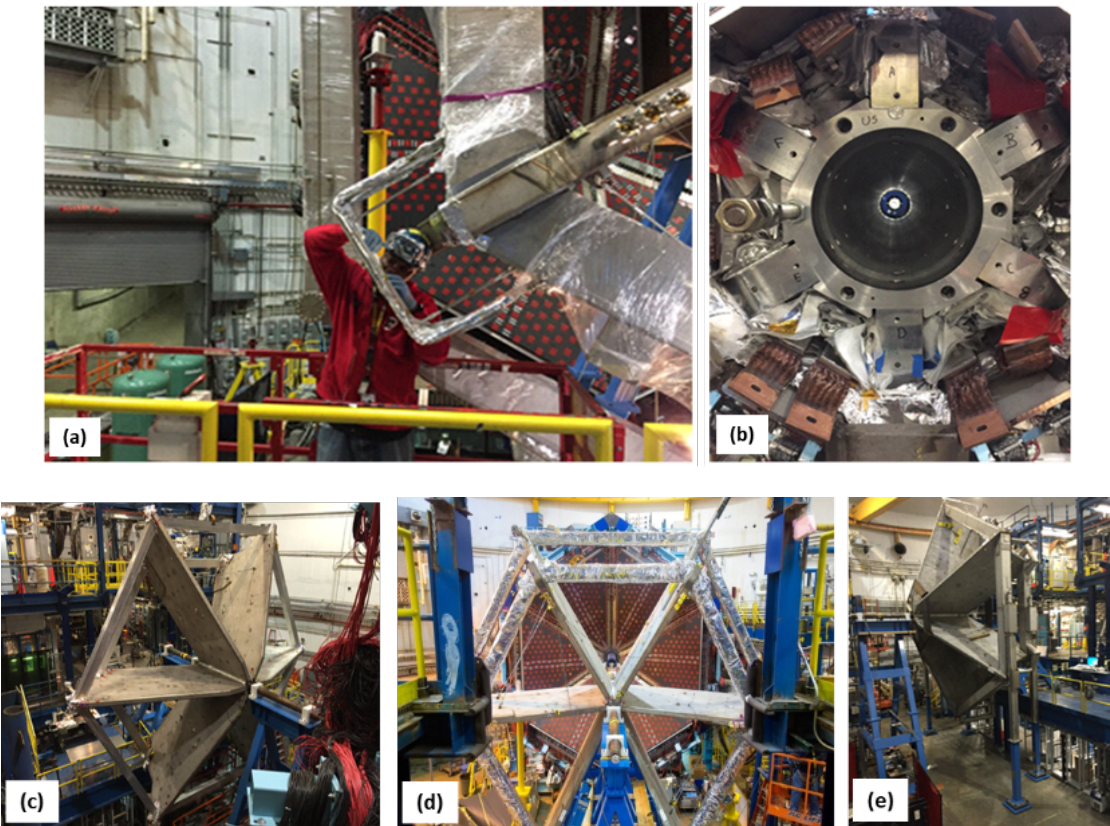


Figure 42: (a) Insulating a cryogenic 'jumper' between hex beams, (b) Aligning and shimming the coils on the hub – the ends of the six coils (A,B,C,D,E,F) can be seen located on the hub, (c) All torus coils and hex beams installed, (d) Hex beams wrapped in MLI, (e) Torus rotated to final position with legs installed.

All connections of each cooling circuit between the coils within the vacuum jacket were made by either welding or brazing. Aluminum welds and copper brazes received a liquid-nitrogen cold shock but stainless-steel welds were exempt. Once each circuit that joined the 6 coils was completed, it was pressure- and leak-tested prior to burying it in MLI. Surveys for alignment were also carried out after attaching each coil to the hub, and a global survey was done at the completion of the hexagon. Torus leak testing did not find any internal leaks, even after the pressure testing. For the external leak testing we employed two leak detectors, one at the TST and one at coil D (6 o'clock position looking downstream). This arrangement was sufficiently accurate in finding external leaks and upon completion of the testing, there was no sign of any leaks even on the most sensitive scale of the leak detectors.

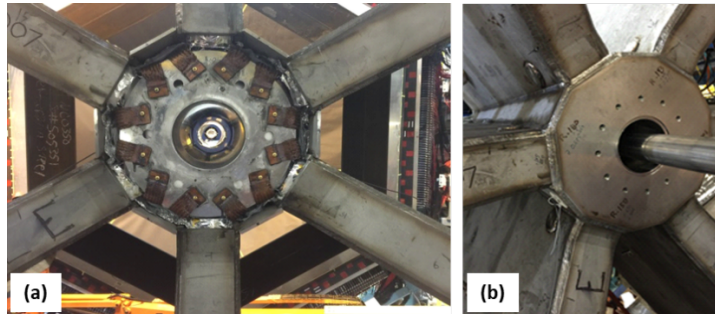


Figure 43: (a) Aluminum thermal shield inside the bore installed with copper thermal straps, (b) Hub vacuum jacket ready to be welded shut.

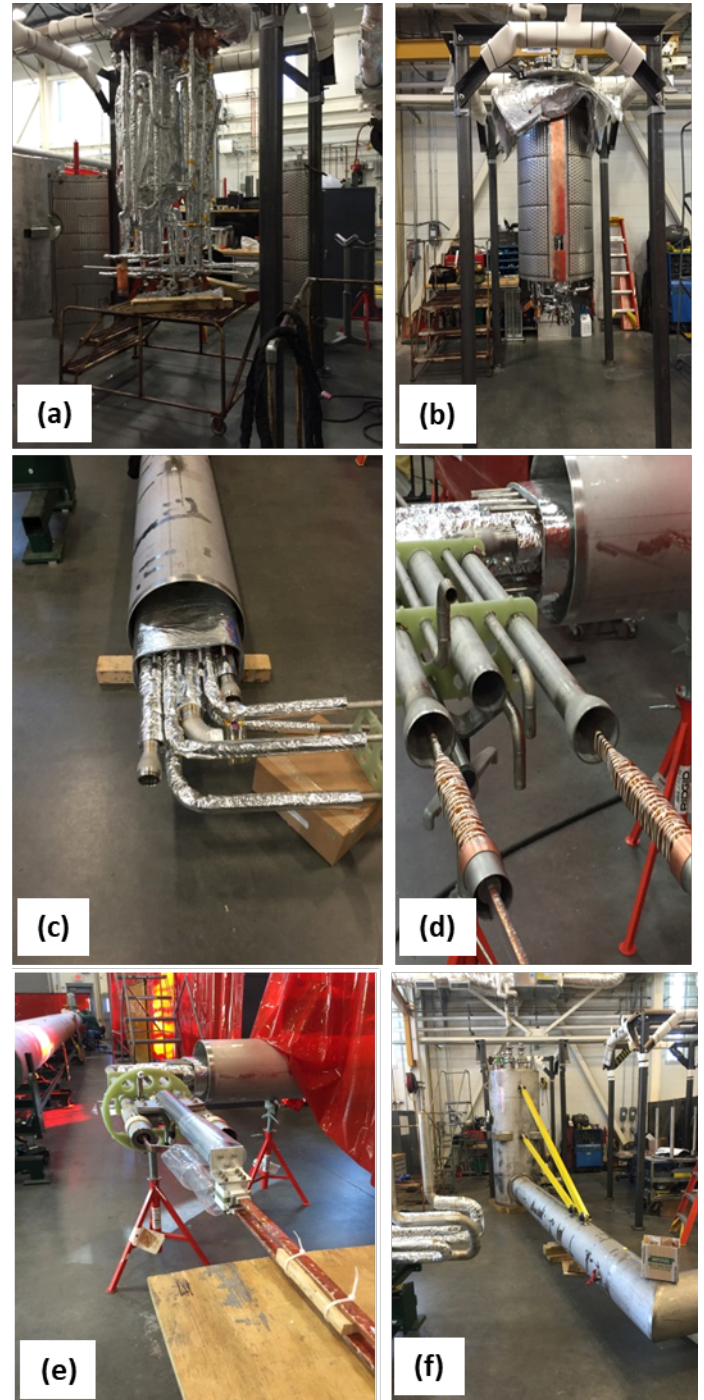


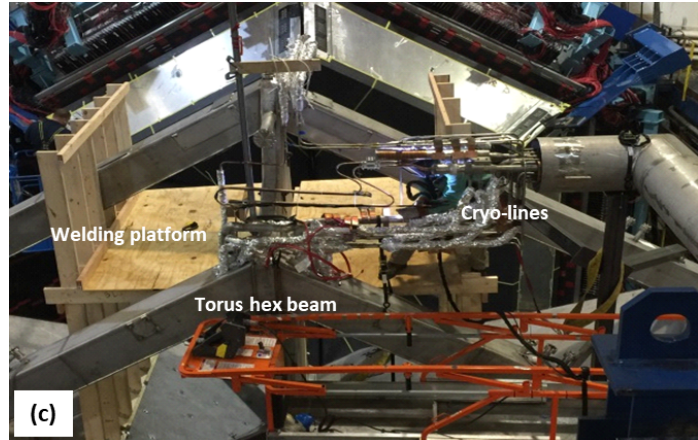
Figure 44: (a) Torus Service Tower (TST) internals insulated with MLI, (b) Thermal shield fitted, (c) Preparing the cryo-duct for attachment to the TST, (d) Superconductor splice joints and leads at the helium-vacuum interface, (e) Insulated leads, (f) Cryo-duct welded to TST body.



(a)



(b)

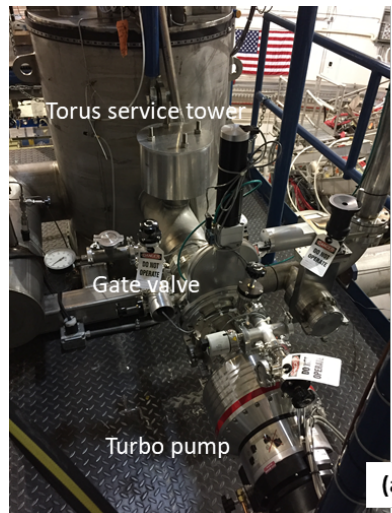


(c)

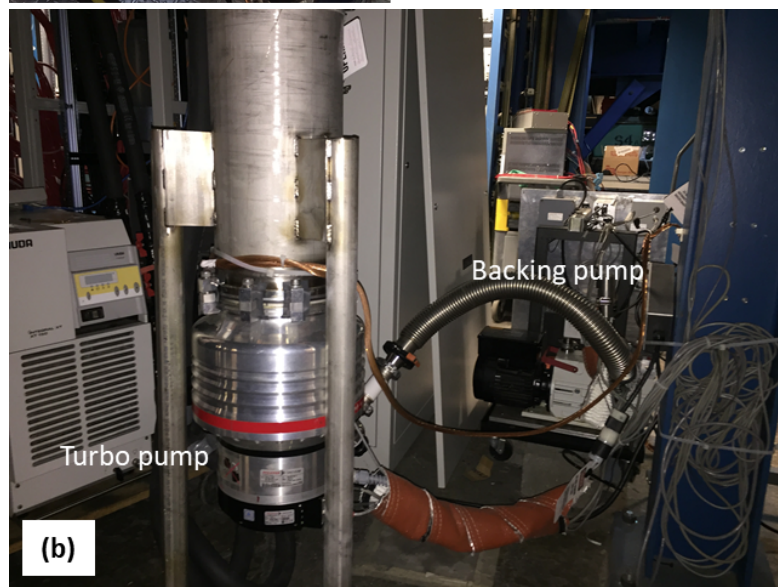


(d)

Figure 45: (a) Cold testing TST pipework, (b) TST in place on the Hall B Space Frame, (c) Cryo-lines connected between the TST and the torus; S-shaped conductor splices completed, (d) Conductor splices in the torus "chimney".



(a)



(b)

Figure 46: (a) Primary pumping system mounted on the service tower, (b) Supplemental pumping system mounted on the hex beam at the lower end of the torus.

torus.

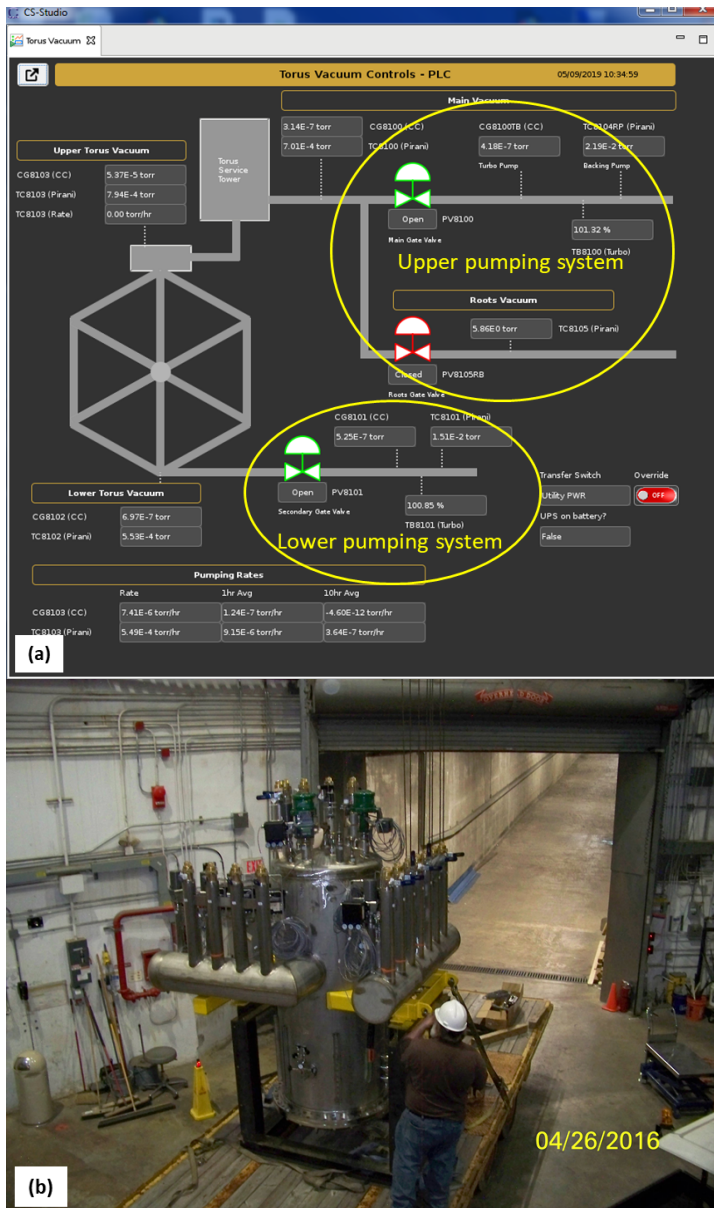


Figure 47: (a) Screen shot of vacuum pumping control screen for the torus, (b) Distribution can being delivered to Hall B, (c) Flexible copper jumpers connecting the torus water-cooled leads to the magnet vapor-cooled leads.

Solenoid

The magnet was built by Everson-Tesla Inc. (ETI) and transported by road to JLab using a purpose-built shipping cradle and vibration isolation transport fixture (see Fig. 48). To assure safe transport, several dummy runs between ETI and JLab were carried out and data on the acceleration loads were collected. These data were used for analysis of the magnet structure with temporary shipping supports.



Figure 48: (a) Solenoid in shipping cradle and transport fixture at vendor, (b) Solenoid arrival at JLab.

Upon arrival at JLab, a visual inspection was completed along with testing of the internal sensors and their wiring. The magnet was then lifted onto its installation cart on the beamline in Hall B. It was rough-aligned by the JLab survey and alignment team and the temporary shipping braces were replaced with the final supports and load cells. The Solenoid Service Tower (SST) built

by JLab was ready several months before the solenoid arrival, and was already in Hall B and roughly positioned upon the space frame above the beamline (see Fig. 49). With the solenoid on the beamline, the SST was then aligned to the solenoid. The two splices that connect the SST to the magnet were completed and instrumented with voltage taps and temperature sensors before the internal welding commenced. Pressure and leak tests followed, similar to the torus. Finally, the multi-layer insulation blankets were applied and the vacuum jacket was welded shut (see Fig. 50).

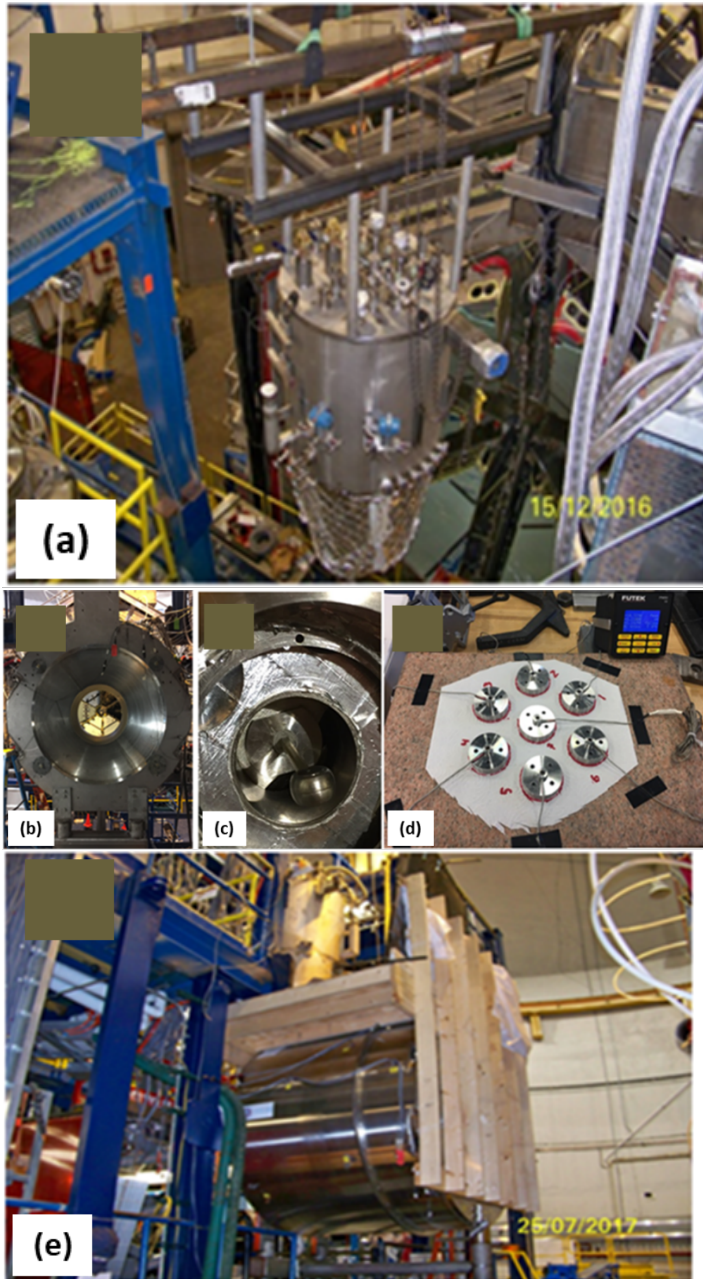


Figure 49: (a) The Solenoid Service Tower being lifted into place on the Hall B Space Frame to await the arrival of the magnet, (b) Solenoid on its cart awaiting removal of axial support shipping fixtures and installation of axial support rods, (c) One of eight axial support rods being fitted within a pocket that will then be connected to a load cell, (d) Axial support load cell readings being checked for consistency prior to installation, (e) Solenoid in position on its "cart" with a temporary wooden platform installed to allow welding of the service tower to the magnet.

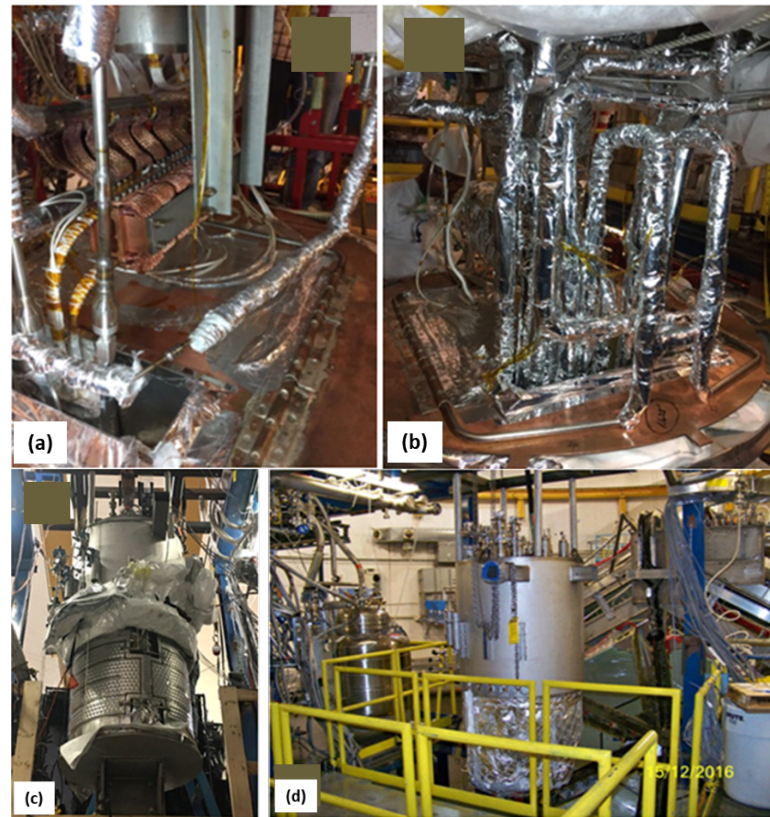


Figure 50: (a) Splices joining the magnet start and end leads to the vapor-cooled leads in the SST, (b) Splice block and cryogenic pipework wrapped in MLI, (c) Service tower thermal shield welding completed, (d) Service tower – ready to have its vacuum jacket closed up.

The magnet arrived from the vendors at the end of June 2017 and was fully installed by early August 2017. The whole installation process took less than 2 months using multiple teams working around the clock. The final installed magnet is shown in Fig. 51.

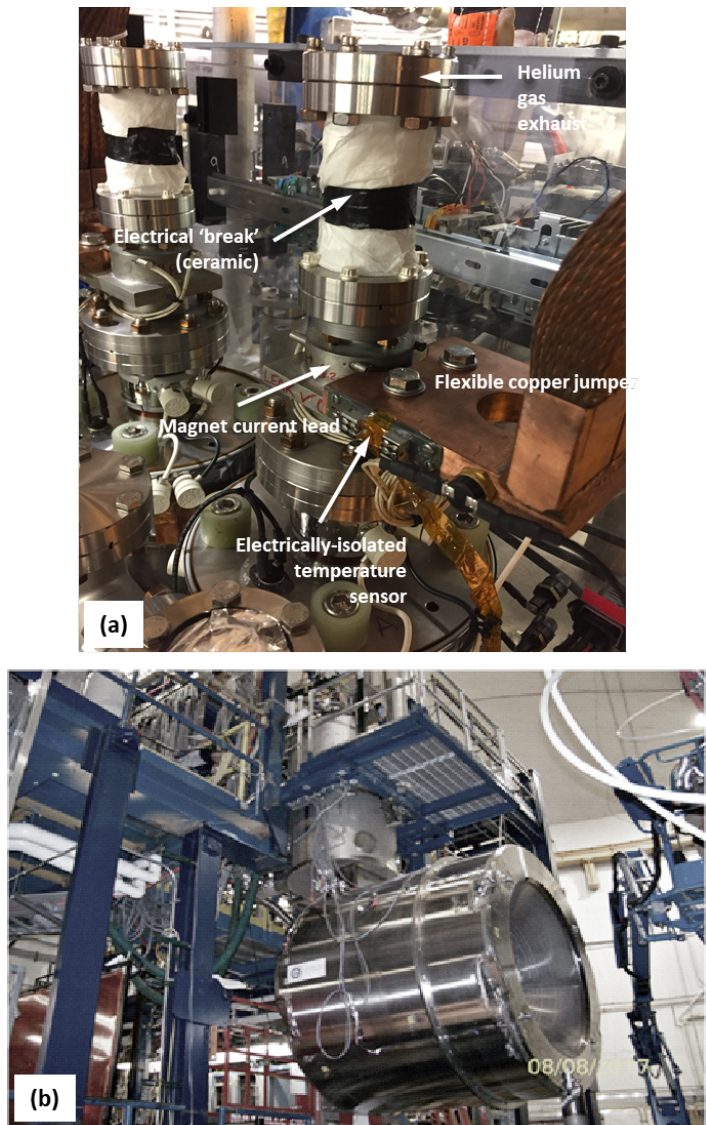


Figure 51: (a) Ceramic break fitted to the top of the magnet vapor-cooled current leads – temporarily wrapped in paper, (b) Solenoid magnet installation complete with “crow’s nest” service platform installed around the SST.

VII. COMMISSIONING AND TEST RESULTS

The vacuum spaces of both magnets were pumped down before being cooled to operating temperature. Then tests were carried out at predefined excitation currents to confirm that the overall system response was as designed. All electromagnetic and cryogenic parameters were monitored during the tests to validate the cryogenic circuit design. Additionally, each magnet was ramped to low currents to minimize its stored energy before a controlled fast discharge was initiated. This allowed the JLab team to check that all system protection mechanisms were operating as designed, thereby mitigating any further risk when the magnets were run at their full operating currents. The torus magnet reached its full operating current of 3770 A without any quenches in November 2016, while the solenoid reached its full operating current of 2416 A in September 2017 with 5 quenches in Coils 3 and 4 attributed to training quenches. The solenoid retained all its quench training.

Each magnet has its own cryogenic service tower, which is fed

from a common cryogenic distribution box. The monitoring, control, protection, power, vacuum, and cooling subsystems are similar but independent for each magnet. Although the systems are separate, a cryogenic “event” in one magnet can affect the other and vice versa since both magnets share the same distribution box [6].

Torus

Pump Down - Before the final vacuum pump down proceeded, all the OOPS were properly set to allow for vacuum jacket deflection. The pump down started gradually at about 2 psig/hr for the first 7 hours to alleviate any coil-case “ballooning” effects and to minimize any movement of the MLI. A roots blower followed by turbo-molecular pumps were used to reduce the pressure to about 10^{-4} Torr before initial cool down and several backfills with gaseous nitrogen were used to assist with the removal of water within the system. The pressure in the system reached about 5×10^{-5} Torr after cool down started.

Purification - A process piping purification process using gaseous nitrogen (GN₂) and gaseous helium (GHe) was used to clean the nitrogen and helium circuits. The nitrogen circuit only needed to be free of water and flow purged with warm GN₂. The helium circuits needed to be free of water, as well as all other contaminant gases.

The initial purification of the torus included purification of the entire Hall B cryogenic system. This included all the warm gas piping, ambient vaporizers, cryogenic transfer lines, distribution box (DBX), U-tubes that interconnect the DBX to the 500-liter helium buffer dewar, U-tubes that interconnect the DBX to the torus, the Buffer Dewar, and the torus. There are 3 cold connections at the End Station Refrigerator (ESR) that are used, 4K helium supply, 4K helium return, and LN₂ supply. There are two warm gas connections to the ESR, 300 K 4 atm helium and 1 atm 300 K return helium.

Cold-connection U-tubes at the ESR were not installed and the warm connection valves were closed. Where possible each circuit was purged with room temperature boil-off nitrogen gas for several days to drive off moisture. The warm helium supply line could not be purged this way because there is no vent on the ESR end. It is also noted that care was taken not to pressurize the helium circuits above 1 atm with nitrogen, to keep from contaminating the operating ESR. The nitrogen circuits were then pumped between 0.5 atm and 0.1 Torr three times and backfilled with nitrogen. At this point the N₂ circuits were considered clean.

The helium circuits were pumped and backfilled through the same pressure range five times. Pumping and backfilling allowed access to the small dead-end ranges of the circuits, such as the pressure transducer and relief valve lines. After pumping and backfilling the helium circuits, purging through the system was done using clean helium from the ESR and sending it back to the refrigerator helium recovery system. This recovery system has nitrogen contamination monitors to verify the level of contamination in the return gas. After the pump and backfills, the return gas to the recovery system indicated that little to no contamination was returned, thus our N₂ purge, helium pump, and backfills were deemed to have been successful and complete. A similar process but on a much smaller scale was performed for the

solenoid.

Cool Down – The unique nature of the torus structure with a cold hub and cold beams made it especially critical to minimize temperature differences between the beams and the coils. Detailed FEA calculations were done and showed that a maximum DT (temperature gradient) of 50 K between them could be tolerated during the cooling process at temperatures between 300 and 100 K for the 4 K mass. The independent nature of the LN₂ shields did not have this physical requirement. The piping of the supercritical circuit is nearly 200 m long with most of it split equally between tubes in the coils and re-coolers. Due to this long length, limited flow at room temperature can be pushed through this circuit with the 4-atm helium supplied to the hall at room temperature. To achieve the required cool down time of 3 weeks, the re-coolers were also designed to be used during the cool down process and performed well.

The cool down of the torus was carried out using variable temperature helium gas provided by the distribution box. Inside the distribution box are two heat exchangers that cool one stream of helium to 80 K. This 80 K helium was mixed with room temperature helium to allow variable temperature gas to be fed to the supercritical circuit and also the shell side of the re-coolers. This then allowed the even cooling of all the coils and the hex beams. During the cool down the maximum difference between the average coil temperature and the average upstream hex beam temperature was 12 K and it averaged about 10 K. For the downstream beams vs. the coils, the maximum difference was 25 K at the beginning, but once the flows were balanced, it averaged about 2 K. With these achieved values we were very safe compared to our allowable difference of 50 K. For safety we had the PLC programmed to shut off all cool down flow if the differences ever exceeded the allowable maximum.

To gently cool the heat shield we took 80 K boil off from the LN₂ pot in the distribution box and with an electrical heater in the U-tube between it and the TST, heated the gas to provide a controlled temperature gas to the shield. Again this was interlocked to turn off the heater and the flow if the maximum difference between any of the six coil shield outlets and the shield supply reached 60 K.

From room temperature to about 100 K the cool down rate of the torus was 0.5-0.7 K/hr. The cool down time from 300 K to about 4 K for the torus was calculated to be about 14 days assuming a maximum temperature differential across the cold mass of 30 K and a helium flow rate of 7 g/s. In reality, the cool down took longer and was carried out in several steps. During the cool down process (at about an average CCM temperature of 209 K), it was

noted (via observation of strain gauge readings on the supports) that the four torus vertical supports were apparently bending. This necessitated a slow-down in the cooling process (to about 170 K) and finally a temporary halt while measurements and strain gauge calibrations were checked. It was discovered that although some of the strain gauges were not being adequately temperature-compensated, the vertical supports were indeed experiencing some level of bending. A risk review was convened to plan the path forward and four options were considered – which included a “worst” case option that required a warm-up to room temperature to repair the vertical supports by cutting into the vacuum jacket. A spare vertical support was tested at liquid-nitrogen temperature and was demonstrated to have a more than adequate strength safety factor under bending (see Fig. 52). It was thus experimentally determined that it was safe to continue with the torus cool down, which was then resumed and the torus achieved its helium operating temperature of 4.5 K without any further issues.



Figure 52: (a) Bend testing a spare torus vertical support.

Steady State Cooling - The upstream (US) cold hex beams contain the cryogenic and electrical connections (splices) between coils, as well as the re-cooler heat exchangers. The re-coolers contain liquid helium and are connected by large tubes to the helium reservoir at 1.3 atm located within the TST. Two small tubes originate at the bottom of the TST and run through the three re-coolers, exiting at the bottom of the re-cooler outer shell. Since the liquid in the small tube is denser than the heated fluid in the re-cooler’s outer shell, a thermo-siphon is used to exchange the cooler reservoir liquid with the shell side fluid. The 1.3 atm. liquid helium cools the 3.0-atm helium before entering each coil.

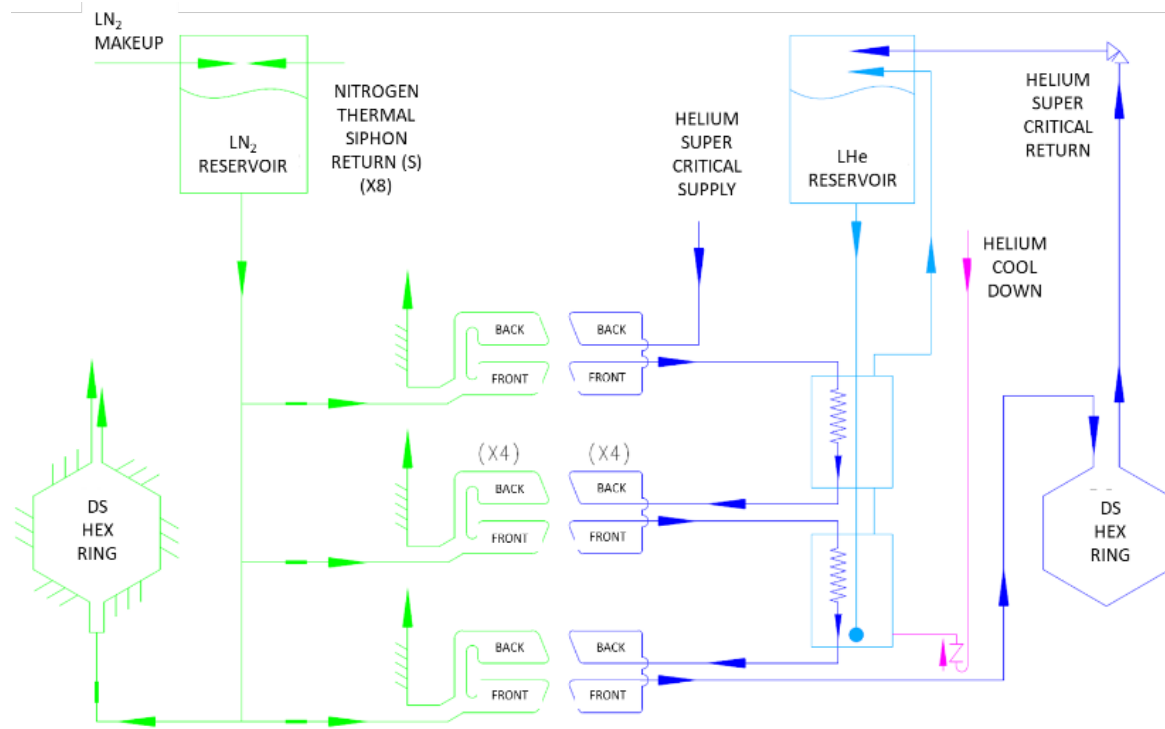


Figure 53: Simplified flow diagram of the CLAS12 torus helium and nitrogen cooling circuits.

The cooling scheme (see Fig. 53) consists of three separate flow circuits as follows:

- 1.3 atm helium circuit** – The LHe reservoir (shown in light blue) within the TST, is filled with liquid helium. LHe then flows down through the re-coolers to the blue dot shown in the figure. Thermal-siphon flow returns helium back up through the re-cooler outer shells and via the upstream hex beams.
- Supercritical helium at 3.0 atm** – This circuit (shown in dark blue) passes through a re-cooler coil within the helium reservoir in the TST. It then flows through six coil and re-cooler units and also through tubes used to cool the

downstream cold hex beams. Finally, it flows through a heat exchanger coil in the TST helium reservoir before flowing through the Joule-Thompson valve that is used to fill the TST reservoir.

- The 1.3 atm LN₂ circuit** – This circuit (shown in green) also uses the thermo-siphon effect. It has one main feed that separates into 8-parallel branches that keep each thermal radiation shield at ~80 K (see Fig. 54). Of the 8 branches, 2 branches cool the downstream hex beam thermal radiation shields, while 6 cool the coil thermal radiation shields.

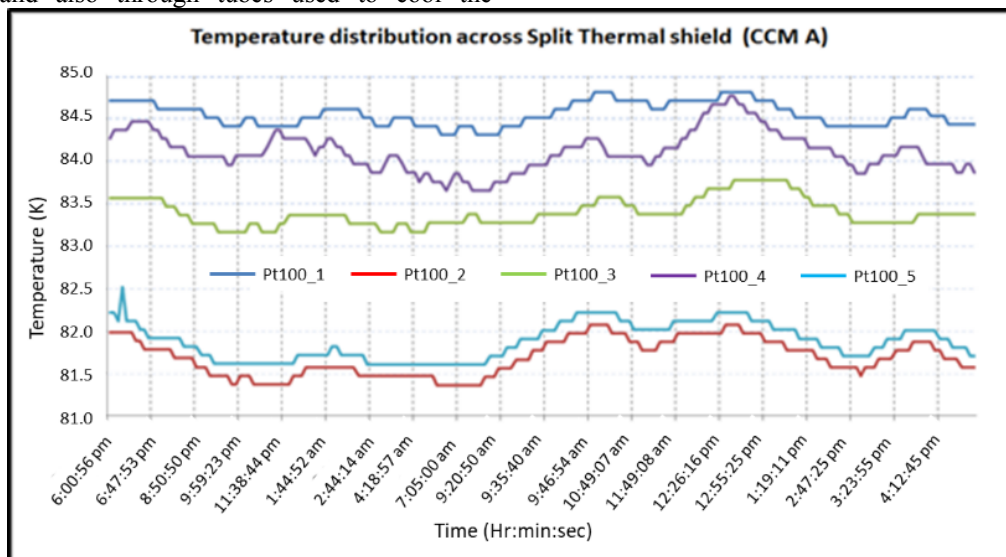


Figure 54: Steady state temperature distribution across one of the thermal shields.

Torus process safety

In Ref. [37] the worst-case scenario was considered of having a loss of vacuum (LOV) and a simultaneous magnet quench, and this work assisted in the development of the operational protocol for the cryogenic process. Pressure relief valves protect the piping systems from over-pressure during an LOV, quench, or fast dump. Five relief valves are used for the 3.0-atm cooling circuit. Three valves are located on the Hex Ring Vacuum Jackets and are set to vent at 5.3 atm; they are located strategically in the path of the CCMs and re-coolers. The remaining two valves are located on the TST and are set to vent at 4.6 atm. A check valve in the supply U-tube prevents any back pressure into the distribution box in the event of a fast dump. The 1.3-atm circuit is protected by a 2.7-atm relief valve located on the TST.

The highest system pressure for this circuit will occur during a LOV and magnet quench at the farthest point from the relief valve in the re-cooler piping. The LOV will impart a major proportion

of the energy to the 1.3-atm circuit while a magnet quench imparts a smaller proportion of energy; first to the 3.0-atm helium flow and then into the 1.3-atm system via the re-coolers.

However, the highest system pressure for the 3.0-atm circuit (during a relief event) occurs at a location buried within the coils and re-coolers, at a point in the circuit between the relief valves, where flow may go both ways. Using a simple model to estimate the system pressure rise (assuming all energy generated is transferred to the helium), the estimated pressure rise (during a fast dump) is shown in Fig. 55. It is apparent that if all the energy from the 3000 A fast dump was transferred to the helium, the design pressure of 20.0 atm of the system would be exceeded. However, using calculations from a more detailed model, it was demonstrated that the 20.0-atm pressure rating of the pipes would not be exceeded in the torus circuit due to the distribution of energy throughout the entire system. Our commissioning tests have since validated the results from this analysis.

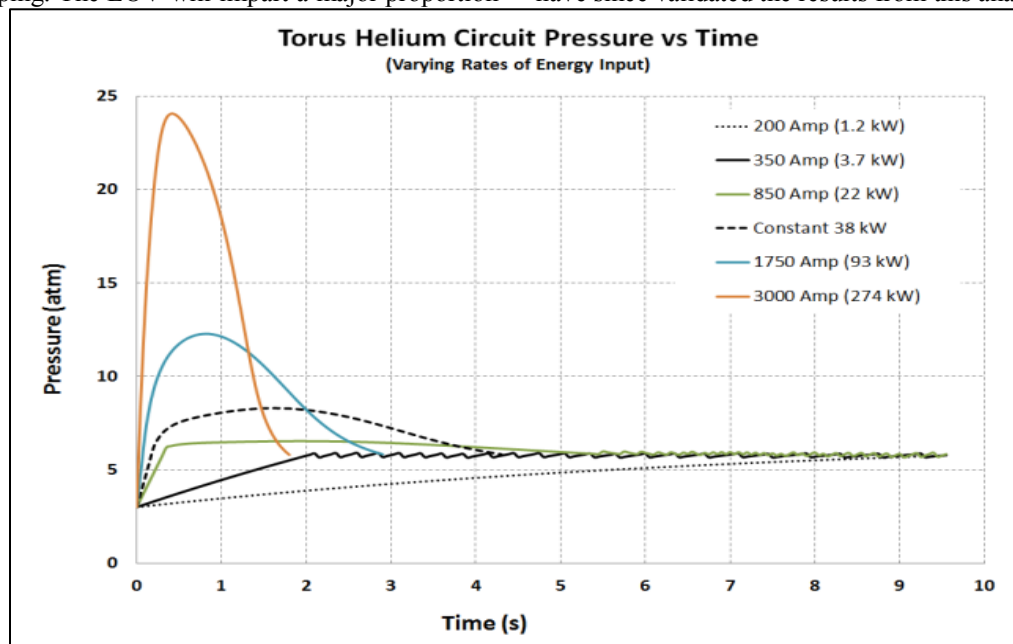


Figure 55: Estimate of torus helium circuit pressure with time at increasing operating currents based on the simple model.

System Energy Balance Modelling – As part of the commissioning process, system heat loads were estimated for each of the energization states. A Detailed Predictive Model (DPM), based on the Wilson model, was used to calculate the heat loads [16]. The DPM assumes that a fast dump would release all of the magnet's stored energy (see Fig. 56). The DPM predicted that the torus could be operated safely, up to the nominal operating current of 3770 A, for all energization states and fault scenarios.

After energization and initial testing at low currents, the magnet was ramped up to 3000 A and parked. An unexpected fast dump was triggered by the PLC comparator controls during this period. The team took advantage of this unexpected event and having reviewed this 3000 A fast dump data, the results clearly indicated that the magnet was safe to also fast dump from 3770 A. These results were also used to calibrate and validate the Detailed Predictive Model.

A maximum average temperature for all the CCMs was recorded as being <40 K during the 3000 A fast dump. The tests and analyses performed validated the pressure relief and the torus cryogenic system design thus confirming that the system was indeed safe.

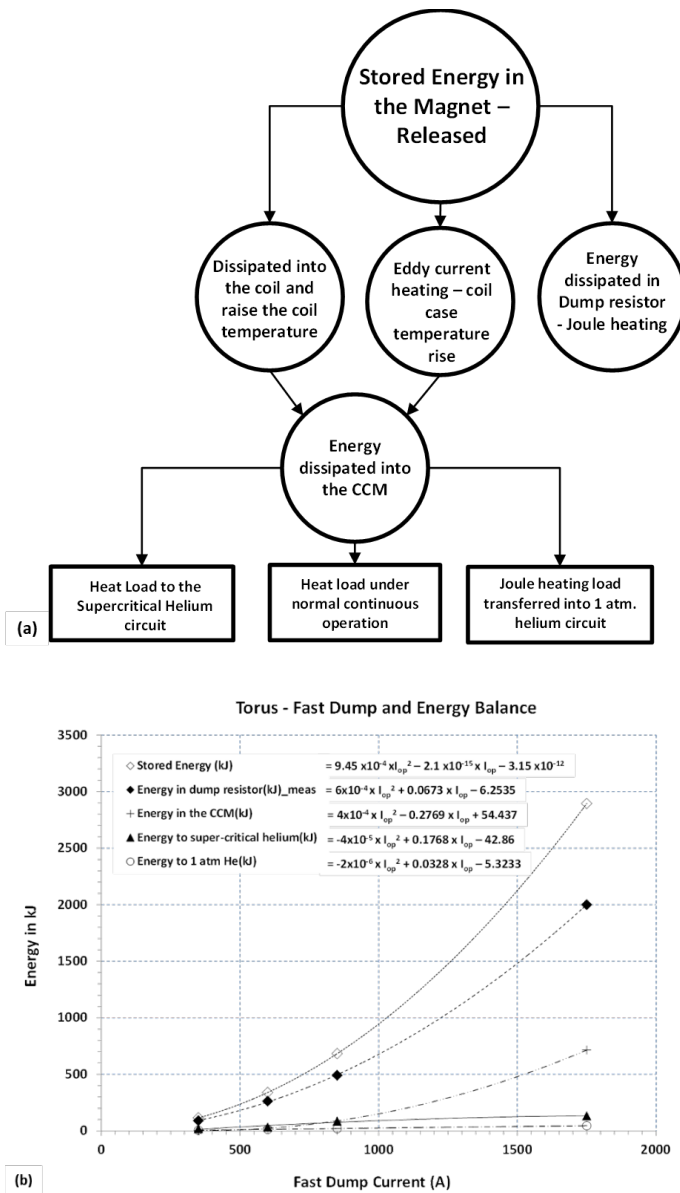


Figure 56: (a) Flow diagram representing the extraction of stored energy in the magnet during a fast dump or in the event of a quench, (b) Plots for the energy calculated based on measured data during fast dump events at various operating currents up to 1750 A (approximated with a polynomial fit to the measured data points).

Solenoid

Pump Down and Purification

The pump down of the solenoid was much faster and easier because the magnet has much less surface area, an overall smaller size, and better conductance between the turbo pump and the magnet. Purification was done similarly to the torus using a GN₂ purge for several days, followed by 5 pump and backfills, then flowing to the purifiers while monitoring the contamination level.

Solenoid Cooling

This five-coil magnet is also conduction cooled by 4.5 K helium, but unlike the torus coils, the heat is directly transferred to liquid instead of supercritical gas. The cool down system for the solenoid is the same one as for the torus and was used while the torus was at 4.5 K. Similar interlocks and controls were used to assure safe cool down. The magnet's liquid helium cooling

channel is located between the two main inner coils and runs around the inner diameter of the bobbin. The thermal shields are cooled using the boil-off from the magnet LHe reservoir. The magnet is held at its operating temperature by conduction cooling via a thermo-siphon helium circuit from the magnet reservoir (see Fig. 57). Adequate instrumentation with redundancy is provided to monitor and control the magnet cool down and steady state operation.

Pre-commissioning checks on all subsystems, controls, and instrumentation were carried out for each magnet prior to starting the commissioning process. The torus and solenoid were cooled in 2-steps. Variable temperature gas was used to cool from 300 K-100 K, followed by LHe to 4.5 K.

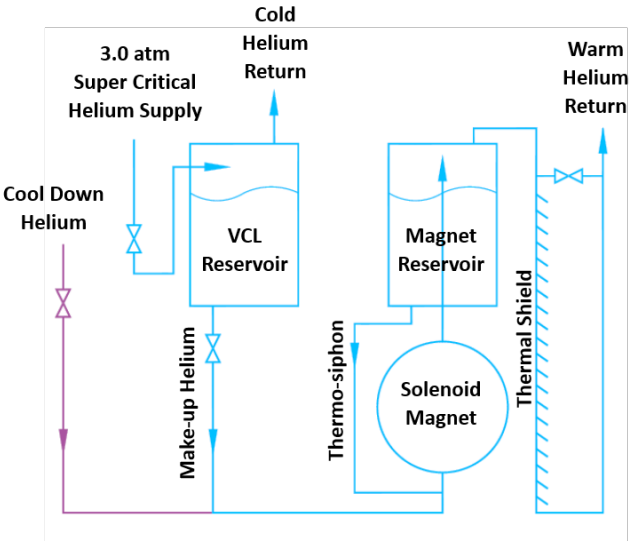


Figure 57: Simplified cooling circuit schematic for the solenoid.

The inlet temperature to the coils, average coil, and outlet temperature were monitored. The maximum cooling rate was limited to 2 K/hr (see Fig. 58).

The experience with magnet cool down for both systems can be summarized as follows:

- Total time = 43 days (torus), 23 days (solenoid);
- Cooling time = 19 days (torus), 23 days (solenoid);
- Helium temperature controlled at 45 K below the maximum metal temperature for the torus and between 35 K and 60 K below maximum metal temperature for the solenoid;
- The maximum allowed metal temperature differences for the torus was limited to 50 K, while for the solenoid it was 46 K. In practice the maximum temperature differences were controlled to about 25 K for the torus and about 40 K for the solenoid;
- Cool down helium flow rate for the torus was 6-7 g/s and 5-6 g/s for the solenoid.

At steady state the solenoid magnet itself requires only 0.4 g/s of liquid helium for its cooling. This flow was measured directly using a room temperature flow meter. This flow rate does not include the amount of flow needed for the VCLs, the lead reservoir, or the primary supply and return U-tubes.

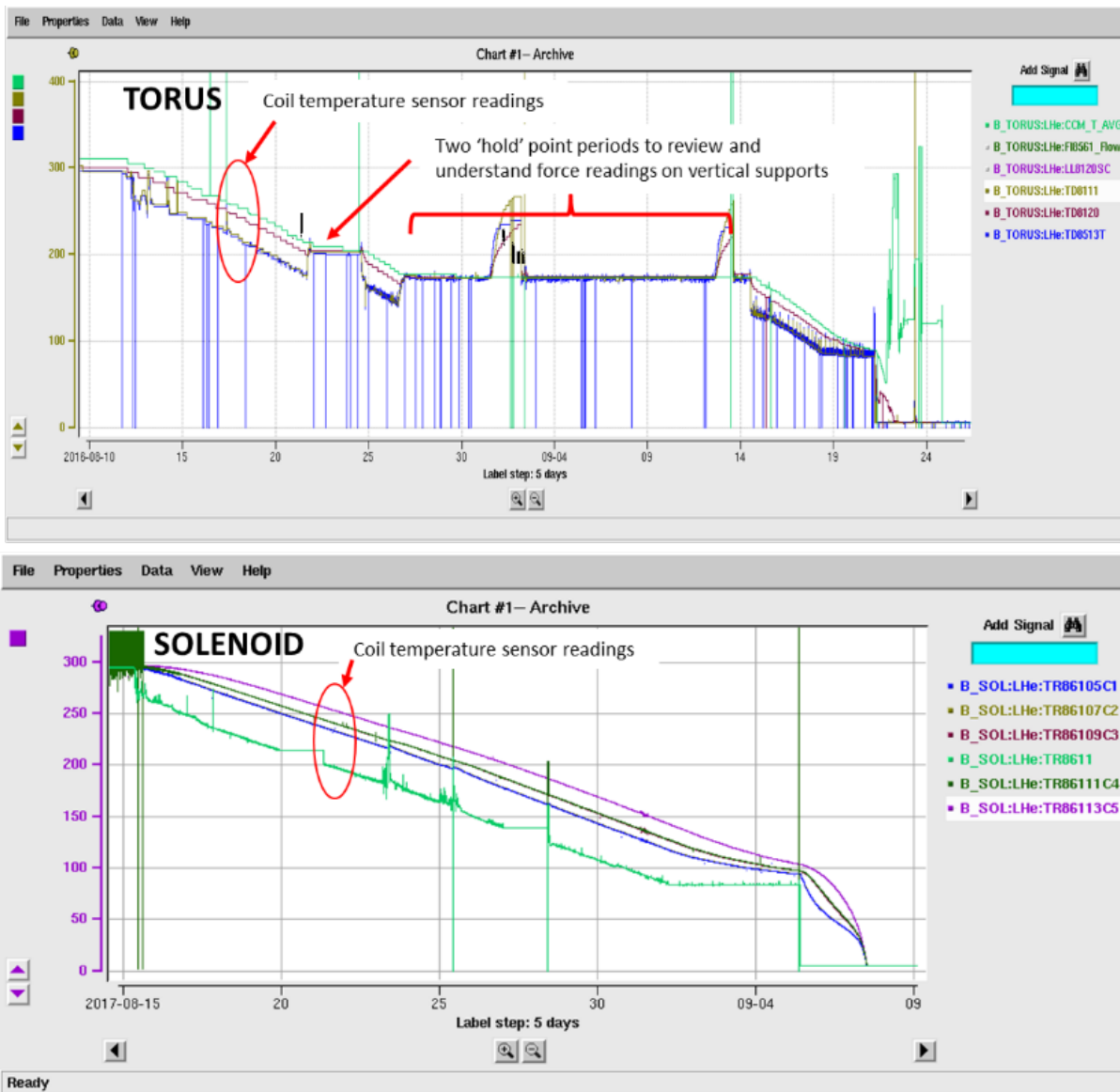


Figure 58: Torus and solenoid cool down (torus cool down: Start-August 12, 2016; Complete-September 22, 2016 and solenoid cool down: Start-August 5, 2017; Complete-September 7, 2017).

During commissioning, [38] both the torus and solenoid were energized in steps to full operating current. Predetermined fast dumps were also carried out to check on the instrumentation and proper functioning of the magnet protection. Typical temperature increases of the torus and solenoid magnet coils during ramp up and down to and from full operating current are shown in Fig. 59

and are a result of eddy current heating within the coils themselves. The temperature increases were modest (no higher than about 0.3 K) and well within the calculated 1.2 to 1.5 K temperature margin of the coils, but were nonetheless used to modify the ramp rates for both magnets to minimize eddy current heating.

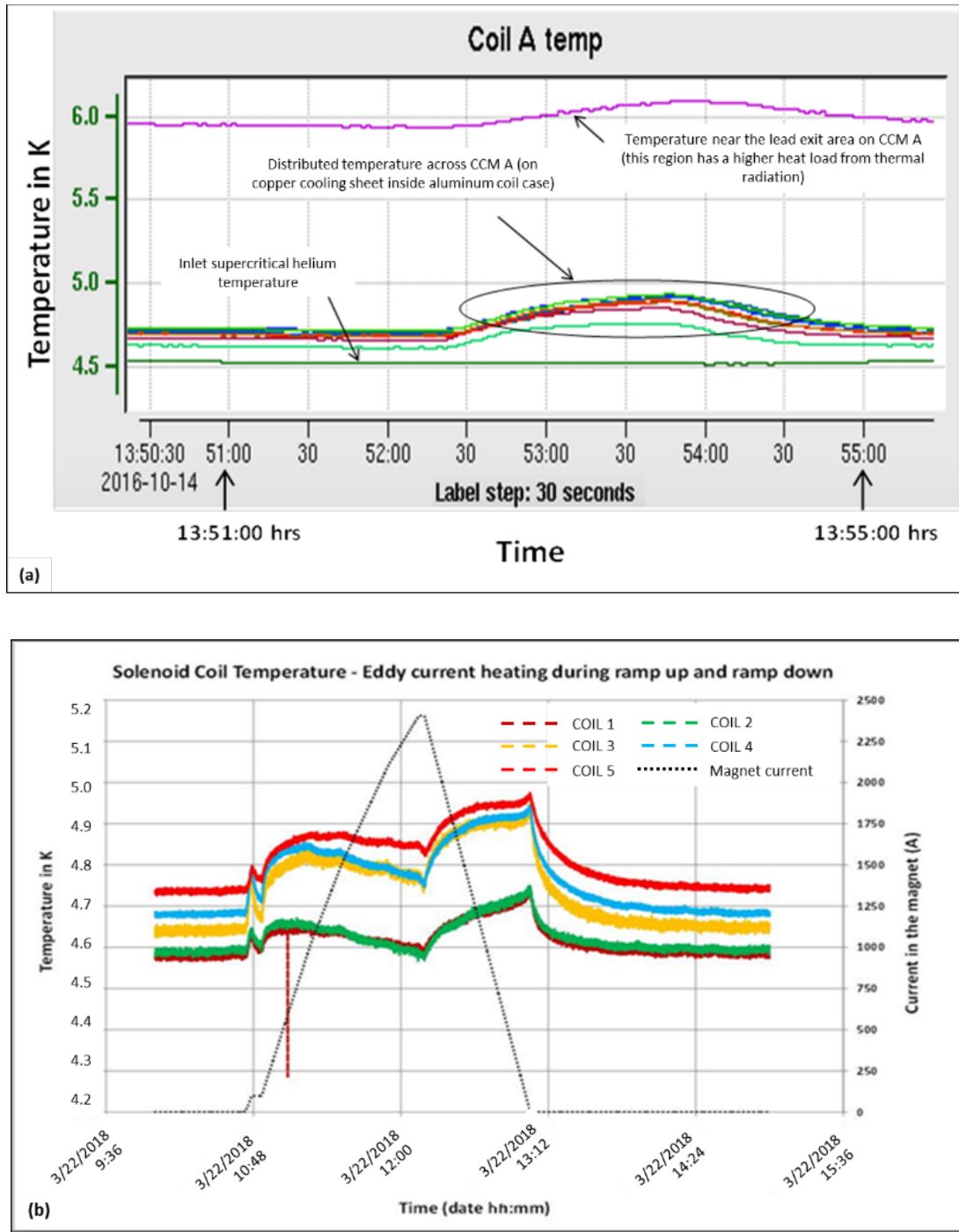


Figure 59: (a) Torus CCM B temperature rise during a ramp to 150 A at 2 A/s due to eddy current heating, (b) A typical plot of temperature rise in the solenoid coils during normal ramp-up and down.

As part of the commissioning process, several fast dumps were carried out at low stored energies in the magnet and were found to match well with the predictive models. All tests carried out indicated that both magnets had more than adequate safety

margins with regards to pressure relief of subsystems and coil temperature rise. The coil temperatures recorded during a fast dump event, 3000 A (torus) and 2047 A (solenoid), are shown in Fig. 60.

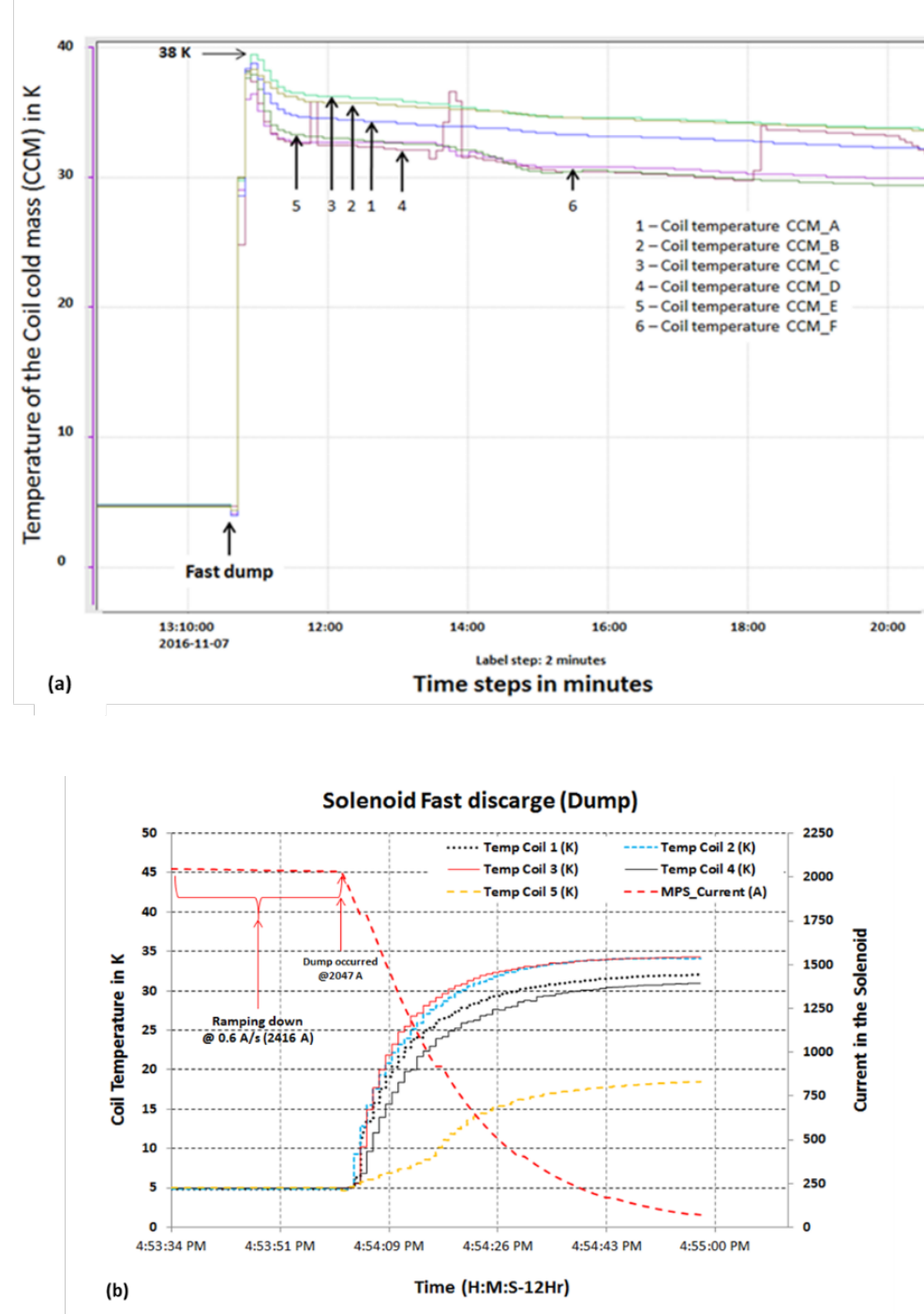


Figure 60: Coil temperature rise - during a fast dump (a) Torus, (b) Solenoid.

There is a level of electromagnetic coupling between the torus and solenoid coils [25]. As the torus is ramped to full field (3770 A) Fig. 61a shows the change in the OOPS load cell readings for the torus CCM-A. This change in force is small and due to a slight mechanical asymmetry in the spacing between the 6 coils. The solenoid radial and axial load cell readings also change during a ramp up of the solenoid to its full operating current of 2416 A, followed by a controlled ramp down to zero amps (see Fig. 61b). Based on the defined load cell limits, the force experienced by the torus coil within its vacuum jacket during energization is not high

enough to initiate a controlled ramp down of the magnet. This behavior is demonstrated by all 6 torus coils with only minor variations depending on the location of the coil on the magnet due to gravity-loading. This behavior was also noted to be extremely repeatable following many cycles of magnet energization and de-energization. For the solenoid, it is encouraging to note that all forces revert back to almost the original values after de-energization, illustrating linear response of the coil support structures. It has also been shown from subsequent runs that this process is very repeatable.

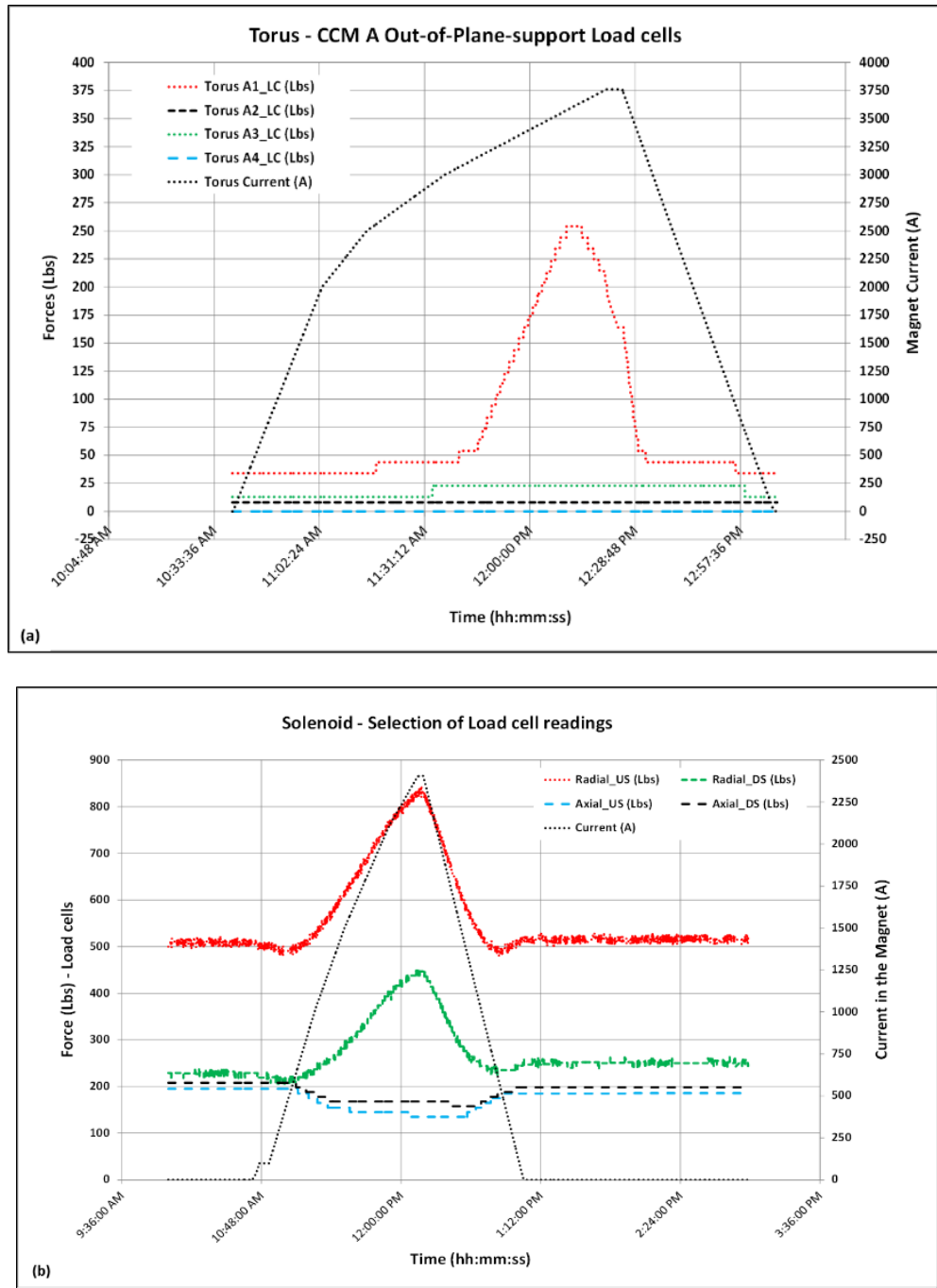


Figure 61: (a) Torus – Change in the torus CCM-A OOPS load cells during ramp up to the full operating current of 3770 A, followed by a controlled ramp down to zero amps, (b) Solenoid - Change in the radial and axial load cells on the solenoid during a ramp up to the full operating current of 2416 A followed by a controlled ramp down to zero amps.

VIII. FIELD MAPPING

Torus

Forward tracks of charged particles (with angles between 5° and 40° of a conical shape in the forward direction) are momentum analyzed by passing through the magnetic field of the torus. The magnet provides an $\int B \cdot dl$ of almost 3 T-m at 5° falling to about 1.0 T-m at 40° . The design requirements for the field mapper are listed in Table XXIX. Such forward tracks will first traverse the

High-Threshold Cerenkov Counter (HTCC) [2] and then enter the first Drift Chamber [39] at a distance of 2.1 m from the target. The track continues through the magnetic field region and its trajectory is measured in two additional Drift Chambers located at 3.3 m and 4.5 m from the target, respectively. The three regions of Drift Chambers are expected to have spatial resolutions of about 300 μm per layer, which allows determination of the momentum to better than 0.5% accuracy. This sets the requirement that we know the $\int B \cdot dl$ to an accuracy of better than 0.3% at small angles.

The field was mapped at four locations within each coil sector (i.e.

between coils) – one measurement at a radius of 30 cm and three measurements at a radius of 46.5 cm but at different Φ angles, as well as within the bore. Multiple measurements were made at each of these locations along the z -axis – i.e. in the direction of the beamline. The mapping equipment consisted of a digital voltmeter, 2-in diameter carbon tube referenced to survey points, three single axis calibrated Hall probes (one for each of the x , y , and z axes) positioned in a cylindrical block of Delrin® spaced 5 cm apart in the z -direction, and a control system (for motion, data-recording, and interlocks) [40]. A commercially available Group 3 MPT-141 series of transverse Hall probes with a DTM-151 Tesla-meter was used for the field measurement. The measurement accuracy of the probes and meter at 25°C, with a shielded cable length of 300 mm \times Ø6.5 mm, is $\pm 0.01\%$ of the full scale reading. The Hall probes are temperature compensated and were also surveyed to a positional accuracy of 0.040 mm within the Hall probe holder. Precisely machined plates were attached to

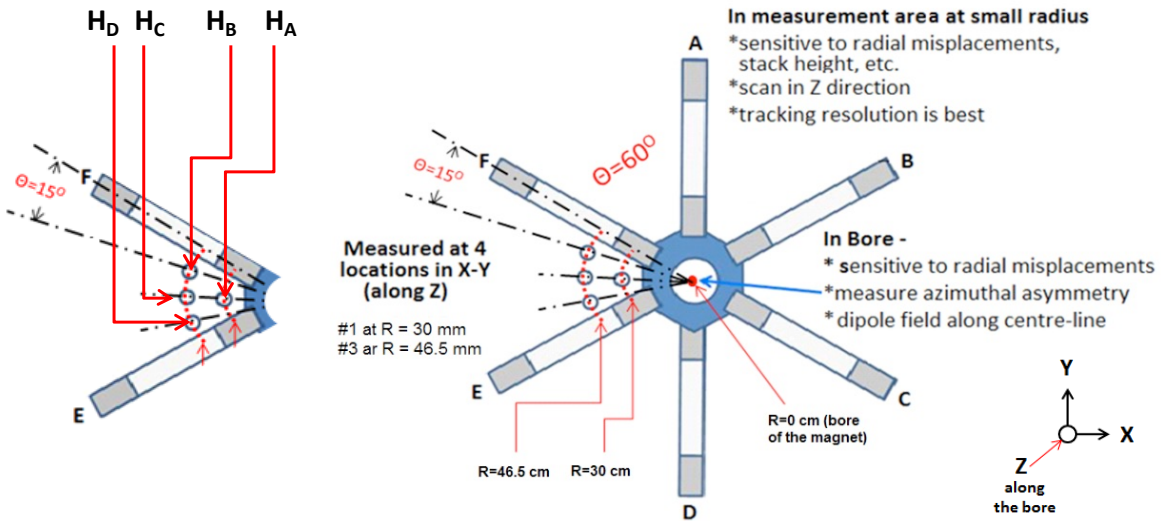
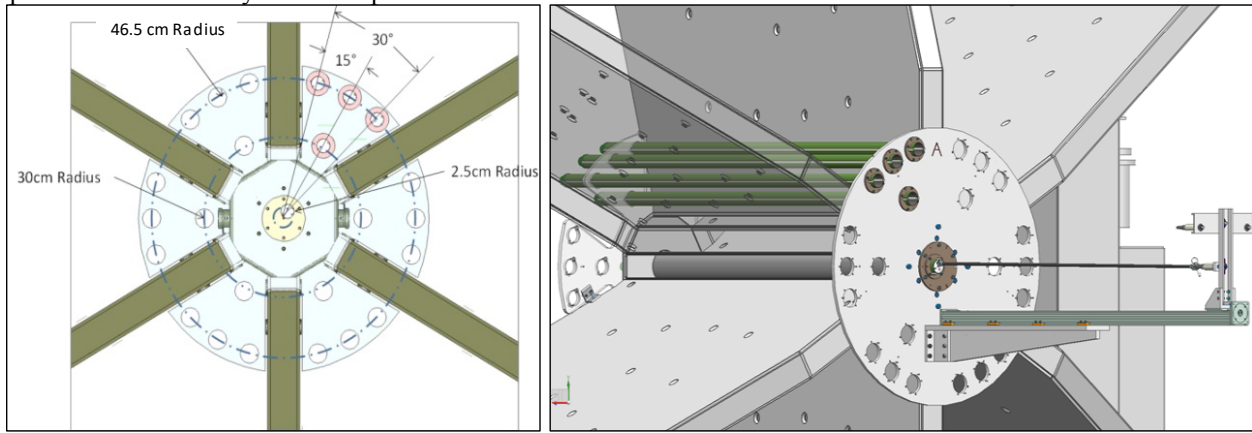


Figure 62: Torus magnetic field measurement locations – 4 locations in each sector and 7 locations in the bore (1 in the center and 6 spaced 60° apart at a radius of 2.5 cm) – field measured at 5 cm increments in z (along the beam axis) along with the torus magnetic field measurement locations (H_A , H_B , H_C , and H_D are within each sector, i.e. between coils).

The magnet field map was created using the original electromagnetic model. This model included thermal contraction effects but was based on a nominal coil design that did not include the real effects of dog-boning, the shimming, or compaction in the areas of tight bend radii.

As stated earlier in the coil fabrication discussion, spacers were

added prior to the first potting to allow more accurate and consistent conductor positioning especially closer to the hub. Data from the optical surveys allowed better knowledge of the actual positioning of conductors within the coil (see Fig. 63). This was then used to create a new electromagnetic model of the coil. That model was compared with data from the field map.



Figure 63: A close-up view of a coil near one bend after the 1st epoxy impregnation to allow data capture of the location of each turn in the coil.

Torus Design Model and Analysis: The torus model coil design was carried out using the commercial OPERA-TOSCA software from Cobham and field maps were produced as the baseline for the magnet field measurement (see Fig. 64). All design models were analyzed utilizing cold (contracted) dimensions with the magnet at its full operating current of 3770 A. The mapping of the field was carried out at 3000 A and the model data was scaled from 3770 A to 3000 A. The measured results obtained were significantly different from the original model data. The results were analyzed to calculate the “distortion field” – i.e. the difference between the measured and calculated field values using a chi-squared function (χ^2) that compared the measured data deviation from the nominal modeled field data [42].

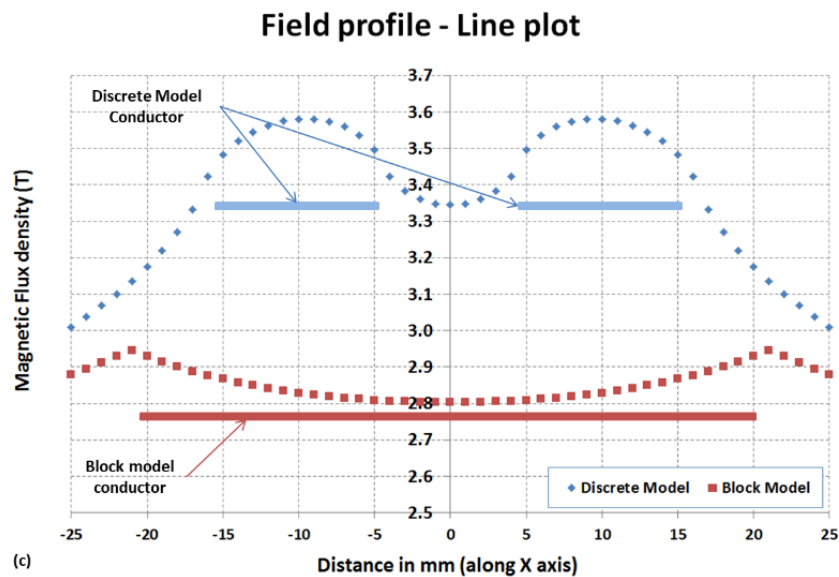
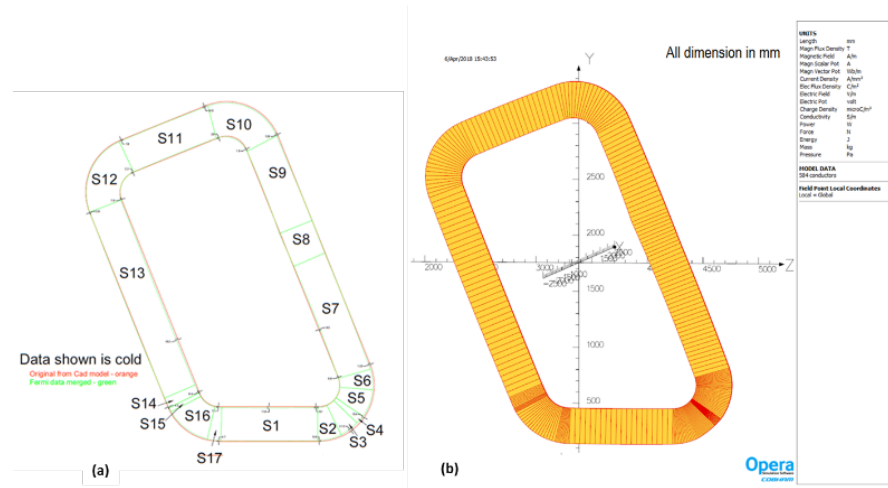


Figure 64: Single pancake of one torus coil (a) Coil survey points from 17 sections in the coil, (b) The design model prepared in Opera® with 17 sections and further discrete subsections, (c) Magnetic flux density variation near and though the coil case of the torus for a simplified version of the conductor (assuming one large contiguous conductor block) and a refined discrete model where the two coil pancakes are modeled individually with current flow only within the superconducting Rutherford cable.

The magnetic field modeling was improved via a 4-stage process:

- *Stage I: Symmetric “Block Model”* - Symmetric ideal coil model (nominal with cold coil dimension, 2 pancake coils simply modeled as one large contiguous block);
- *Stage II: Asymmetric Block Model*- Block model combined with relocated coil position;
- *Stage III: Symmetric “Discrete Model”* - Symmetric coil model with surveyed conductor location (with cold coil dimension), with 2-individual pancakes; Current in individual pancakes considered;
- *Stage IV: Asymmetric Discrete Model* – coil model with surveyed conductor locations combined with relocated coil positions.

The absolute field data plot is presented in Fig. 65. The plots show that the variation in the magnetic field distribution is about +4.96 % for the block model and about -0.9 % for the discrete model in a sector when compared to the measurements.

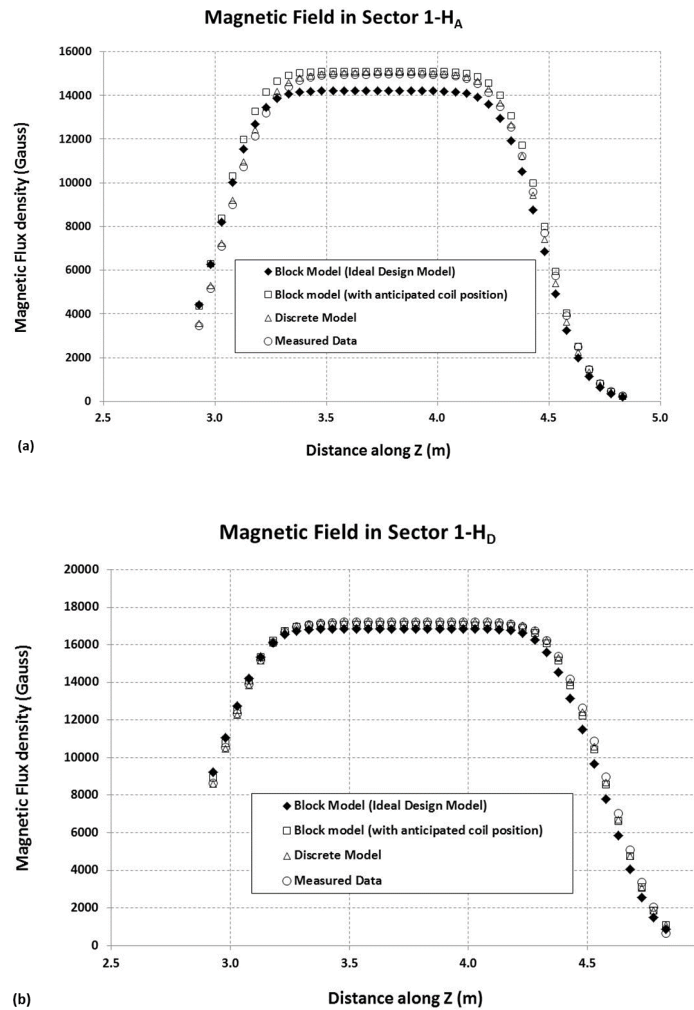


Figure 65: Magnetic flux density distribution (a) sector 1 - H_A (b) sector 1 – H_D, between block model – symmetric, asymmetric, and “discrete model” compared with measured data.

Summary of findings - At distances far from the hub and coils, all models accurately represent the field, but since the detector needs a model that accurately represents the field at small angles (near the hub), as well as over a large azimuthal angle in ϕ (from one coil to the next), only the discrete model should be used. Work continues to confirm that the $\int B \cdot dl$ is known better than 0.3 % accuracy at small angles.

- a. The percentage variations cited are for one-to-one comparisons using two-dimensional percentage analysis (*block model and discrete model*) and the averages were calculated separately based on χ^2 .
- b. Average inner (30 cm radial position) measurements indicate a 0.5% deviation from the measured data.
- c. Average outer (46.5 cm radial position) measurements indicate a 0.05% deviation from the measured data.
- d. Fluctuations in the inner measurement deviations are consistent and attributed to the effect of a 1.5 mm change to the outer radius of the coil shape.

An additional benefit of adopting the detailed model was to allow us to re-calculate the peak field on the torus coil; the peak field increased by just over 1% from 3.58 T (using a simple model) to 3.62 T (using the detailed model) confirming that the load lines shown earlier are still valid.

Solenoid

Measurements were carried out to establish the following:

- a. To quantify the magnetic length of the solenoid;
- b. To verify the high homogeneity region (over a 25 mm diameter x 40 mm length cylinder) at the center of the magnet;
- c. To measure the magnetic fringe fields at the specified detector locations.

The torus mapper was adapted for the field mapping of the solenoid magnet. The external fixture holds the 2-in diameter carbon fiber tubes at precise x-y positions and uses a linear stage drive to move the probes in the z-direction. The Hall probe holder was placed within the carbon-tube in order to zero the z-position of the linear slide before the start of the z-map for the particular location in question. The z-map consisted of driving the Hall probe holder in 5 cm steps along z and pausing for 5 s for the Hall probes to settle before recording the probe data for each of the 3-sensors. Figure 66 shows the typical arrangement for the solenoid magnet field measurement along the bore and off-center locations.

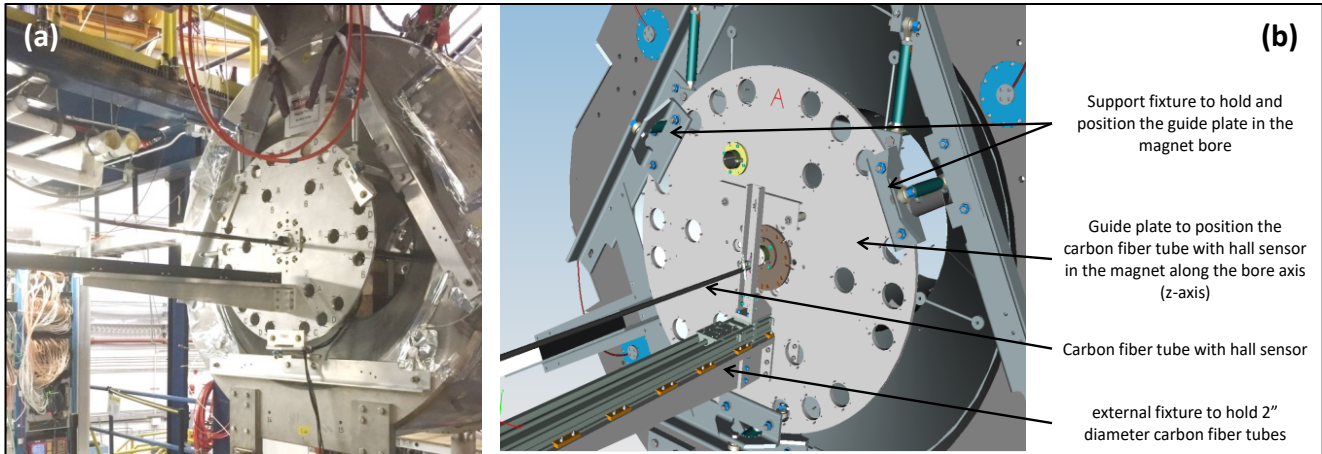


Figure 66: Typical arrangement for the solenoid magnet field measurement along the bore and off-center locations.

During commissioning of the solenoid magnet, the field mapping was carried out at different operating currents in order to confirm the design specifications. Field mapping was performed along the z direction at 9 locations; one at the geometrical center of the magnet and at 8° to 45° positions at a radius of 12.5 mm. The magnetic field was also measured along the z -axis at a 30 cm radius at a 60° angle from horizontal. To verify the field homogeneity of the magnet, measurements were taken at the center of the magnet at 10 mm intervals along the z -axis.

The magnet length, L , defined as $B_0^{-1} \int B dl$ was measured to be 1.41 m. The measured homogeneity, $\Delta B/B_0$, over a 40-mm-long \times ϕ 25 mm cylinder was better than 300 ppm and satisfied the present physics experimental requirements. To achieve the desired 100 ppm for planned future polarized target experiments, the JLab Target Group is intending to design and install small superconducting corrector coils that will be positioned directly over the target. Fringe field measurements at the detector locations were carried out using a hand-held field probe and a template board to help position the probe.

The central field of the solenoid is 5 T, but the Hall sensors were calibrated only to 3 T. Therefore, field mapping was limited to 3 T (corresponding to an operating current of 1450 A). The central field at higher currents was verified using an NMR probe.

Another limitation of this mapper was the extent to which it could map in the z -direction, as the linear stage was limited to about 1.9 m. The measured field over this length was compared with the model data to find the effective length of the magnet. The field mapping results are summarized in Table XXX.

TABLE XXX
 SOLENOID – REQUIRED AND MEASURED PERFORMANCE PARAMETERS

Performance Parameter	Broad Specification	Actual Measured
B_0	5T	5.0 T
$L = B_0^{-1} \int B dl$ (B_0 field at the center (0,0,0) of solenoid)	$L = 1$ to 1.4 m	1.41 m
Field uniformity in target area	$\Delta B/B_0 < 10^{-4}$ in cylinder 25 mm diameter \times 40 mm length (100 ppm)	318 ppm <i>(to be improved using superconducting corrector coils around the target)</i>
Field at HTCC PMT locations	$B < 35$ G - for the four HTCC PMT locations	$B = 6$ -22 G
Field at CTOF PMT locations	$B < 1200$ G - for the two CTOF PMT locations	$B = 43$ -1041 G

The mapped data was compared with the as-wound cold-contracted (4.5 K) coil model data. There is still a slight discrepancy between the two data sets for the central field and the field at a radius of 30 cm. The model uses 208 block conductors, as follows - each layer for the inner and intermediate coils is assumed to be one block conductor, while each layer for the shield coil has been split into 2 block conductors:

- 2*42 layers for inner coils (84 block conductors);
- 2*46 layers for intermediate coils (92 block conductors);
- The shield coil has 16 layers, but each layer was divided into 2 block conductors (32 block conductors).

The discrepancy between the model and measured data could be attributed to coil positioning errors or coil movement during energization. The theoretical model is being improved to better match the mapped data. One of these improvements involves moving the inner and intermediate coils radially or axially - these results are shown in Figs. 67 - 70. Figure 67 shows the comparison of model, mapped and data produced with an inner coil axial movement; Figure 67a shows the field in the central region while Fig. 67b shows the off-axis field data. It is clear from Fig. 67 that an inner coil axial movement alone is not sufficient to reproduce the mapped data. Figure 68 shows the same data with a radial movement of the inner coils and again the mapped data and data modeled with this radial change do not match. Figures 69 and 70 show similar data with the middle (intermediate) coil moved axially and radially. It is clear from the manipulation of the modeled data that a single coil movement alone cannot fully explain the variation between the modeled and mapped data. A combination of inner and middle coil movement together with a movement variation in the shield coil might result in a better match between model and mapped data. This work is still in progress.

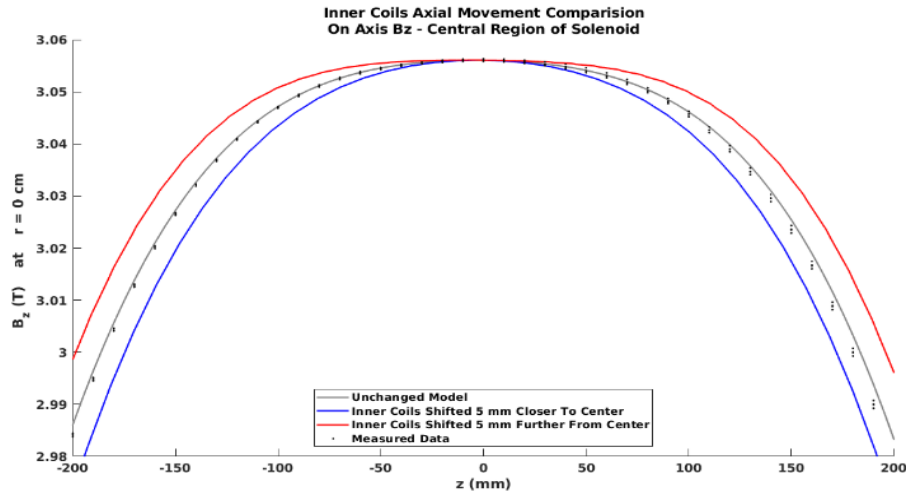


Figure 67: (a) Comparison of model and mapped data at $r=0$ cm with the inner coils moved axially.

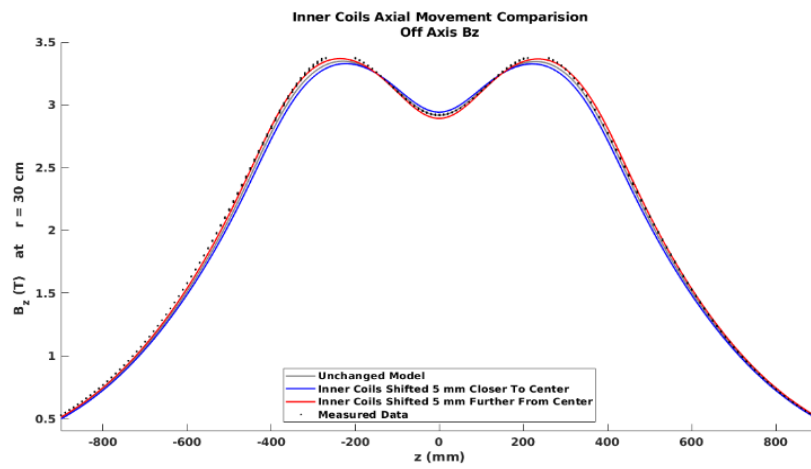


Figure 67: (b) Comparison of model and mapped axial data at $r=30$ cm with the inner coils moved axially.

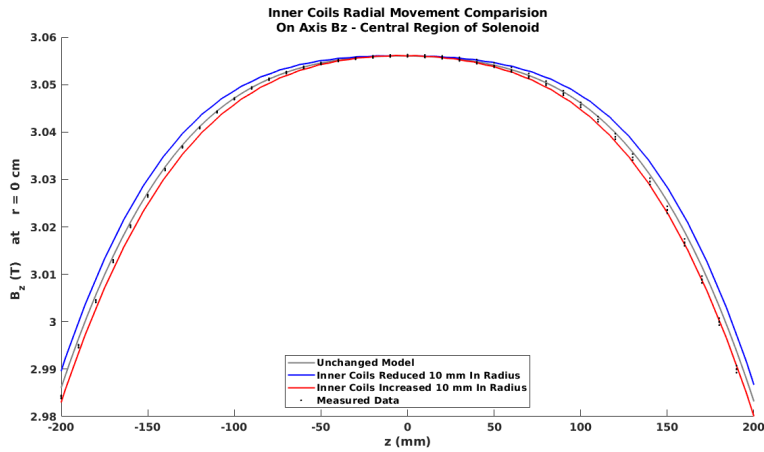


Figure 68: (a) Comparison of model and mapped data at $r=0$ cm with the inner coils moved radially.

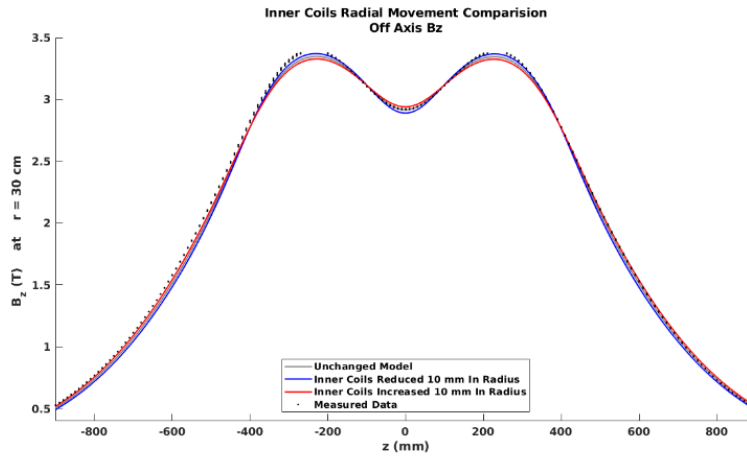


Figure 68: (b) Comparison of model and mapped axial data at $r=30$ cm with the inner coils moved radially.

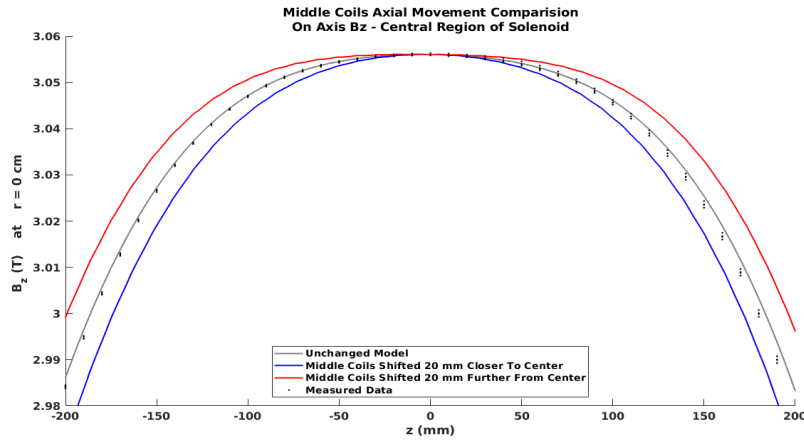


Figure 69: (a) Comparison of model and mapped data at $r=0$ cm with the middle (intermediate) coils moved axially.

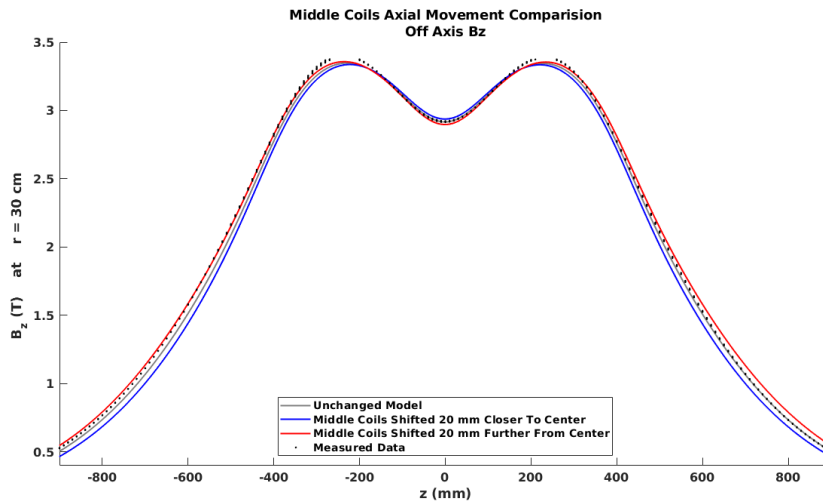


Figure 69: (b) Comparison of model and mapped axial field data at $r=30$ cm with the middle (intermediate) coils moved axially.

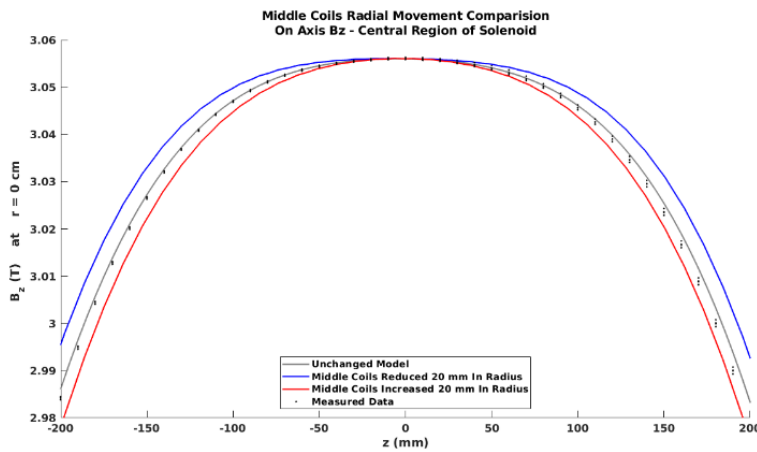


Figure 70: (a) Comparison of model and mapped data at $r=0$ cm with the middle (intermediate) coils moved radially.

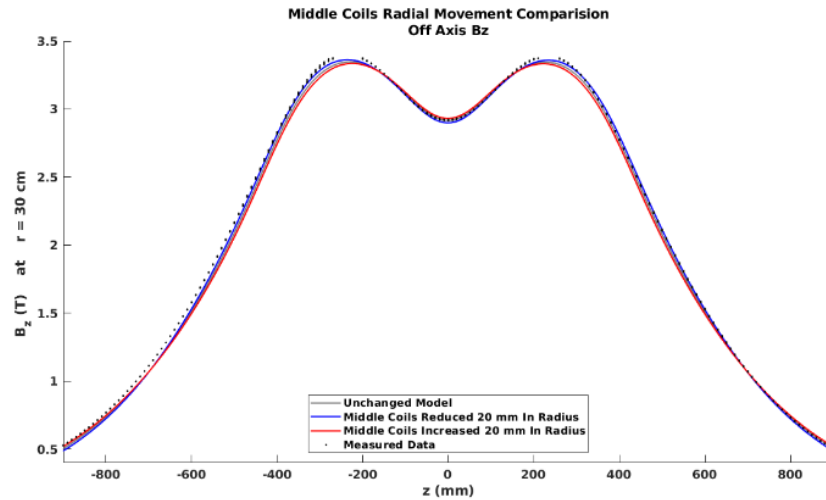


Figure 70: (b) Comparison of model and mapped radial field data at $r=30$ cm with the middle (intermediate) coils moved axially.

Operational Experience

Both the torus and the solenoid have performed very well since being commissioned in 2016 and 2017, respectively [38]. However, between September 2017 and February 2019 there were a total of 15 fast dumps of the solenoid – i.e. the dump switch would open and the magnet would run down through its dump resistor. One fast dump was attributed to a malfunctioning mechanical switch on the voltage tap diagnostic panel and a second being due to an incorrectly set quench detection threshold setting. The remaining 13 dumps were initially incorrectly identified as being due to magnet coil voltages exceeding their set quench detection thresholds. Several causes were postulated:

- The voltage thresholds apparently being exceeded were those associated with the vapor-cooled leads. Thus initial thoughts were that a resistance was developing across these leads perhaps due to a deteriorating joint. However, examination of all the data collected thus far indicated that all of the joints were good and none displayed any deviation from normal

expected resistances for all operating currents and varying helium levels within the lead reservoir. Movements of the leads producing induced voltages were also ruled out due to the robust mechanical support of the leads within the reservoir and the extremely low magnetic field in that region.

- We eliminated any potential issues with our fast data acquisition and quench detector electronics by carrying out a series of voltage injection tests. We also reviewed and improved some of the grounding for our wiring and electronics.

Investigation of the way in which we were recording and “packaging” the voltage tap data via our fast data acquisition electronics indicated that our data had unintended offsets in the time stamps - hence the false voltage tap triggers that we believed caused the fast dumps. This data packaging and translation has now been improved.

Additional diagnostics and relays were fitted to the power supply and dump switch so we could time stamp when the dump switch

opened with respect to the triggering of the quench detection units. Examination of the time stamps of subsequent solenoid fast dumps clearly indicated that the trips were originating from the power supply interlocks, which unfortunately had been masked by the false voltage trip data. A more detailed investigation revealed a strong correlation with temporary reductions in cooling water flow to the magnet power supply. This phenomenon was traced to the low conductivity water (LCW) expansion tank, (which is also shared by two other experimental halls), being topped up at intervals thus affecting the regulation of water flow to the hall and thus the magnet power supply. We made several improvements to the overall system including adding more margin for the flow switches within the power supply itself, using larger diameter pipework from the water manifold to the power supply, and most importantly, improving the regulation of the expansion tank and thus the flow of water to our experimental hall.

A re-examination of the data associated with the 13 fast dumps revealed that indeed there was a correlation with a reduction of the LCW to the hall and the power supply. To date, the solenoid has not suffered from any additional fast dumps and both magnets continue to operate within all normal expected parameters.

Summary

As with any typical project, the key drivers were technical reliability, schedule, and cost. These drivers encouraged the team to adopt and extensively use the Failure Modes and Effects Analysis (FMEA) methodology for both magnets from design through to installation and commissioning. Regular reviews such as the Magnet Advisory Group reviews, JLab Director's Reviews, and U.S. Department of Energy Office of Project Assessment Reviews, provided a clear focus and boundaries for the JLab project team. The skills, resourcefulness, and outstanding work ethic of the members of the 12 GeV Magnet Task Force, coupled with the support and commitment of other groups and departments within the laboratory, enabled the project team to flex its planning, management, and execution strategies to overcome all manner of obstacles, including sub-standard potting of torus coils, vendor quality issues on the distribution box, cool down issues involving vertical supports for the torus, and the later than expected delivery of the solenoid to name the key ones.

Ultimately both the superconducting torus and solenoid magnets developed and constructed to be used for the new CLAS12 spectrometer have met the required system specifications that will enable the full physics program to be carried out.

Acknowledgements

The authors would like to acknowledge the contributions and support from all Hall B staff, Hall D staff, the Engineering Division, Magnet Measurement Group, DC Power Group, Cryogenics Group, Detector Support Group, Target Group, Fast Electronics Group, Engineering Support Services, SRF, Procurement Team, Travel, ESH&Q, Human Resources, Payroll, Planning, Finance, Information and Technology (IT), JLab management and, in particular, the 12 GeV leadership team, the 12 GeV Project Support Staff and the technicians at JLab. The authors would also like to thank reviewers, to name a few in

particular, S. Prestemon (LBNL), B. Flora (FNAL), and H. ten Kate (CERN). Thanks are also due to Fermilab for the fabrication of the torus coils and the key vendors, Advanced Engineering Systems (conductor soldering), Tesla Engineering Limited (Solenoid design), Everson Tesla Inc. (solenoid build), Meyer Tool (distribution box), and the University of Durham (conductor splice testing). A special mention is also due to the following individuals who have contributed to the success of this project: M. Anerella, J. Ballard, K. Bruhwel, G. Cheng, J. Creel, J. Fischer, J. Gomez, S. Gregory, V. Hagen-Gates, D. Hampshire, L. Harwood, V. Lagerquist, A. Makarov, M. Marchlik, F. Martin, W. Oren, S. Plate, L. Quettier, S. Radovic, B. Reinhart, P. Rossi, E. Salpietro, W. Schneider, K. Smith, E. Stallworth, M. Stirbet, J. Szal, C. Wiggins, T. Willard, and M. Zarecky.

This material is based upon work supported by the U.S. Department of Energy, Office of Science, and Office of Nuclear Physics under contract DE-AC05-06OR23177. The U.S. Government retains a non-exclusive, paid-up, irrevocable, worldwide license to publish or reproduce the published form of this manuscript, or allow others to do so, for United States Government purposes.

REFERENCES

1. V.D. Burkert et al., "The CLAS12 Spectrometer at Jefferson Laboratory", to be published in Nucl. Inst. and Meth. A, (2020). (see this issue)
2. Y.G. Sharabian et al., "The CLAS12 High Threshold Cherenkov Counter", to be published in Nucl. Inst. and Meth. A, (2020). (see this issue)
3. D. S. Carman et al., "The CLAS12 Central Time-of-Flight System", to be published in Nucl. Inst. and Meth. A, (2020). (see this issue)
4. Luongo, C., Ballard, J., Biallas, G., Elouadrhiri, L., Fair, R., Ghoshal, P., et al., "The CLAS12 Torus Detector Magnet at Jefferson Lab", *IEEE Transactions on Applied Superconductivity*, V26 (4), 2016, DOI - 10.1109/TASC.2015.2510336.
5. Krave, S., Velev, G., Makarov, A., Nobrega, F., Kiemschies, O., Robotham, B., et al., "Overview of Torus magnet coil production at Fermilab for the Jefferson Lab 12-GeV Hall B upgrade", *IEEE Transactions on Applied Superconductivity*, V26 (4), 2016, DOI 10.1109/TASC.2016.2533264.
6. Ghoshal, P. K., Bachimanchi, R., Fair, R. J., Kashy, D., Rajput-Ghoshal, R., Hogan, J., Sandoval, N., Young, G., "Instrumentation and Control Selection for the 12 GeV Hall-B Magnets at Jefferson Lab", *Supercon. Sci. and Tech.*, V31 (9), 095007, 2018, DOI: 10.1088/1361-6668/aad277.
7. Fair, R. J. & Young, G. R., "Superconducting Magnets for the 12 GeV Upgrade at Jefferson Laboratory", *IEEE Transactions on Applied Superconductivity*, V25 (3), 2015, DOI - 10.1109/TASC.2014.2365737.
8. Ghoshal, P. K., Biallas, G., Fair, R. J., Rajput-Ghoshal, R., Schneider, W., Legg, R., et al., "FMEA on the Superconducting Torus for the Jefferson Lab 12GeV Accelerator Upgrade", *IEEE Transactions on Applied Superconductivity*, V26 (4), 2016, DOI 10.1109/TASC.2016.2533264.

- Superconductivity*, V25 (3), 4901005, 2015, DOI - 10.1109/TASC.2015.2388591.
9. Ghoshal, P., Pastor, O., Kashy, D., Schneider, W., Wiseman, M., Zarecky, M., et al., "Electromagnetic and Mechanical Analysis of the Coil Structure for the CLAS12 Torus for 12 GeV Upgrade", *IEEE Transactions on Applied Superconductivity*, V25(3), 4500705, 2015, DOI 10.1109/TASC.2014.2382604.
 10. de Hoog, F. R., Cozijnsen, M., Yuen, W. Y. D. and Huynh, H. N., "Predicting Winding Stresses for Wound Coils of Linear Orthotropic material", in *Proc. Instrumentation Mech. Engineers, Part C, J. Mechanical Engineering Science*, 218 (C1), 13–25, 2004.
 11. Li, S and Cao, J., "A Hybrid Approach for Qualifying the Winding Process and Material Effects on Sheet Coil Deformation", *J. Engineering Materials and Technology*, V126, pp. 303-313, July 2004.
 12. Knight, C. E., "Residual Stress and Strength Loss in Filament-wound Composites", *Composite Materials: Testing and Design (Eighth Conference)*, Editor: J. D. Whitcomb, ASTM, 1988.
 13. Arp, V., "Stresses in Superconducting Magnets", *Journal of Applied Physics*, V48, No. 5, pp. 2026-2036, May 1977
 14. Pojer, M., Devred, A & Scandale, W., "A Finite Element Model for Mechanical Analysis of LHC Main Dipole Magnet Coils", *LHC Project Report 1001, Applied Superconductivity Conference (ASC 2006)*, 2006.
 15. P. K. Ghoshal, R. J. Fair, D. Hampshire, V. Hagen-Gates, D. Kashy, R. Legg, R. Rajput-Ghoshal, Y. Tsui, "Design and Evaluation of joint resistance in SSC Rutherford type cable splices for Torus magnet for the Jefferson Lab 12 GeV Upgrade," *IEEE Transactions on Applied Superconductivity*, 2016; V26(4), DOI - 10.1109/TASC.2016.2517922
 16. M. N. Wilson, "Superconducting magnets," *Oxford University Press*, UK, 1983
 17. V. S. Kashikhin, L. Elouadrhiri, P. K. Ghoshal, D. Kashy, A. Makarov, O. Pastor, et al., "Torus CLAS12-Superconducting Magnet Quench Analysis," - *IEEE Trans on Appl. Superconductivity*, Vol 24. No. 3, June 2014 (DOI 10.1109/TASC.2014.2299531).
 18. P K Ghoshal, R. J. Fair, R. Rajput-Ghoshal, "Torus Analytical Quench analysis - Single coil quench analysis Hall B Torus", *JLab Internal Document # B00000401-A012* (April 23, 2013)
 19. OPERA-3D User Guide, Version 18R2, Cobham Technical Services, Network House, Langford Locks, Kidlington, U.K., May 2016.
 20. Pastor, O., Willard, T., Ghoshal, P., Kashy, D., Wiseman, M., Kashikhin, V., Young, G., Elouadrhiri, L., & Rode, C., "Structural Analysis of Thermal Shields During a Quench of a Torus Magnet for the 12 GeV Upgrade", *IEEE Transactions on Applied Superconductivity*, V25 (3), 2015, DOI-10.1109/TASC.2014.2371820.
 21. Fazilleau, P., Ball, J., Hervieu, B., & Pes, C., "CLAS 12 Solenoid Magnet Technical Design Report", *Centre de Saclay, A-CRYOM-02-07-01-01-RT05*.
 22. M.A. Antonioli et al., "The CLAS12 Silicon Vertex Tracker", to be published in Nucl. Inst. and Meth. A, (2020). (see this issue)
 23. P. Chatagnon et al., "The CLAS12 Central Neutron Detector", to be published in Nucl. Inst. and Meth. A, (2020). (see this issue)
 24. F. Bossu et al., "The CLAS12 Micromegas Vertex Tracker", to be published in Nucl. Inst. and Meth. A, (2020). (see this issue)
 25. Rajput-Ghoshal, R., Ghoshal, P. K., Fair, R. J., Hogan, J., & Kashy, D., "An investigation into the electromagnetic interactions between a superconducting torus and solenoid for the Jefferson Lab 12 GeV Upgrade", *IEEE Transactions on Applied Superconductivity*, V25 (3), June 2015, DOI - 10.1109/TASC.2014.2372049.
 26. Neilsen, C., "Design Report USA 502337-201, Hall B Torus/Solenoid MPS", *MPS 854 - Danfysik System 8500*, www.danfysik.com, June 2014.
 27. Pfeffer, H., Flora, B., & Wolff, D., "Protection of Hardware: Powering Systems (Power Converter, Normal-Conducting, and Superconducting Magnets)", *US Particle Accelerator School, Batavia*, Aug 2016, DOI: 10.5170/CERN-2016-002.343
 28. Ghoshal, P. K., Bachimanchi, R., Fair, R. J., Gelhaar, D., Kumar, O., Philip, S., & Todd, M., "Superconducting Magnet Power Supply and Hard Wired Quench Protection at Jefferson Lab for 12 GeV Upgrade", *IEEE Transactions on Applied Superconductivity*, V27 (8), 4703006, 2017, DOI - 10.1109/TASC.2017.2759280.
 29. Ekelof, S., "The genesis of the Wheatstone bridge", *Engineering Science and Education Journal*, V10 (1), Feb 2001, DOI: 10.1049/esej:20010106
 30. Lakeshore Cryotronics - Cernox temperature sensor technical data (2017).
http://www.lakeshore.com/Documents/LSTC_appendixB_1.pdf, p168, Online at <http://www.lakeshore.com>
 31. P. K. Ghoshal, R. Bachimanchi, P. Bonneau, P. Campero Rojas, B. Eng, R. Fair, T. Lemon, N. Sandoval, "Development of FPGA-based multi-sensor excitation low voltage (MSELV) chassis at Jefferson Lab", *Rev. Sci. Instrum.*, 90(12), 124701, Dec 2019 (DOI: 10.1063/1.5127460)
 32. Compact-sized FPGA development platform for prototyping circuit designs, <http://www.terasic.com.tw/cgi-bin/page/archive.pl?Language=English&CategoryNo=139&No=593>
 33. Single Resistor Gain Programmable Precision Instrumentation Amplifier, Online link information at <http://cds.linear.com/docs/en/datasheet/1167fc.pdf>
 34. Designers Guide for Applying Instrument Amplifiers Effectively, <http://www.analog.com/media/en/training-seminars/designhandbooks/designers-guide-instrumentamps-chV.pdf>
 35. Wiseman, M., Elementi, L., Elouadrhiri, L., Gabrielli, G., Gardner, T. J., Ghoshal, P. K., et al., "Design and Manufacture of the Conduction Cooled Torus Coils for The Jefferson Lab 12 GeV Upgrade", *IEEE Transactions on Applied Superconductivity*, V25 (3), 2015, DOI 10.1109/TASC.2014.2376964.
 36. Legg, R., Kashy, D., Fair, R., Ghoshal, P., Bachimanchi, R., Bruhwel, K., et al., "Liquid Nitrogen Tests of a Torus Coil

- for the Jefferson Lab 12-GeV Accelerator Upgrade”, *IEEE Transactions on Applied Superconductivity*, V25 (3), 2015, DOI - 10.1109/TASC.2014.2360139.
37. Ghoshal, P. K., Biallas, G., Fair, R. J., Kashy, D., Matalevich, J., & Luongo, C., “Commissioning Validation of CLAS-12 Torus Magnet Protection and Cryogenic Safety System”, *IEEE Transactions on Applied Superconductivity*, V28 (6), 2018, DOI 10.1109/TASC.2018.2841928.
38. P. K. Ghoshal, R. Banchimanchi, G. Biallas, P. Campero, B. Eng, R. Fair, A. Hoebel, J. Hogan, D. Insley, D. Kashy, O. Kumar, C. Luongo, T. Lemon, J. Matalevich, M. Mestayer, R. Miller, W. Moore, R. Rajput-Ghoshal, N. Sandoval, G. Young, “Commissioning of the CLAS12 Hall-B Solenoid & Torus Detector Magnets at Jefferson Lab”, Presented at ASC2018-Seattle (ASC_ID 2986822, 3L0r2B-02), *JLab Document #JLAB-PHY-18-2856*, DOE/OR/23177-4570 (Dec 2018)
39. M.D. Mestayer et al., “The CLAS12 Drift Chambers”, to be published in Nucl. Inst. and Meth. A, (2020). (see this issue)
40. Ikeda, T., Chapman, M. D., Igarashi, Y., Imazato, J., Lee, J. M., Khabibullin, M. M., *et al.*, “High-precision magnetic field mapping with a 3D Hall probe for a T-violation experiment in $K_{\mu 3}$ decay”, Elsevier Publications, Nuclear Instruments and Methods in Physics Research, Sec A, 401, pp243-262, 1997.
41. Rajput-Ghoshal, R., Fair, R., Meyers, J., Beck, M., Brakman, D., Mestayer, M., *et al.*, “Field Mapper for Superconducting Torus Magnet for the Jefferson Lab 12GeV Upgrade”, *International Magnetic Meas. Workshop, IMMW-20*, Oxford (UK), June 2017 (Talk).
42. Ghoshal, P. K., Beck, J. M., Fair, R. J., Kashy, D., Mestayer, M. D., Meyers, J., Newton, J., Rajput-Ghoshal, R., Tremblay, K., Wiggins, C. L., “Magnetic Field Mapping of the CLAS12 Torus—A Comparative Study Between the Engineering Model and Measurements at JLab”, *IEEE Transactions on Applied Superconductivity*, V29 (4), 4000310, 2019, DOI - 10.1109/TASC.2018.2884968.